UNIVERSITY OF CALIFORNIA

Santa Barbara

The Bioavailability of Seasonally Accumulated Dissolved Organic Carbon and its Contribution to Export in the Western North Atlantic

A dissertation submitted in partial satisfaction of the

requirements for the degree Doctor of Philosophy

in Marine Science

by

Nicholas Q. Baetge

Committee in charge:

Professor Craig Carlson, Chair

Professor Alyson Santoro

Professor David Siegel

September 2021

The dissertation of Nicholas Q. Baetge is approved.

_____

David Siegel

_____

Alyson Santoro

_____

Craig Carlson, Committee Chair

June 2021

The Flux and Fate of Dissolved Organic Carbon Over the Annual Phytoplankton Bloom in the Western North Atlantic

Nicholas Q. Baetge

ACKNOWLEDGEMENTS

This dissertation represents not only my work, but the collective effort and support of my mentors, family, friends, and colleagues. I am grateful to my committee members and the many professors, researchers, research staff, and *R/V* crew members I have interacted with at UCSB and at sea for their guidance, patience, knowledge, and assistance. Craig Carlson has been an exceptional mentor and role model whose example and advice I will draw from throughout my career. Thank you, Craig, for showing me the way, believing in me, and always going up to bat for me.

Sincerest thanks to the entire Carlson lab, past and present, who have been a wonderful science family to grow up as a part of; to the NASA NAAMES, ACIDD, and BIOS-SCOPE teams, who have encouraged and challenged me to not only push the envelope, but also myself as a person and scientist; to my many fellow graduate students and friends for embracing me and enjoying life with me; to the IGPMS, MSI, and Marine Biotech staff for supporting me and my research behind the scenes; and to my family and dog, Casper, for their unconditional love that fills my heart every day.

Finally, I am deeply grateful for my mom, Lien Baetge, whose life has been shaped by the trauma and hardships of escaping the Việt Cộng, surviving as a refugee, and acculturing into American society as a young girl. Let this dissertation be a testament to her success in providing her kids with an entirely different life and the opportunity to pursue their dreams.

VITA OF Nicholas Q. Baetge
April 2021

EDUCATION

Bachelor of Science in Aquatic Biology, University of California, Santa Barbara, June 2013 (with distinction)
Doctor of Philosophy in Marine Science, University of California, Santa Barbara, June 2021 (expected)

PROFESSIONAL EMPLOYMENT

2013-2014: Junior Research Specialist, Marine Science Institute, University of California, Santa Barbara
2014-2021: Teaching Assistant, Department of Ecology, Evolution and Marine Biology, University of California, Santa Barbara

PUBLICATIONS

Wagner, S., Harvey, E., **Baetge, N.**, McNair, H., Arrington, E., & Stubbins, A. Investigating atmospheric inputs of dissolved black carbon to the Santa Barbara Channel during the Thomas Fire (California, USA). Journal of Geophysical Research: Biogeosciences. DOI: 10.1029/2021JG006442

N Baetge, MJ Behrenfeld, J Fox, KH Halsey, KD Mojica, A Novoa. BM Stephens, CA Carlson. 2021. The Seasonal Flux and Fate of Dissolved Organic Carbon through Bacterioplankton in the Western North Atlantic. Frontiers in Microbiology. DOI: 10.3389/fmicb.2021.669883

LM Bolaños, CJ Choi, AZ Worden, **N Baetge**, CA Carlson, S Giovannoni. 2021. Seasonality of the microbial community composition in the North Atlantic. Frontiers in Marine Science. 8, 23. DOI: 10.3389/fmars.2021.624164

BN Hendrickson, SD Brooks, DCO Thornton, RH Moore, E Crosbie, LD Ziemba, CA Carlson, **N Baetge**, JA Mirrielees, AN Alsante. 2021. Role of Sea Surface Microlayer Properties in Cloud Formation. Frontiers in Marine Science. 7:596225. DOI:10.3389/fmars.2020.596225

G Saliba, C Chen, S Lewis, LM Russell, PK Quinn, TS Bates, TG Bell, MJ Lawler, ES Saltzman, KJ Sanchez, R Moore, Mi Shook, L Rivellini, A Lee, **N Baetge**, CA Carlson, MJ Behrenfeld. 2020. Seasonal Differences and Variability of Concentrations, Chemical Composition, and Cloud Condensation Nuclei of Marine Aerosol over the North Atlantic. Journal of Geophysical Research: Atmospheres. 25(19), e2020JD033145. DOI: 10.1029/2020JD033145

S Liu, R Parsons, K Opalk, **N Baetge**, S Giovannoni, LM Bolaños, EB Kujawinski, K Longnecker, Y Lu, E Halewood, CA Carlson. 2020. Different carboxyl-rich alicyclic molecules proxy compounds select distinct bacterioplankton for oxidation of dissolved organic matter in the mesopelagic Sargasso Sea. Limnology and Oceanography. 65(7), 1532-1553. DOI: 10.1002/lno.11405

N Baetge, JR Graff, MJ Behrenfeld, CA Carlson. 2020. Net Community Production, Dissolved Organic Carbon Accumulation, and Vertical Export in the Western North Atlantic. Frontiers in Marine Science. 7, 227. DOI: 10.3389/fmars.2020.00227

KM Bisson, **N Baetge**, SJ Kramer, D Catlett, G Girling, H McNair, E Arrington, D Hayes, C Jacobs, A James, I Closset, A D Fischer, S Wagner, M Reading, J Comstock, S Amiri, E Harvey, C Carlson, P Gaube, K Drushka, DL Valentine. 2020. California wildfire burns boundaries between science and art. Oceanography. 33(1), 16-19. DOI: 10.5670/oceanog.2020.110.

S Liu, **N Baetge**, J Comstock, K Opalk, RJ Parsons, E Halewood, C English, SJ Giovannoni, LM Bolaños, CE Nelson, K Vergin, CA Carlson. 2020. Stable isotope probing identifies bacterioplankton lineages capable of utilizing dissolved organic matter across a range of bioavailability. Frontiers in Microbiology. 11, 2364. DOI: 10.3389/fmicb.2020.580397

MJ Behrenfeld, RH Moore, CA Hostetler, J Graff, P Gaube, LM Russell, G Chen, SC Doney, S Giovannoni, H Liu, C Proctor, LM Bolaños, **N Baetge**, C Davie-Martin, TK Westberry, TS Bates, TG Bell, KD Bidle, ES Boss, SD Brooks, B Cairns, C Carlson, K Halsey, EL Harvey, C Hu, L Karp-Boss, M Kleb, S Menden-Deuer, F Morison, PK Quinn, AJo Scarino, B Anderson, J Chowdhary, E Crosbie, R Ferrare, JW Hair, Y Hu, S Janz, J Redemann, E Saltzman, M Shook, DA Siegel, A Wisthaler, MY Martin, L Ziemba. 2019. The North Atlantic Aerosol and Marine Ecosystem Study (NAAMES): Science motive and mission overview. Frontiers in Marine Science. 6, 122. DOI: 10.3389/fmars.2019.00122

G Saliba, C Chen, S Lewis, LM Russell, L Rivellini, AKY Lee, PK Quinn, TS Bates, N Haëntjens, ES Boss, L Karp-Boss, **N Baetge**, CA Carlson, MJ Behrenfeld. 2019. Factors driving the seasonal and hourly variability of sea-spray aerosol number in the North Atlantic. Proceedings of the National Academy of Sciences. 116(41), 20309-20314. DOI: 10.1073/pnas.1907574116

AWARDS

ACIDD: Across the Channel, Investigating Diel Dynamics. UC Santa Barbara Coastal Fund, 2017

ACIDD: Across the Channel, Investigating Diel Dynamics. UC Ship Funds, 2017

US Congressional Antarctic Service Medal, 2014

ABSTRACT

The Bioavailability of Seasonally Accumulated Dissolved Organic Carbon and its Contribution to Export in the Western North Atlantic

by

Nicholas Q. Baetge

Phytoplankton blooms are major sources of net community production (NCP) in the Western North Atlantic and represent important sinks for atmospheric CO_2, influencing the balance of carbon between the ocean and atmosphere. The organic matter produced by these blooms are subject to a variety of food web processes that dictate the partitioning of organic carbon into the particulate and dissolved phases. Some of the dissolved organic matter (DOM) is used to fuel instantaneous bacterial carbon demand (BCD) for biomass production and respiration. The DOM that resists or escapes rapid bacterioplankton utilization can accumulate, of which a fraction can persist. This persistent DOM is subject to being exported to depths below the sunlit ocean due to winter convective mixing and thus, can represent an important export pathway for carbon produced by phytoplankton blooms. This dissertation seeks to clarify the magnitude and divers of surface DOC accumulation over the course of the annual phytoplankton bloom in the Western North Atlantic, the contribution of DOC to annual vertical carbon export (aka biological carbon pump) via deep convective overturn, and the fate of surface accumulated DOC following physical export.

The work described here is centered on the NASA interdisciplinary field program, the North Atlantic Aerosols and Marine Ecosystems Study (NAAMES), which was designed to resolve the dynamics and drivers of the annual phytoplankton bloom and their subsequent impacts on the atmosphere. The work I describe here was supported by an independent companion grant from the National Science Foundation. As a part of the science program, I collected microbial and geochemical data from four 26-day repeat meridional ship transects in the Western North Atlantic, spanning different seasons over four years.

In Chapter II, I combined autonomous float and ship-collected data to constrain the fraction of NCP that was partitioned into seasonally accumulated DOC. This analysis allowed estimation of the export potential of DOC and its contribution to the biological carbon pump in this Western North Atlantic. The results also revealed seasonality in the partitioning of NCP, with an increased contribution of accumulated DOC further from the peak of the annual phytoplankton bloom. In addition, results suggested that non-siliceous picophytoplankton can serve as species indicators for the partitioning of NCP, which helps to narrow future research seeking to elucidate controls on DOC accumulation.

Chapter III describes the microbial remineralization experiments conducted aboard three of the cruises which demonstrate seasonality in the bioavailability of accumulated DOC to the heterotrophic microbial community. Empirically derived estimates of bacterioplankton growth efficiency from these experiments allowed for the estimation of gross bacterioplankton production, constraining the flux of labile DOC (i.e., BCD) through bacterioplankton. Many previous studies have investigated either BCD or the seasonal accumulation of a persistent pool of DOC. This work is unique in that it evaluates both fluxes in order to better resolve how heterotrophic bacterioplankton mediate carbon cycling

in the Western North Atlantic. Results indicated that while the BCD became more strongly coupled to the source of NPP as seasons transitioned from high to low productivity, a larger fraction of the DOM production accumulated and persisted.

Finally, Chapter IV describes a rare field opportunity to observe how microbes respond to organic matter exported from the euphotic zone into the mesopelagic zone following deep convection. In May of 2016, we occupied a retentive anticyclonic eddy over three days and track the temporal evolution of phytoplankton and bacterioplankton processes as the mixed layer shoaled from ~250 m upon arrival on station to < 25 m over three days. This chapter reports rapid changes in bacterioplankton carbon and carbon demand throughout the water column, but relatively smaller and more gradual changes in community composition in response to physical stratification following deep convection.

TABLE OF CONTENTS

I. Introduction

The Western North Atlantic Ocean is a region where winter-time convective overturn drives deep water formation (Dickson and Brown, 1994) and initiates massive annual phytoplankton blooms (Behrenfeld, 2010). Winter-time convective overturn deepens the mixed layer and dilutes encounter rates between phytoplankton and their predators, allowing phytoplankton division to exceed loss rates. As deep convection subsides into the spring, the shoaling mixed layer shoals increases encounter rates between phytoplankton and their predators. However, the increased light availability and continued nutrient availability in the euphotic (sunlit) zone accelerates phytoplankton division, which can continue to outpace herbivory long enough for phytoplankton to bloom (Behrenfeld and Boss, 2018). By consuming CO_2 and elemental nutrients while simultaneously generating oxygen and new organic matter, these phytoplankton blooms provide the energy and carbon that support oceanic food webs and are central to biogeochemical cycling in regions including the Western North Atlantic (Duursma, 1963; Lochte et al., 1993; Sieracki et al., 1993; Carlson et al., 1998; Falkowski et al., 1998; Behrenfeld, 2010).

The organic matter (particulate [POM] and dissolved [DOM]) produced by these blooms is subject to three export pathways that can transport organic carbon to depths where a portion can remain sequestered from the atmosphere for decades to centuries (Ducklow et al., 2001b). These pathways together represent the biological carbon pump and include the passive sinking flux of POM (McCave, 1975) physical deep mixing of DOM (Copin-Montégut and Avril, 1993; Carlson et al., 1994) or suspended POM (Dall'Olmo et al., 2016; Lacour et al., 2019), and zooplankton-mediated transport by vertical migration (Steinberg et al., 2000). The magnitude of phytoplankton blooms as well as the strength of the biological

carbon pump affect the ability of the oceans to absorb atmospheric CO_2 and mitigate the accelerating pace of global climate change.

Globally, phytoplankton account for less than 0.2% of Earth's photosynthetic biomass, but are responsible for nearly half of the planet's annual net primary production (NPP)(Field et al., 1998). NPP in the global oceans results in the production of approximately 50 Pg C y^{-1} in the form of POM and DOM (Dunne et al., 2007; Carlson and Hansell, 2015). Apart from the direct extracellular release of DOM by phytoplankton, a variety of food web processes following NPP also control the production of DOC including viral-induced or auto-lysis of phytoplankton cells, grazing activity (i.e., sloppy feeding, excretion, and egestion by herbivores), and solubilization of organic particles (see review in Carlson and Hansell, 2015). DOM is operationally defined as the fraction of organic matter that passes through a submicron filter and can, as a result, constitute a myriad of compounds depending on the filter type or pore size used (Repeta, 2015). There is no universal standard filter used to distinguish POM from DOM due to differences in methodological and analytical requirements, but filter pore sizes typically range between 0.2 and 0.7 μm. Consequently, the DOM pool can include truly dissolved chemical species, viruses, bacteria-sized particles, and colloidal organic matter (Repeta, 2015).

Regardless, the production of DOM in the global oceans (3 – 20 Pg C y^{-1}) supports marine heterotrophic bacterioplankton, which are small in size, ranging from 0.2 – 0.6 μm in diameter, but numerically abundant, ranging from 10^4 to > 10^6 cells ml^{-1} (Azam et al., 1983). In fact, the combined biomass of heterotrophic bacterioplankton is estimated to exceed that of the ocean's fishes and zooplankton (Pomeroy et al., 2007). Heterotrophic bacterioplankton rapidly recycle DOM as a source for energy and biomass synthesis (Azam

et al., 1983) and those living in the ocean's surface waters are responsible for remineralizing a majority of newly produced DOM (Azam et al., 1993), making them a dominant mechanism of nutrient cycling within the ocean's water column.

Oceanic DOM is conceptually separated into multiple carbon pools (dissolved organic carbon, DOC) defined by their bioavailability to heterotrophic bacterioplankton as well as their intrinsic turnover times (Carlson and Hansell, 2015). With turnover time of centuries to millennia, refractory DOC pool comprises up to 70% of the global DOC. In fact, the mean age for DOC in the interior of the North Pacific was radiocarbon dated to be 6240 years which is six times the estimated turnover time for global ocean circulation (Williams and Druffel, 1988; Hansell and Carlson, 1998a). This refractory pool, while representing an important reservoir of reduced carbon, does not contribute significantly to export flux nor does it support biological productivity. On the other extreme, the labile DOC pool is present at low concentrations (nM to a few μM) and is made up of organic monomers and polymers that are used to support the energy and nutrient requirements of heterotrophic microbes. While important to microbial ecology and the rapid cycling of elemental nutrients, the low concentration of the labile DOC pool combined with its high turnover rates (minutes to days) preclude it from being an important contributor to export flux. The semi-labile and semi-refractory DOM pools are dynamic pools with turnover rates of months to decades. The chemical composition of these pools remains largely uncharacterized but can include compounds like humic substances and carboxyl-rich aliphatic matter (CRAM) (Hertkorn et al., 2006) that can supplement heterotrophic metabolism, but are inherently resistant to rapid biological degradation and thus, less energy yielding (Moran and Hodson, 1990, 1994; Amon and Benner, 1994; Repeta, 2015).

Labile and semi-labile DOC together represent bioavailable DOC (BDOC), and their concentration can be operationally determined as the amount of carbon removed over various time scales in microbial remineralization incubation experiments. In these experiments, the growth of a naturally-occurring bacterioplankton populations are monitored simultaneously with changes in bulk DOC and associated specific compounds (i.e., neutral aldoses or amino acids) over time scales of days to weeks. DOC remineralization is generally characterized by an initially fast decay rate, followed by a decreasing rate that reaches an asymptote over time. The difference between the DOC concentration at the initiation of the experiment and the DOC concentration at the incubation's asymptote is used to operationally define BDOC (Carlson and Ducklow, 1996; Halewood et al., 2012; Wear et al., 2015a).

Net heterotrophic bacterioplankton production (BP) is the primary conduit for the uptake of BDOC and its passage to higher trophic levels, a key carbon-flow pathway that defines the microbial loop and shapes the ocean carbon cycle (Azam et al., 1983; Azam, 1998). Net BP has been shown to be positively correlated with NPP and chlorophyll a standing stock. It ranges from 0.03 – 12.75 μmol C L^{-1} d^{-1} and generally comprises 15 – 20% of local NPP, suggesting that it is modest in comparison to NPP (Cole et al., 1988; Ducklow et al., 2000). However, estimates of carbon flux through heterotrophic bacteria based solely on net BP are underestimated. Gross bacterioplankton production, also termed bacterioplankton carbon demand (BCD), provides a more accurate estimate of the cumulative energy and carbon flux through bacterioplankton. BCD can be estimated as the sum of net BP and the carbon that is respired as CO_2 or the division of net BP by a bacterioplankton growth efficiency (BGE) (Ducklow et al., 1999, 2002).

BGE represents the assimilation efficiency of bacterioplankton, i.e., the amount of bacterial biomass produced per unit DOC consumed. (Del Giorgio and Cole, 1998; Carlson et al., 2002; Carlson and Hansell, 2015). A bacterioplankton community with a low BGE implies that its constituents are diverting more energy to respiration and cell maintenance than to reproduction and biomass accumulation. BGE in the oceans is generally < 50%, ranging from < 10% in oligotrophic systems to > 20% in eutrophic coastal systems (Del Giorgio and Cole, 1998) and has been shown to be affected by the concentration and composition of organic matter, the composition of the heterotrophic community, nutrient availability, temperature, pH, and UV irradiation (Carlson and Hansell, 2015). With microbial remineralization experiments, BGE is determined empirically as the ratio between change in bacterial carbon biomass and the change in DOC concentration over time (Carlson et al., 1994, 2004; Wear et al., 2015a). By applying empirically derived BGE estimates with *in situ* observations of BP, one can estimate the gross flux of carbon through the bacterioplankton community using the following formula:

$$BCD = BP/BGE \qquad \text{(Eq. 1)}$$

Comparing BCD to NPP provides a useful index for evaluating the degree to which NPP can support BCD (BCD:NPP) (Cole et al., 1988; Ducklow, 2000), allowing identification of regions of net heterotrophy where the net out-gassing of CO2 can occur (Hoppe et al., 2002). Reported values of BCD:NPP have been as low as 0 (Pomeroy and Deibel, 1986; Pomeroy and Wiebe, 2001), indicative of net autotrophy, and have also exceeded 1 (Duarte and Agustí, 1998; Hoppe et al., 2002), indicative of net heterotrophy. The BCD:NPP ratio can also serve as a prelude to DOC accumulation on diel to seasonal time scales. For instance, over three bloom seasons in the Sargasso Sea, DOC consumption

was unable to match the rate of DOC release (i.e., low BCD:NPP), resulting in nearly half of the seasonally-produced DOC escaping rapid microbial to accumulate (Carlson et al., 1998).

The condition where BCD:NPP is low has been termed the “malfunctioning microbial loop” (Thingstad et al., 1997) and can lead to DOC accumulation over timescales of days to years. The factors that control this accumulation of DOM remain largely unconstrained, but a number of scenarios have been proposed. Some suggest that DOM is physically, chemically or biologically altered to a molecular structure that appears to "shield" the labile components from biological oxidation (Benner et al., 1992; McCarthy et al., 1996; Borch and Kirchman, 1997). Thus, DOC compounds resulting from NPP and subsequent food web processes can accumulate because they are intrinsically resistant to or slowly degraded by heterotrophic utilization (Hansell, 2013; Shen and Benner, 2020). Indeed, phytoplankton have been observed to directly produce of recalcitrant compounds (Aluwihare et al., 1997) or precursors to recalcitrant compounds (Arakawa et al., 2017). Additionally, labile DOC can be altered to recalcitrant compounds by heterotrophic microbes or phototransformation (Kieber et al., 1997; Benner and Biddanda, 1998; Ogawa et al., 2001; Gruber et al., 2006; Jiao et al., 2010). It has also been proposed that the shear molecular diversity of the DOC pool precludes any one individual compound from existing at concentrations detectable to a heterotrophic bacterium; thus, the encounter rate is low between an individual compound and a microbe with appropriate uptake mechanism (Kattner et al., 2011). The accumulated DOC pool thus reflects the sum of these low-concentration compounds (Kattner et al., 2011; Dittmar, 2015).

It can be argued that DOC accumulates not because it is chemically resistant to degradation but because the energetic costs of oxidizing particular compounds outweigh the

nutritional and metabolic benefits to the microbe directly exposed to the compounds (Carlson et al., 2009; Treusch et al., 2009; Giovannoni, 2017; Landry et al., 2017; Saw et al., 2020). Nutrient limitation (Zweifel et al., 1995; Cotner et al., 1997; Church, 2008) or accelerated predation (Thingstad et al., 1997) on BCD have been proposed as controls of DOC accumulation. BCD may more closely track grazer or viral-mediated release of DOM instead of instantaneous phytoplankton production (Kirchman et al., 1994). Lastly, some BCD may be supported by volatile organic compounds which are not captured in estimates of NPP measured by contemporary methods (Davie-Martin et al., 2020; Moore et al., 2020). A disconnect between BCD and NPP can arise from the combined effects of any or all of these mechanisms, which together describe the functional recalcitrance of DOC to microbial consumption. The magnitude of this functional recalcitrance, or how much the supply of DOC outpaces microbial consumption, leads to seasonal accumulation DOC in the surface waters of the ocean (Zakem et al., 2020).

Throughout the global ocean, the resistance of the semi-labile and -refractory DOM pools to rapid microbial remineralization allows them to accumulate to appreciable concentrations that can create vertical gradients of up to 40 μM from the surface sunlit ocean to the dark deep ocean (Duursma, 1963; Eberlein et al., 1985; Carlson et al., 1994; Hansell and Carlson 2009). The elemental stoichiometry of this seasonally accumulated DOM does not adhere to the canonical Redfield ratio of 106C:16N:1P, instead having mean values of 199C:20N:1P in both coastal and offshore regions of the North Atlantic and North Pacific central gyre (Hopkinson and Vallino, 2005). The C-rich character of seasonally accumulated DOM suggests that semi-labile and -refractory DOM can play important roles in the downward vertical export of atmospheric CO_2 (i.e., the biological carbon pump) if

they persist long enough to be physically redistributed to depth by mixing or subduction (Carlson et al., 1994; Børsheim and Myklestad, 1997; Hansell et al., 1997b, 1997a).

Studies have observed that the accumulation of organic carbon in the DOM pool can be greater or equal to that of the POM pool over the course of a phytoplankton bloom, supporting the importance of DOM to the biological carbon pump (Duursma, 1963; Ittekkot et al., 1981; Carlson et al., 1994; Williams, 1995). During the JGOFS 1989 North Atlantic Bloom Experiment (NABE), investigators reported that the DOC pool in the surface 80 m was, at times, ten times greater than the POC pool without apparent seasonal changes (Lochte et al., 1993). This finding, however, was shrouded in controversy due to uncertainty around the measurement of seawater DOC concentrations via the high-temperature combustion (HTC) technique (Sharp et al., 1993). By contrast, other studies suggested that the contribution of DOC to carbon export is minimal in the North Atlantic. During the 2008 North Atlantic Bloom Experiment (NAB08), a study of the temporal evolution of a single phytoplankton patch using a suite of autonomous instruments in a Lagrangian framework, investigators used profiling floats to estimate the O_2:NO_3 ratio, a proxy for the net production of nitrogen-deficient DOM. They found that the ratio was close to the canonical Redfield ratio and concluded that carbon export via DOM was likely minimal in the region as the accumulation of C-rich DOM was absent during their study (Alkire et al., 2012). It is possible that the productive water mass sampled by the study may represent an anomalous feature relative to the mean biological climate of the North Atlantic.

DOC distributions along meridional transects in the North Atlantic reveal enhanced DOC concentrations in the mesopelagic and bathypelagic zones at latitudes poleward of 40˚N (Carlson et al., 2010). Coupled to data of CFC-derived water mass ventilation ages,

these distributions suggest that accumulated DOC in the epipelagic is entrained to depth by physical mixing in the North Atlantic (Hansell et al., 2009; Carlson et al., 2010). It was estimated from these data that approximately 0.081 Pg C of DOM are exported out of the upper 100 m of the water column annually, indicating that the North Atlantic is indeed a quantitatively important region of DOC export (Carlson et al., 2010). While it is clear that DOM can accumulate and be physically entrained to depth in the North Atlantic, it remains unclear how the annual phytoplankton bloom and its associated food web processes drive that accumulation or how DOM export varies in differing regions of the North Atlantic.

Additionally, the fate of accumulated DOM after being exported to depth remains unresolved. It has been observed that accumulated DOC resistant to rapid microbial utilization at one geographical location or depth can be readily used at another (Carlson et al., 2011). Surface-accumulated DOC delivered by wintertime convective overturn can support net heterotrophic processes in the ocean interior. Indeed, absolute bacterioplankton abundance in the upper mesopelagic at BATS has been observed to increase in the weeks following deep convection (Carlson et al., 2009), with increases in relative abundance by certain bacterioplankton taxa like SAR11 subclade II, *OCS116*, *SAR202*, and marine *Actinobacteria* (Morris et al., 2005; Carlson et al., 2009; Treusch et al., 2009; Vergin et al., 2013; Liu et al., 2020a). However, the magnitude and rate at which mesopelagic bacterioplankton respond to the export of surface-accumulated DOC on shorter timescales of hours to days remains unclear. Understanding the role of DOM in the biological carbon pump requires not only constraining the magnitude and drivers of DOC accumulation, but also the fate of accumulated DOC following physical export on various timescales.

This dissertation seeks to clarify the magnitude and divers of surface DOC accumulation over the course of the annual phytoplankton bloom in the Western North Atlantic, the contribution of DOC to annual vertical export via deep convective overturn, and the fate of surface accumulated DOC following physical export. Chapters II – III describe field and experimental work conducted as a part of the NASA North Atlantic Aerosols and Marine Ecosystems Study (NAAMES), a program designed to improve understanding of the annual phytoplankton bloom and its impacts on the atmosphere. This program, detailed in Behrenfeld et al (2019), was comprised of four field campaigns in the Western North Atlantic involving repeated meridional ship transects between 39˚N and 56˚N latitude and -38˚W to -47˚W longitude. Each cruise accordingly took place at a different time of the year at four different phases of the annual phytoplankton bloom cycle. NAAMES 1 occurred in the early winter ("winter transition": November - December 2015), NAAMES 2 in the late spring ("climax transition": May 2016), NAAMES 3 in the early autumn ("depletion phase": September 2017), and NAAMES 4 in the early spring ("accumulation phase": April 2018). The design of the NAAMES study provided an ideal framework to explore the cumulative influence of microbial processes on the accumulation, bioavailability, and persistence of DOC across a large latitudinal range and over different phases of the annual phytoplankton bloom. In addition, NAAMES 2 afforded a rare opportunity to track and observe microbial and geochemical processes in the mesopelagic zone following a deep convection event. Together, the chapters presented here help to further elucidate the biogeochemical role of DOC in the biological carbon pump in the Western North Atlantic.

II. Net Community Production, Dissolved Organic Carbon Accumulation, and Vertical Export in the Western North Atlantic

Reprinted From: N Baetge, JR Graff, MJ Behrenfeld, CA Carlson. 2020. Net Community Production, Dissolved Organic Carbon Accumulation, and Vertical Export in the Western North Atlantic. Frontiers in Marine Science. 7, 227. DOI: 10.3389/fmars.2020.00227

Abstract

The annual North Atlantic phytoplankton bloom represents a hot spot of biological activity during which a significant fraction of net community production (NCP) can be partitioned into dissolved organic carbon (DOC). The fraction of seasonal NCP that is not respired by the heterotrophic bacterial community and accumulates as seasonal surplus DOC (ΔDOC) in the surface layer represents DOC export to the upper mesopelagic zone, and in the North Atlantic this is facilitated by winter convective mixing that can extend to depths >400 m. However, estimates of ΔDOC and vertical DOC export for the western North Atlantic remain ill-constrained and the influence of phytoplankton community structure on the partitioning of seasonal NCP as ΔDOC is unresolved. Here, we couple hydrographic properties from autonomous *in situ* sensors (ARGO floats) with biogeochemical data from two meridional ship transects in the late spring (~ 44 – 56˚N along ~ -41˚W) and early autumn (~ 42 – 53˚N along ~ -41˚W) as part of the North Atlantic Aerosols and Marine Ecosystems Study (NAAMES). We estimate that 4 – 35% of seasonal NCP is partitioned as ΔDOC and that annual vertical DOC export ranges between 0.34 – 1.15 mol C m^{-2} in the temperate and subpolar North Atlantic. Two lines of evidence reveal that non-siliceous

picophytoplankton, like *Prochlorococcus*, are indicator species of the conditions that control the accumulation of DOC and the partitioning of NCP as ΔDOC.

Introduction

Phytoplankton blooms spanning the subtropical to the polar latitudes of the North Atlantic occur annually and are central to biogeochemical cycling in the global ocean (Duursma, 1963; Lochte et al., 1993; Sieracki et al., 1993; Carlson et al., 1998; Falkowski et al., 1998; Behrenfeld, 2010). These blooms are net autotrophic events initiated by an imbalance between phytoplankton division and loss rates, created by favorable abiotic conditions for incident sunlight and subsurface attenuation, surface mixing layer dynamics, nutrients, and temperature(Behrenfeld and Boss, 2018).

When photoautotrophy exceeds net heterotrophic processes within the surface layer, the seasonal net community production (NCP, moles C per unit volume or area per time) can be estimated from the biological production of oxygen (Plant et al., 2016) or the net drawdown of total carbon dioxide or nitrate as it is fixed to organic matter (Codispoti et al., 1986; Hansell et al., 1993; Hansell and Carlson, 1998b). Organic matter resulting from NCP has three main fates: (1) accumulation as particulate organic carbon (POC) in the surface layer followed by export via the passive sinking flux (McCave, 1975), (2) export from the surface layer via vertical migrating zooplankton (Steinberg et al., 2000) and (3) accumulation as suspended organic matter (i.e. dissolved organic carbon (DOC) and suspended POC (POC_s)) in the surface layer followed by export via physical transport (Carlson et al., 1994; Hansell and Carlson, 1998b; Sweeney et al., 2000; Dall'Olmo et al., 2016). The present study examines the third fate, focusing on the accumulation and subsequent vertical export of

DOC. We refer to the seasonal accumulation rate of surplus surface layer DOC as ΔDOC (vertically-integrated moles C m^{-2} time $period^{-1}$ or moles C L^{-1} time $period^{-1}$).

ΔDOC has been reported to represent a significant fraction of NCP in a variety of environments and ecological states (Carlson et al., 1998; Hansell and Carlson, 1998b; Romera-Castillo et al., 2016; Bif and Hansell, 2019). For example, Hansell and Carlson (1998) reported that as much as 59% - 70% of NCP was partitioned as ΔDOC shortly following a spring bloom in the Sargasso Sea. More recently, Romera-Castillo et al. (2016) analyzed data from seven US Repeat Hydrography cruises (currently called GO-SHIP) and three Spanish cruises (OVIDE, Good Hope, CAIBOX) and found that ΔDOC:NCP largely ranged between 0.10 and 0.40 throughout the Atlantic basin, with an average ΔDOC:NCP of 0.17 for the basin. The ratio was then applied to climatological nitrate data to model ΔDOC throughout the region. While extensive hydrographic data were used in this analysis, there was a paucity of data from the temperate and subpolar western North Atlantic. Furthermore, the data used did not permit the authors to diagnose seasonal variability in ΔDOC:NCP. Seasonal measures of NCP and ΔDOC for the western North Atlantic may help to constrain estimates of NCP partitioning and consequently, outputs from models seeking to predict changes in ΔDOC. Constraining estimates of ΔDOC is necessary to improve evaluations of vertical DOC export in the western North Atlantic.

A variety of food web processes can lead to the production of DOC, including passive and active dissolved organic matter (DOM) release by phytoplankton, grazer-mediated release and excretion, viral cell lysis, and particle solubilization (see review by Carlson and Hansell, 2015). Controlling factors that result in ΔDOC in the surface layer remain unknown but have been linked to nutrient limitation (Cotner et al., 1997; Thingstad et al.,

1997), the direct production of recalcitrant compounds by phytoplankton (Aluwihare et al., 1997; Wear et al., 2015b), the alteration of labile DOM by heterotrophic microbes or phototransformation to recalcitrant compounds (Kieber et al., 1997; Benner and Biddanda, 1998; Fukuda et al., 1998; Gruber et al., 2006; Jiao et al., 2010), and the composition and metabolic potential of the extant microbial community (Carlson et al., 2004; Morris et al., 2005; DeLong et al., 2006a).

In addition, because different phytoplankton species release different quantities and qualities of DOM, the identity of the dominant phytoplankton in a community may regulate the magnitude of ΔDOC (Conan et al., 2007; Wear et al., 2015b). For example, the dominance of large eukaryotic phytoplankton has been linked to the production of bioavailable DOC that can lead to limited variability in the bulk DOC pool (Carlson et al., 1998; Wear et al., 2015a, 2015b), while the dominance of picophytoplankton in tropical and subtropical systems has been linked to elevated ΔDOC (Hansell and Carlson, 1998b; Hansell et al., 2009). Blooms of large eukaryotic phytoplankton relative to picophytoplankton may reflect conditions that favor the production of more bioavailable DOC that has a low potential to accumulate as ΔDOC (Carlson et al., 1998). If distinct phytoplankton species or group can be linked to ΔDOC or ΔDOC:NCP, they may be useful indicators for the conditions that control DOC production and accumulation. Absolute cell abundance data or sequencing data can be used to reveal phytoplankton community structure at the time of sampling; inorganic nutrient drawdown ratios provide information that integrates a previous community's activity and how that community affects nutrient pools. In the Ross Sea, Sweeney et al., (2000) used ΔSiO_4:ΔNO_3 ratios to distinguish phytoplankton populations dominated by diatoms from those dominated by non-siliceous species, with greater ratios

indicative of a greater relative importance of diatoms. These metrics of phytoplankton community structure can all be used to explore whether distinct species or groups can be used as indicators for the conditions controlling ΔDOC and ΔDOC:NCP. In the North Atlantic where massive spring blooms have been associated with diatoms and the depletion of silicate relative to nitrate (Sieracki et al., 1993), one might expect diatoms to disproportionately contribute to NCP but also produce DOC with high bioavailability, leading to low ΔDOC. Understanding the role of diatoms in the partitioning of NCP may be important in elucidating the mechanisms and conditions that regulate ΔDOC and ΔDOC:NCP.

Regardless of the controls on DOC production and accumulation, ΔDOC in the surface layer has been observed throughout the global ocean (Duursma, 1963; Eberlein et al., 1985; Carlson et al., 1994; Børsheim and Myklestad, 1997; Hansell and Carlson, 1998b; Halewood et al., 2012). ΔDOC resisting or escaping rapid microbial degradation is available for horizontal or vertical export via physical processes (Hansell et al., 1997b). Seasonal deep convective overturn mixes ΔDOC into the ocean's interior, where it can support net heterotrophic processes (Carlson et al., 1994, 2004). It is estimated that approximately 0.081 Pg C of DOM are exported out of the upper 100 m of the water column annually in the North Atlantic basin, making this region a quantitatively important location for vertical DOC export (Carlson et al., 2010). However, refining estimates of local ΔDOC and vertical DOC export in the western North Atlantic remains difficult because of limited DOC observations under deeply mixed conditions and the necessary assumptions to approximate those conditions (Hansell and Carlson, 1998b; Romera-Castillo et al., 2016).

Here we present a seasonal composite of local ΔDOC and NCP based on shipboard and ARGO float data collected in the temperate and subpolar western North Atlantic as a part of the ARGO and NASA North Atlantic Aerosols and Marine Ecosystems Study (NAAMES) programs. The repeated meridional ship transects and the extensive spatiotemporal coverage of the deployed floats provide a unique opportunity to examine DOC dynamics in the context of the annual plankton cycle. Here, we 1) consider the relationship between seasonal NCP and the partitioning of the resulting organic matter into the dissolved pool in the context of both space and time, 2) estimate vertical DOC export, and 3) examine the ΔDOC:NCP as it relates to variability in environmental conditions and phytoplankton community composition.

Materials and Methods

Study Region

The NAAMES program, detailed in Behrenfeld et al (2019), was designed to resolve the annual dynamics and drivers of the North Atlantic phytoplankton bloom and its subsequent impact on the atmosphere. It was comprised of four field campaigns from 2015 to 2018, each involving coordinated ship, aircraft, remote sensing, and autonomous *in situ* sensing (ARGO and Biogeochemical-ARGO floats) measurements during transects between 39˚N and 56˚N latitude and -38 to -47˚W longitude (Figure 2.1). Here, we focus on two NAAMES campaigns at extreme ends of the seasonal cycle, NAAMES 3 in September 2017 (early autumn) and NAAMES 4 in April 2018 (early spring), respectively. The stations occupied during these campaigns were classified into subregions defined by Della Penna

and Gaube (2019). The present study represents an ancillary companion project seeking to resolve temporal and spatial DOC dynamics in the western North Atlantic Ocean.

Environmental Data

NAAMES field campaign data are available through NASA's Ocean Biology Distributed Active Archive Center (OB.DAAC). Conductivity-temperature-depth (CTD), discrete inorganic nutrient, and flow cytometry data used here were retrieved from the SeaWiFS Bio-optical Archive and Storage System (SeaBASS; https://seabass.gsfc.nasa.gov/). All CTD casts and seawater samples were collected on the *R/V Atlantis* using a Sea-Bird Scientific SBE-911+ CTD outfitted with a Wet Labs ECO-AFL fluorometer and 24 ten-liter Niskin bottles in a typical rosette mount. Chlorophyll Maxima (CMs) were estimated for each profile using downcast data from the CTD fluorometer.

Inorganic nutrient concentrations (µmol N or Si L^{-1}) were determined for 15 depths over the surface 1500 m at each station (nominally 5, 10, 25, 50, 75, 100, 150, 200, 300, 400, 500, 750, 1000, 1250, and 1500 m). Samples were gravity filtered directly from the Niskin bottles through in-line 47 mm PC filtration cartridges loaded with 0.8 µm polycarbonate filters into sterile 50 mL conical centrifuge tubes. Resultant samples were then stored at -20˚C for later analysis using the Lachat QuickChem QC8500 automated ion analyzer at the University of Rhode Island Graduate School of Oceanography Marine Science Research Facility (GSO-MSRF). Precision for nitrite + nitrate and nitrite analyses are ~0.3 µmol L^{-1}, while precision for silicate analysis is ~0.1 µmol L^{-1}.

DOC concentrations (µmol C L^{-1}) were determined from replicate samples at the same 15 depths where nutrient samples were collected. Samples were gravity filtered directly

from the Niskin bottles into pre-combusted (4 h at 450°C) 40 mL EPA borosilicate glass vials. Filtration was performed using 47 mm PC filtration cartridges loaded with pre-combusted (4 h at 450˚C) 0.7 µm GF/ F filters. Filters were flushed with ~100 mL of sample water before collection. Vials were rinsed three times with sample water before being filled. All DOC samples were acidified to a pH of 2 by adding 50 µl DOC-free 4N HCl to 35 ml of sample immediately after collection. Samples were stored at ~ 14 ˚C in an environmental chamber free of volatile organics until analysis at the University of California, Santa Barbara.

DOC concentrations were measured in batches on Shimadzu TOC-V or TOC-L analyzers using the high-temperature combustion technique (Carlson et al., 2010). Each batch analysis was calibrated using glucose solutions of 25 – 100 µmol C L^{-1} in low carbon blank water. Data quality was assessed by measuring surface and deep seawater references (sourced from the Santa Barbara Channel) after every 6 – 8 samples as described in Carlson et al., (2010). Precision for DOC analysis is ~1 µmol L^{-1} or a CV of ~2%. Local seawater reference waters were calibrated with DOC consensus reference material provided by D. Hansell (Hansell, 2005). All DOC data for the NAAMES project are available in the SeaWiFS Bio-optical Archive and Storage System (SeaBASS; https://seabass.gsfc.nasa.gov/).

Phytoplankton concentrations (cells L^{-1}) were determined for 6 depths over the surface 100 m at each station (nominally 5, 10, 25, 50, 75, and 100 m) within hours of collection. Samples were analyzed using a BD Influx Flow Cytometer to estimate phytoplankton concentrations for four major groups (*Prochlorococcus*, *Synechococcus*, *Picoeukaryotes* (< 3 µm), and *Nanoeukaryotes* (3 - ~10 µm) (see methods in Graff and Behrenfeld, 2018). The

Phytoplankton Abundance Maximum (PAM) for each profile was defined as the depth where the sum concentration of the four major groups was greatest.

Concentrations for nutrients, DOC, and phytoplankton measured at 5 m were assumed to be equivalent to surface concentrations (0 m) as the mixed layer depth was greater than 5 m for all stations and all cruises (Figure 2.2). All profiles were averaged for each station containing multiple casts (Appendix Figures 2.1 – 2.3, 2.7).

Maximum Mixed Layer Depth Calculations from ARGO Floats

We used temperature, salinity, and pressure data provided by Biogeochemical-ARGO and ARGO (hereafter both referred to as ARGO) profiling floats to determine the maximum annual mixed layer depths in the vicinity of stations sampled during the ship campaigns. To match float profiles with station data, the NAAMES region was subdivided into 1˚ latitudinal bins. Stations and float profiles were binned to the nearest half degree based on their latitudinal coordinates. For example, a station location of 47.49˚N and a float location of 46.50˚N were both assigned to the 47˚N bin (Figure 2.1, Table 2.1).

ARGO float data were retrieved from the NAAMES data page (https://naames.larc.nasa.gov/data2018.html). All ARGO floats used were located in the area of study and were either deployed during the NAAMES campaigns or previously by the ARGO or the remOcean programs in support of NAAMES (n = 18). Float data spanned from May 5, 2014, to December 2, 2018, and encompassed 2425 unique profiles.

Mixed layer depths (Z_{MLD}) were determined for each float profile using a threshold of the Brunt-Väisälä buoyancy frequency, N^2, which was calculated using the function *swN2*() from the package *oce* (v 1.0-1) in *R*. Following Mojica and Gaube (in review), Z_{MLD} was defined as the depth below 5 m at which N^2 was greater than its standard deviation:

$$Z_{MLD} = Z_{N^2>|\sigma(N^2)|} \quad (2.1)$$

The deepest Z_{MLD}, including its corresponding month and year, recorded for each 1˚ latitudinal bin throughout the float sampling period was reported as that bin's annual maximum mixed layer depth, $Z_{Max\ MLD}$ (Figure 2.1, Table 2.1).

Seasonal Nitrate Drawdown and NCP Calculations

Estimates of surface layer-integrated NO_3 drawdown (ΔNO_3, mol N m^{-2} t^{-1}) between deep mixed and bloom or post-bloom stratified conditions have been used to determine seasonal NCP for a variety of ecosystems (Codispoti et al., 1986; Takahashi et al., 1993; Yager et al., 1995; Bates et al., 1998; Hansell and Carlson, 1998b; Siegel et al., 1999; Sweeney et al., 2000). The challenge with this approach is capturing the surface layer NO_3 distribution during deep winter convective mixing when nutrients from depth are redistributed to the surface. In the absence of direct measurements of NO_3 during deep convection, we devised an approach to approximate the NO_3 profiles at the time of convection ($NO_{3\ Mixed}$) for each 1˚ latitudinal bin around each NAAMES station. Specifically, each station's NO_3 profile measured during the post-bloom stratified condition was integrated to the corresponding $Z_{Max\ MLD}$ of its latitudinal bin. The integrated NO_3 stock was then depth-normalized to the $Z_{Max\ MLD;}$ thus, providing a volumetric estimate of mixed NO_3 concentrations for that station (vertical dashed line in Figure 2.2a). In cases where latitudinal bins contained stations from both the late spring and early autumn campaigns (44, 48, and 50˚N), the $NO_{3\ Mixed}$ profile generated from the early autumn profiles was applied to the late spring campaign. In cases where latitudinal bins only contained stations from the late spring (54 and 56˚N), $NO_{3\ Mixed}$ profiles were generated from the late spring profiles.

Depth-integrated NO_3 drawdown ($\Delta NO_3^{100\,m}$, mol N m^{-2} t^{-1}) over the surface 100 m (Figure 2.3a) from the time of deep convection to the time of observation (t) were calculated for each profile as:

$$\Delta NO_{3\ 100m} = \frac{\int_0^{100}(NO_{3_{Mixed}})dz - \int_0^{100}(NO_{3_{Observed}})dz}{t} \quad (2.2)$$

The drawdown was then converted to seasonal net community production ($NCP_{100\,m}$, mol C m^{-2} t^{-1}) by employing the C:N ratio from Redfield (1963) as done by previous studies (Hansell et al., 1993; Yager et al., 1995; Romera-Castillo et al., 2016; Bif and Hansell, 2019).

$$NCP_{100\,m} = \Delta NO_3 \times 6.6 \quad (2.3)$$

Seasonal depth-integrated NCP was also calculated for the depth horizons of the chlorophyll maximum (CM) and the phytoplankton abundance maximum (PAM) to examine how it changed over various depths within the surface layer.

ΔDOC and Export Calculations

Seasonal depth-integrated ΔDOC ($\Delta DOC_{100\,m}$, mol C m^{-2} t^{-1}) over the surface 100 m from the time of deep convection to the time of observation (t), shown in figure 2.3b, was calculated for each profile, as follows:

$$\Delta DOC_{100\,m} = \frac{\int_0^{100}(DOC_{Observed})dz - \int_0^{100}(DOC_{Mixed})dz}{t} \quad (2.4)$$

$\Delta DOC_{100\,m}$ at each station from the time of deep convection to early autumn stratified period provides an approximation of the magnitude of annual DOC export from the surface layer (Carlson et al., 1994; Hansell and Carlson, 2001b). Demarcating the surface layer at

100 m is consistent with previous studies that have used the same depth horizon to define DOC export from the surface layer into the mesopelagic (Sweeney et al., 2000; Carlson et al., 2010; Hansell et al., 2012). Thus, annual DOC export out of the surface 100 m ($DOC_{Export\ 100\ m}$, mol C m^{-2} t^{-1}) was calculated as the difference in the integrated DOC stocks (100 m to the maximum MLD for each station) between the mixed and the early autumn stratified condition (Figure 2.3b), as follows:

$$DOC_{Export\ 100\ m} = \frac{\int_{100}^{Max\ MLD}(DOC_{Observed})dz - \int_{100}^{Max\ MLD}(DOC_{Mixed})dz}{t} \quad (2.5)$$

We acknowledge that ΔDOC is subject to surface circulation and can be advected to a location with enhanced, dampened, or negligible vertical mixing. Because we do not have an explicit means to constrain lateral advection with the available data, the DOC export values reported here assume a static view of the system and represent local vertical export.

The partitioning of seasonal NCP into ΔDOC was calculated as the ratio between ΔDOC and NCP (Figure 2.4c, Appendix Figure 2.6). To examine how ΔDOC and ΔDOC:NCP changed over various depth horizons within the surface layer, they were estimated within the surface 100 m, the chlorophyll maximum (CM), and the phytoplankton abundance maximum (PAM).

Seasonal Silicate Drawdown Calculations

The depth-integrated seasonal drawdown of SiO_4 ($\Delta SiO_{4\ 100\ m}$) relative to $\Delta NO_{3\ 100\ m}$ was used as an index of the relative importance of diatoms in NO_3 drawdown, as opposed to other phytoplankton groups. Greater ΔSiO_4:ΔNO_3 ratios indicate the greater relative importance of diatoms in contributing to $NCP_{100\ m}$ (Sweeney et al., 2000). $\Delta SiO_{4\ 100\ m}$ was calculated following the same approach described above to determine $\Delta NO_{3\ 100\ m}$.

Statistical Analyses

Model I linear regressions were used to assess the comparability of ΔDOC:NCP estimates as well as latitudinal trends in those estimates. Regressions were computed using the function *lm*() from the package *stats* (v 3.5.1) in *R* (v 3.5.1). Model fits with p-values ≤ 0.05 are described herein as 'significant', while those with p-values ≤ 0.01 are described as 'highly significant'. T-tests were used to determine if slopes were different from 0, with p-values ≤ 0.05 indicating significant likelihood. The Breusch-Pagan test against heteroskedasticity was performed on each model using the function *bptest*() from the package *lmtest* (v 0.9-37) with the argument *studentized* set to TRUE in *R* (v 3.5.1). From this test, p-values ≤ 0.05 suggest heteroskedasticity and indicate that the spread of the residuals is not constant with the fitted values. In this case, the regression model's ability to predict a dependent variable is not consistent across all values of that dependent variable. Standardized (reduced) major axis model II linear regressions were used to explore relationships among deep mixed conditions, NCP, ΔDOC:NCP, ΔDOC, inorganic nutrients, and broad phytoplankton groups. As with the model I linear regressions, model fits with p-values ≤ 0.05 are described as 'significant' and those with p-values ≤ 0.01 are described as 'highly significant'. A Welch Two Sample T-test was performed to compare ΔDOC:NCP between seasons using the function *t.test*() from the package *stats* (v 3.5.1) in *R* (v 3.5.1).

Results

ARGO Float-Based Maximum Mixed Layer Depth Estimates

A total of 2425 profiles were recorded in the NAAMES study region between May 5, 2014 and December 2, 2018. The minimum and maximum number of profiles for each 1˚

latitudinal bin within the NAAMES study region were n = 17 (40˚N) and n = 375 (53˚N), respectively, with a mean of n = 127 and the median of n = 92. Figure 2.1 illustrates the temporal coverage obtained by combining data from the ARGO floats in the vicinity of each station (within 1° latitudinal bin). The maximum MLD ($Z_{Max\ MLD}$) determined for each 1˚ latitudinal bin in the NAAMES region occurred between the months of November and April and ranged from 110 – 508 m. A total of 1491 profiles were recorded during this period, with a minimum, maximum, mean, and median number of profiles for each 1˚ latitudinal bin at 5 (57˚N), 274 (52˚N), 78, and 49, respectively (Table 2.1). The range, mean, and median of $Z_{Max\ MLD}$ was greater than the mixed layer depths recorded for all cruises within the NAAMES campaign, which ranged between 6 and 214 m (Figure 2.2), indicating that conditions reflecting deep convection were not captured during the NAAMES occupations.

$Z_{Max\ MLD}$ determined for each bin was then used to reconstruct mixed nutrient and DOC profiles required to calculate seasonal NCP and ΔDOC.

NCP, ΔDOC, and Vertical DOC Export

Estimates of seasonal NCP from the mixed condition to the early autumn stratified period ranged between 1.67 and 6.70 mol C m^{-2}, with a median of 4.69 and a mean of 4.29 mol C m^{-2} (Table 2.2). ΔDOC:NCP over the same period ranged from 0.14 to 0.35, with a median and mean of 0.17 and 0.20, respectively (Table 2.2).

Vertical profiles of volumetrically-estimated NCP (difference between $NO_{3\ Mixed}$ and $NO_{3\ Observed}$ at each depth x 6.6) and ΔDOC (difference between $DOC_{\ Observed}$ and $DOC_{\ Mixed}$ at each depth) show that NCP and ΔDOC were both most pronounced within the shallowest depth horizons of the surface layer (Figure 2.4, Appendix Figures 2.4 – 2.5). ΔDOC:NCP estimates were similar whether calculated for the upper 100 m, to the depth of the

chlorophyll maximum (CM), or the depth of the Phytoplankton Abundance Maximum (PAM) (Appendix Table 2.1).

Using the local $Z_{Max\ MLD}$ for each station, we estimated annual $DOC_{Export\ 100m}$ for each station along the NAAMES meridional transect (42˚N – 53˚N) to range between 0.34 and 1.15 mol C m^{-2} (Table 2.2), with a mean of 0.77 mol C m^{-2}. $DOC_{Export\ 100m}$ is purposely not reported in table 2.3, which represents data from the late spring. It would be inappropriate to calculate DOC export in the late spring due to its timing being far removed from the timing of deep convection. It is the bulk DOC pool during the stratified condition, just before the late autumn/winter, that will be subject to deep convection. Mesopelagic DOC concentrations in the early autumn were observed to be lower than those of the mixed condition (Figure 2.3, Appendix Figure 2.2), suggesting that after DOC is exported, it is remineralized by the mesopelagic community (Carlson et al., 2004, 2011). Vertical DOC export was observed to increase in magnitude with increasing NCP (Figure 2.6b). ΔDOC:NCP over a range of NCP magnitudes was observed to be significantly greater in the early autumn (mean 0.20 ± 0.06) than the late spring (mean 0.11 ± 0.06) (Table 2.2, 2.3, Figure 2.5, 2.6a).

Partitioning of NCP

ΔSiO_4:ΔNO_3 in the early autumn generally increased with increasing latitude and ranged from 0.36 – 0.70, which would suggest that 36 – 70% of phytoplankton biomass in the region was represented by diatoms or other siliceous phytoplankton like silicoflagellates. ΔDOC:NCP displayed a strong and highly significant negative relationship with ΔSiO_4:ΔNO_3 (Figure 2.7). ΔDOC:NCP also showed significant moderate to strong direct relationships with *Prochlorococcus* abundance within the depth horizons of the CM and

PAM (Figure 2.8). When compared to flow cytometry cell abundance estimates of other broad phytoplankton groups (*Synechococcus,* picoeukaryotes and nanoeukaryotes), the ΔDOC:NCP ratio only demonstrated a weak negative relationship with picoeukaryotes over the PAM depth horizon (Appendix Table 2.2).

Discussion

Of the ~9 Pg C of global annual carbon export to the ocean interior by the biological carbon pump (DeVries and Weber, 2017), approximately 1.27 Pg C are exported in the North Atlantic alone, indicating that the biological carbon pump in the North Atlantic is an important component of the global carbon cycle (Sanders et al., 2014). The biological carbon pump is driven by a complex set of processes, including a passive sinking flux of organic particles (McCave, 1975), an active transport of organic carbon and CO_2 by vertically migrating zooplankton (Steinberg et al., 2000), and the physical transport of dissolved and suspended organic matter by subduction and convective mixing (Carlson et al., 1994; Hansell et al., 2009; Dall'Olmo et al., 2016). To predict changes in the North Atlantic biological carbon pump under different climate scenarios, it is necessary to reduce the uncertainties in the magnitude and contribution of these different pathways (Sanders et al., 2014; Siegel et al., 2016).

Although contributions by passive fluxes and vertical migrating organisms to carbon export can be obtained on individual research campaigns, assessing the contribution of the vertical redistribution of suspended particulate or dissolved organic carbon (POC_s and DOC, respectively) to carbon export requires an understanding of the interplay between the seasonal net production of POC_s and DOC and the extent of physical convective mixing at any given location. By combining ARGO float data with satellite estimates of POC, one

study demonstrated that the seasonal accumulation and physical removal of total POC in the North Atlantic could account for 23 - >100% of the carbon export flux into the mesopelagic (Dall'Olmo et al., 2016). Applying this approach to estimate the contribution of DOC to vertical carbon export would be difficult without a remote-sensing proxy for the bulk DOC pool in the open ocean. Direct measurements of DOC at regular temporal intervals over numerous annual cycles at time-series study sites is arguably the most powerful approach to resolving the contribution of DOC to vertical carbon export (Copin-Montégut and Avril, 1993; Carlson et al., 1994; Børsheim and Myklestad, 1997; Hansell and Carlson, 2001b). This approach, however, is only feasible at a limited number of locations.

Constraints on Post-convection Conditions Challenges Estimations of ΔDOC and NCP

Studies that make direct DOC measurements at the time of deep convection and during stratified periods (i.e. post-bloom) can provide estimates of seasonal DOC accumulations (ΔDOC). Concomitant measurements of TCO_2, inorganic nutrients, or oxygen between those periods permit estimates of net community production (NCP) (Codispoti et al., 1986; Hansell et al., 1993; Bates et al., 1998; Plant et al., 2016). Combining the corresponding ΔDOC and NCP estimates provides insight into how much of NCP becomes seasonally accumulated DOC (ΔDOC:NCP), thereby providing constraint on vertical DOC carbon export estimates (Hansell and Carlson, 1998b; Carlson et al., 2000; Sweeney et al., 2000; Hansell and Carlson, 2001b). A major challenge to estimating ΔDOC:NCP is being able to capture direct measures of DOC and inorganic nutrients at the time of deep mixing when their respective concentrations are homogenously distributed throughout the deep mixed layer. Measures of DOC and inorganic nutrient profiles during both seasonally vertically stratified and maximally mixed conditions allow for the calculation of net DOC production

from NO_3 drawdown (estimates of NCP). However, capturing maximal deep convective mixing events is difficult at best.

In the absence of direct measurements, previous studies have defined criteria to predict pre-bloom nutrient and surface DOC concentrations. In their study of upwelling-driven phytoplankton blooms in the northwestern portion of the Santa Barbara Channel, California, Wear et al. (2015a) used nutrient and salinity fields to characterize recently upwelled water at 5 m and then identified waters meeting those nutrient and salinity conditions as "pre-bloom" source waters, reflective of initial mixed conditions. DOC values in these source waters were used as background concentrations from which ΔDOC values were calculated. In Romera-Castillo et al (2016), the authors applied a representative ΔDOC:NCP value derived from cruise-based estimates to climatological nitrate data to model ΔDOC throughout the Atlantic. They calculated ΔDOC and NCP as the difference in DOC and nitrate concentrations, respectively, between the surface and underlying source waters, which varied with latitude. In the North Atlantic, mixed condition values for DOC and nitrate concentrations were taken from 200 m with the reasoning that winter vertical mixing commonly reaches that depth. Here, we used ARGO float observations to retrieve the maximum MLDs measured in 1˚ latitudinal bins in the NAAMES study region (Figure 2.1, Table 2.1). We then redistributed early autumn stratified DOC and NO_3 profiles over their corresponding local maximum MLD to estimate DOC_{Mixed} and $NO_{3\ Mixed}$ concentrations (Figure 2.3), allowing estimations of ΔDOC and NCP at occupied stations.

Leveraging ARGO Datasets Empower Analysts to Simulate Pre-bloom Conditions

With a current global fleet of over 3900 autonomous floats, the ARGO program has made great contributions to improving our understanding of physical and biogeochemical

variability in the oceans (Riser et al., 2016; Claustre et al., 2020). Probing the rich dataset generated by these floats can provide reasonable estimates of annual maximum MLDs across expansive areas of the ocean at 1˚ latitudinal resolution (Figure 2.1, Table 2.1). These estimates of annual maximum MLDs can then be used to simulate the redistribution of DOC and nitrate profiles observed during the early autumn stratified periods and allow approximate reconstructions of the mixed profiles for each variable (Figure 2.3). Combining ARGO data collected in the NAAMES region with profiles collected during the early autumn stratified period, we were able to estimate mixed DOC and nutrient concentrations in the absence of direct measurements.

As these estimates were the foundation for calculating approximate ΔDOC, its contribution to *NCP*, and potential *DOC* export flux in western North Atlantic (Table 2.2, Table 2.3, Figure 2.3), we sought to compare them against wintertime (January – March) data from two publicly available data products, the Global Ocean Data Analysis Project version 2 2019 (Gv2_2019) and the World Ocean Atlas 18 (WOA18) (see analyses in Appendix). Unfortunately, these two data products contained limited wintertime data for the NAAMES study region and the available data displayed relatively shallow winter MLDs compared to our maximum MLD estimates. For these reasons, using Gv2_2019 and WOA18 data to constrain the conditions under deep convection for the NAAMES region was problematic and made comparisons with this study's data equivocal. However, interrogating these publicly available data products did underscore the difficulty in defining the magnitude and conditions of deep mixing for the western North Atlantic, even with extensive, historical datasets. Data from the ARGO program, as used in this study, can help to hone estimates of the maximal extent of deep convective mixing, critical to constraining

ΔDOC, its contribution to NCP, and potential DOC export flux. However, this is not an infallible approach either.

Our approach to capturing deep convective mixing over a wide range of latitudes at 1˚ resolution using ARGO float data can also be limited by sampling resolution (i.e., number of floats, profiling frequency). While the float data for most of the latitudinal bins in the NAAMES region contain mixing estimates deeper than 200 m (Table 2.1, Figure 2.2), it is possible that the ARGO floats missed deeper mixing events at or near our station locations, leading to underestimates of local deep mixing. However, the ARGO-based maximum mixed layer depths presented here are deeper than the winter mixed layer depths from the Gv2_2019 and WOA18 data products, from wintertime ARGO climatological data, as well as those observed on the late autumn NAAMES campaign (i.e., closest campaign to the timing of deep convection (November 2015)) (see analyses in Appendix, Appendix 2.12). Regardless, the derived variables (i.e., ΔDOC, NCP, and vertical DOC export) presented here are realistically constrained but should be considered conservative estimates. Other caveats with the approach have been noted in previous studies that have calculated NCP from nutrient deficits and are summarized below.

Caveats Limit Approximations of NCP from Nitrate Drawdown

NCP derived from nitrate drawdown is taken as an approximation of new production, that is, the net production utilizing inorganic nitrogen provided from outside sources such as deep mixing and/or upwelling (Dugdale and Goering, 1967). This approximation ignores the contributions of new nitrogen from atmospheric deposition, river inputs, and nitrogen fixation, which may lead to underestimates of NCP. Recent convergent estimates from an inverse biogeochemical and a prognostic ocean model suggest that the input of newly fixed

nitrogen from microbial fixation, atmospheric deposition, and river fluxes can account for up to 10% of carbon export in the NAAMES region (Wang et al., 2019). In addition, nitrification within the surface layer can lead to underestimates of new production (Santoro et al., 2010). Though direct measures of nitrification rates are scarce, previous studies have demonstrated that nitrification can be an insignificant source of nitrate in the euphotic zone of the subarctic North Atlantic and the Sargasso Sea (Fawcett et al., 2015; Peng et al., 2018). The approach used here does not allow us to constrain the contributions of new nitrogen from the processes described above, thus nitrate drawdown was our best approximation of NCP.

Redfield stoichiometry (C:N = 6.6) is commonly used to convert nitrate drawdown to NCP in carbon units (Hansell et al., 1993; Yager et al., 1995; Romera-Castillo et al., 2016; Bif and Hansell, 2019). We recognize that DOM production and accumulation in the surface layer can be C-rich relative to Redfield stoichiometry, having C:N ratios ranging from 12-15 in surface waters (Williams, 1995; Hansell and Carlson, 2001b; Hopkinson and Vallino, 2005), and that these values may change over the course of a phytoplankton bloom (Sambrotto et al., 1993; Bury et al., 2001; Körtzinger et al., 2001). Using Redfield stoichiometry to convert NO_3 drawdown to NCP may underestimate true NCP if a significant fraction of organic matter production was C-rich relative to Redfield stoichiometry, ultimately leading to slight overestimates of ΔDOC:NCP. While Laws (1991) argues that applying the Redfield ratio to seasonal nitrate drawdown can underestimate NCP by as much as 15-30%, other studies have demonstrated that the seasonal drawdown of TCO_2 relative to NO_3 drawdown is close to 6.6 in some high latitude

systems (Yager et al., 1995; Bates et al., 1998). Thus, employing Redfield stoichiometry is a useful approach when comparing ΔDOC:NCP with previously published studies.

ΔDOC:NCP Linked to Ecosystem State

The range of ΔDOC:NCP reported here is comparable to those previously reported from a variety of locations in the North Atlantic under different ecological states and NCP magnitudes (Hansell and Carlson 1998; Romera-Castillo et al., 2016 and references therein). ΔDOC:NCP increased from late spring to early autumn and vertical DOC export increased as seasonal NCP increased into the early autumn (Table 2.2, Table 2.3, Figures 2.5, 2.6). This may reflect changes in both ecosystem state (i.e. nutrient availability) and plankton community composition (Hansell and Carlson, 1998b; Carlson et al., 2000). Differences in predominant phytoplankton community members might lead to differences in the magnitude of DOM accumulation, perhaps due to differences in the quantity and quality of the DOM produced (Conan et al., 2007). We observed a seasonal progression in the partitioning of NCP into ΔDOC, with ΔDOC:NCP increasing between the late spring and early autumn (Figure 2.5). This finding is consistent with previous bloom observations in the Ross Sea (Carlson and Hansell, 2003). Prior studies have shown phytoplankton bloom progression is coincident with increases in DOC production and accumulation, which could be in part due to nutrient limitation (Duursma, 1963; Ittekkot et al., 1981; Eberlein et al., 1985; Billen and Fontigny, 1987; Carlson et al., 1994; Williams, 1995; Wear et al., 2015a), but these relationships are not universal (Carlson et al., 1998). While some studies have demonstrated increases in DOC concentrations with increases in *Phaeocystis* primary production and biomass (Eberlein et al., 1985; Billen and Fontigny, 1987), Carlson et al. (1998) observed little change in the bulk DOC pool during the early phase of an Antarctic *Phaeocystis* bloom. The authors reported low total

DOC production (0.44 mol C m^{-2}) in the Antarctic relative to the oligotrophic Sargasso Sea (1.7 mol C m^{-2}). Also, the authors observed that while ~50% of the newly produced DOC in the Sargasso Sea escaped microbial consumption and instead accumulated as ΔDOC, only ~28% accumulated as ΔDOC in the Antarctic, indicating that newly produced DOC in the Antarctic was largely bioavailable to the extant heterotrophic microbial community and was largely removed prior to deep convective mixing. These observations led to the hypothesis that the low seasonal production of DOC and its high bioavailability in the Ross Sea may have been tied to the size structure and composition of the phytoplankton community there.

Blooms of large eukaryotic phytoplankton relative to picophytoplankton may reflect conditions that favor the production of more bioavailable DOC that has a low potential to accumulate as ΔDOC (Carlson et al., 1998). Wear et al. (2015a, 2015b) demonstrated in field and experimental work at a coastal upwelling site that, as diatom dominated blooms transition from a nutrient-replete to a Si-stressed state, there were corresponding increases in the fraction of bloom-produced DOC that is bioavailable to heterotrophic bacterioplankton. Comparatively in tropical and subtropical systems, the dominance of picophytoplankton appears to lead to greater DOC accumulation (Carlson et al., 1998; Hansell and Carlson, 1998b; Hansell et al., 2009). It is important to emphasize, however, that the relative contribution of a phytoplankton size class does not necessarily dictate the magnitude of ΔDOC and the fractionation of NCP into ΔDOC. Rather, their relative abundance may be indicative of the environmental conditions that control the net partitioning of NCP as ΔDOC. For instance, higher ΔDOC:NCP ratios may reflect greater extracellular DOC release from primary production due to differences in cell surface area: volume ratios (Karl et al., 1996). In hydrographically stable conditions, elevated ΔDOC:NCP ratios may reflect

the increased transformation of labile DOM to more recalcitrant compounds due to nutrient limitation of heterotrophic bacterioplankton production, physical separation of bacterioplankton assemblages capable of using recalcitrant DOM, or further transformation by by phototransformation (Cotner et al., 1997; Kieber et al., 1997; Benner and Biddanda, 1998; Jiao et al., 2010). Conversely, cell physiological stress in response to physical mixing may also lead to the increased production of DOC, resulting in higher ΔDOC:NCP ratios (Hansell and Carlson, 1998b).

The contribution of larger phytoplankton, like *Phaeocystis* and diatoms, may also illuminate what conditions drive NCP partitioning. For example, the larger contribution of *Phaeocystis* relative to picoeukaryotes observed by Carlson et al. (1998) may reflect conditions that favor the production of more bioavailable DOC that has a low potential to accumulate as ΔDOC. In support of this, the authors noted that the increased production of bioavailable DOC in SiO_4-limited conditions may be an adaptive strategy by diatoms to promote heterotrophic remineralization of dead diatom frustules to dissolved SiO_4. Thus, in waters where silicate drawdown exceeded nitrate drawdown, we may infer that they were not only occupied by silicifying phytoplankton like diatoms but also that those phytoplankton may have become Si-limited over time, producing bioavailable DOC inconsequential to carbon accumulation and vertical export. Indeed, the ratios of nutrient deficits, particularly ΔSiO_4 and ΔNO_3, and NCP have been used to provide a crude signature of the composition of the community that may have been responsible for NCP and ΔDOC (Sweeney et al., 2000; Carlson and Hansell, 2003). With knowledge of either or both phytoplankton community composition and signatures of nutrient limitation, we can glean the environmental conditions that control the partitioning of NCP into ΔDOC.

ΔDOC:NCP and Vertical DOC Export Reflect Conditions Favoring Non-Siliceous Phytoplankton

To determine whether linkages could be made between the observed partitioning of NCP and distinct ecosystem states, we explored the relationships between ΔDOC:NCP, ΔSiO_4:ΔNO_3, and distinct phytoplankton groups along the NAAMES meridional transect. Because the North Atlantic spring bloom has been associated with diatoms and the depletion of silicate relative to nitrate (Sieracki et al., 1993), we expected elevated ΔSiO_4:ΔNO_3 ratios where diatom blooms might disproportionately contribute to NCP. However, because DOC produced by diatoms has been shown to be characterized by high bioavailability under Si-stress (Wear et al., 2015b), we also expected that in locations with elevated ΔSiO_4:ΔNO_3, ΔDOC would be low. We found that ΔSiO_4:ΔNO_3 increased at the higher latitudes, suggesting a higher frequency or magnitude of blooms by silicifying phytoplankton like diatoms in the northern section of the NAAMES region (Figure 2.7). However, the model regression between ΔSiO_4:ΔNO_3 and latitude was heteroskedastic, suggesting that latitude alone is not a good predictor for silicate versus nitrate drawdown. ΔSiO_4:ΔNO_3 ranged from 0.36 to 0.70, indicating that phytoplankton communities comprised of siliceous phytoplankton like diatoms and silicoflagellates were responsible for 36 – 70% of SiO_4 and NO_3 drawdown. The ratio displayed a strong and highly significant inverse relationship with ΔDOC:NCP (Figure 2.7), consistent with previous field and culture reports (Wear et al., 2015a, 2015b). An alternate interpretation is that the inverse relationship between ΔSiO_4:ΔNO_3 and ΔDOC:NCP indicates when Si drawdown is low and where the phytoplankton community is dominated by functional groups other than siliceous

phytoplankton (e.g. picoeukaryotes and cyanobacteria) there is a larger partitioning of NCP into ΔDOC.

We did not find significant relationships between ΔDOC:NCP and the abundance of *Synechococcus* or *nanoeukaryotes* (3- ~10 μm) (Appendix Table 2.2) . However, we did find that the abundance of *Prochlorococcus* was a moderate to strong indicator of ΔDOC:NCP and DOC accumulation within both the depth horizons of the chlorophyll and phytoplankton abundance maximums (Figure 2.8). This relationship, in combination with those of the nutrient deficits aforementioned, is intriguing. Together, they suggest that in stratified waters with a higher presence of *Prochlorococcus*, DOC accumulation and ΔDOC:NCP are elevated.

It is not clear in our study if elevated *Prochlorococcus* concentrations lead to the direct production of recalcitrant DOC or if the group simply represents an environmental indicator of other physical and / or food web interactions that result in ΔDOC. It has been proposed that *Prochlorococcus* may disproportionally contribute to the enhanced concentrations and long-term stability of DOC in the oligotrophic ocean (Braakman et al., 2017). The correlations between elevated *Prochlorococcus,* reduced ΔSiO_4:ΔNO3, increased DOC accumulation, and increased ΔDOC:NCP reported here is consistent with this hypothesis. The linkages made here may be important to understand the specific mechanisms that drive the partitioning of NCP and the accumulation of ΔDOC and would benefit from future experimental work targeting the role of *Prochlorococcus* in these processes.

DOC is an Important Vertical Export Term in Temperate and Subtropical Western North Atlantic

In this study, we have estimated that 20 ± 6% NCP accumulated as ΔDOC by early autumn in the western North Atlantic region occupied by NAAMES (Table 2.2). Applying this estimate to a climatological model like that of Romera-Castillo et al. (2016) may help constrain estimates of ΔDOC throughout the western North Atlantic at a higher resolution. An annual DOC export of 0.34 – 1.15 mol C m^{-2} (mean 0.77 mol C m^{-2}) out of the surface 100 m indicates that physical mixing of DOC is an important component of the biological carbon pump for this portion of the North Atlantic. Because the ARGO floats used here may not have captured the deepest local mixing event at any given station location, our estimates of annual ΔDOC are considered conservative. Similar to previous studies we calculate ΔDOC in the surface 100 m to be equivalent to vertical DOC export (Hansell and Carlson, 2001b; Romera-Castillo et al., 2016; Bif and Hansell, 2019). However, a fraction of ΔDOC could be laterally transported and/or remineralized by heterotrophic bacterioplankton, thus becoming unavailable to downward mixing by convective overturn. We may further constrain our estimates of DOC export by distinguishing horizontal from vertical transport and also accounting for the bioavailable fraction of DOC that is rapidly remineralized by microorganisms (Copin-Montégut and Avril, 1993; Carlson et al., 1994; Børsheim and Myklestad, 1997). DOC bioavailability and its impact on vertical DOC export for the NAAMES study region will be discussed in a subsequent manuscript. Finally, our data suggest that in conditions resulting in low Si-drawdown, *Prochlorococcus* or the conditions they reflect may play a significant role in the accumulation of annual ΔDOC and the

partitioning of NCP, providing a framework for future investigations of the mechanisms driving these processes.

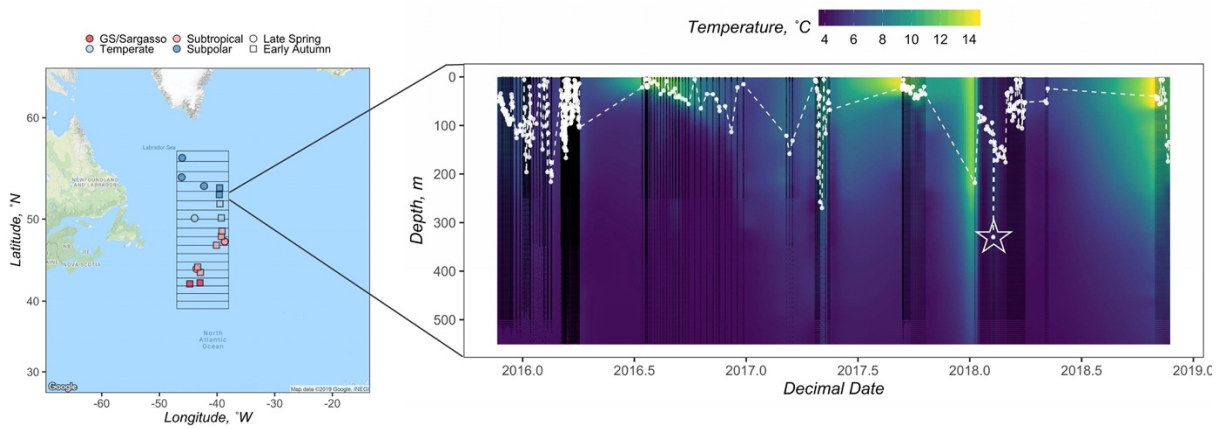

Figure 2.1. Geographical map of the NAAMES study region (left), with station locations for the late spring and early autumn cruise designated as circles and squares, respectively. Stations are colored by subregional classification based on Della Penna and Gaube (2019). Gridded box displays the bounds of the in 1˚ latitudinal bins from which float data were available. Displayed on the right is an example composite of float data from the 52˚ latitudinal bin. Black points denote when water column data were collected by an ARGO float. The white points and dashed line mark the depth of the mixed layer (n = 348). $Z_{max\ MLD}$ for this latitudinal bin was recorded as 330 m. Interpolated temperature data from the corresponding float profiles are shown in the background.

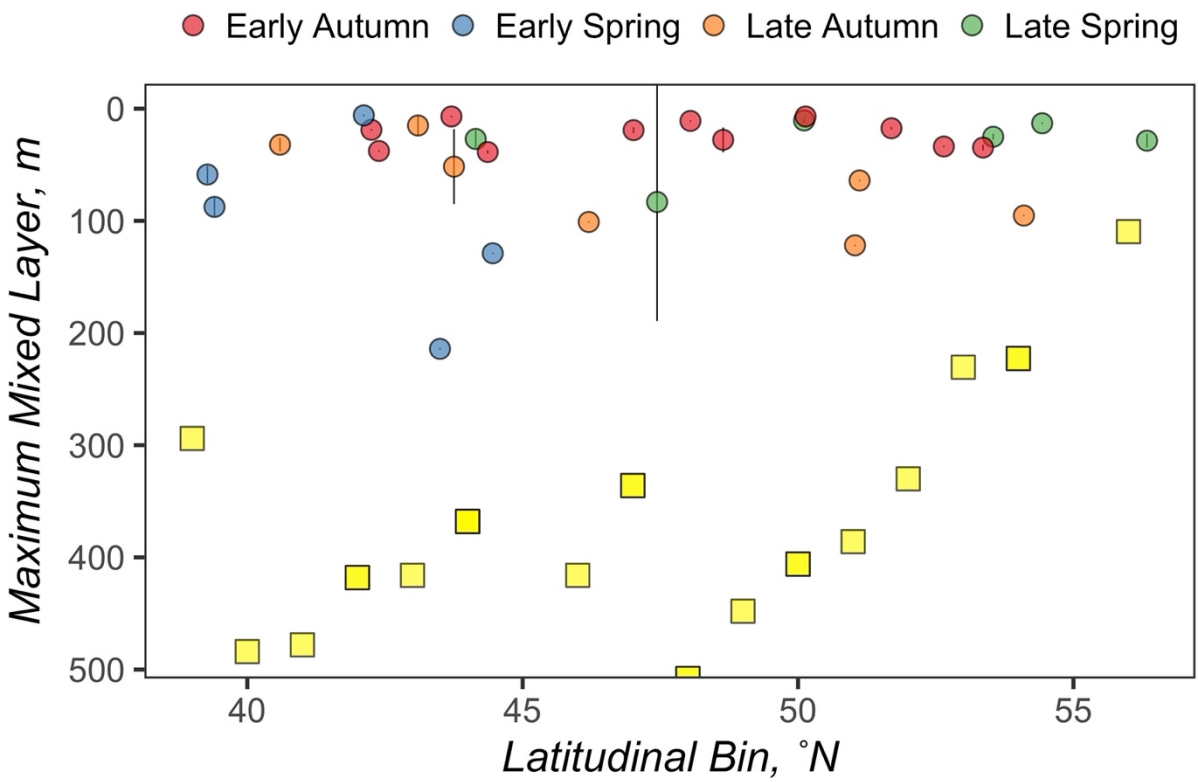

Figure 2.2. The average mixed layer depth between all CTD casts at a station is represented by an individual circle, the color of which represents the season when that mixed layer depth was observed. Error bars represent standard deviations. Yellow squares represent the maximum mixed layer depths measured by the NAAMES ARGO floats for each latitudinal bin.

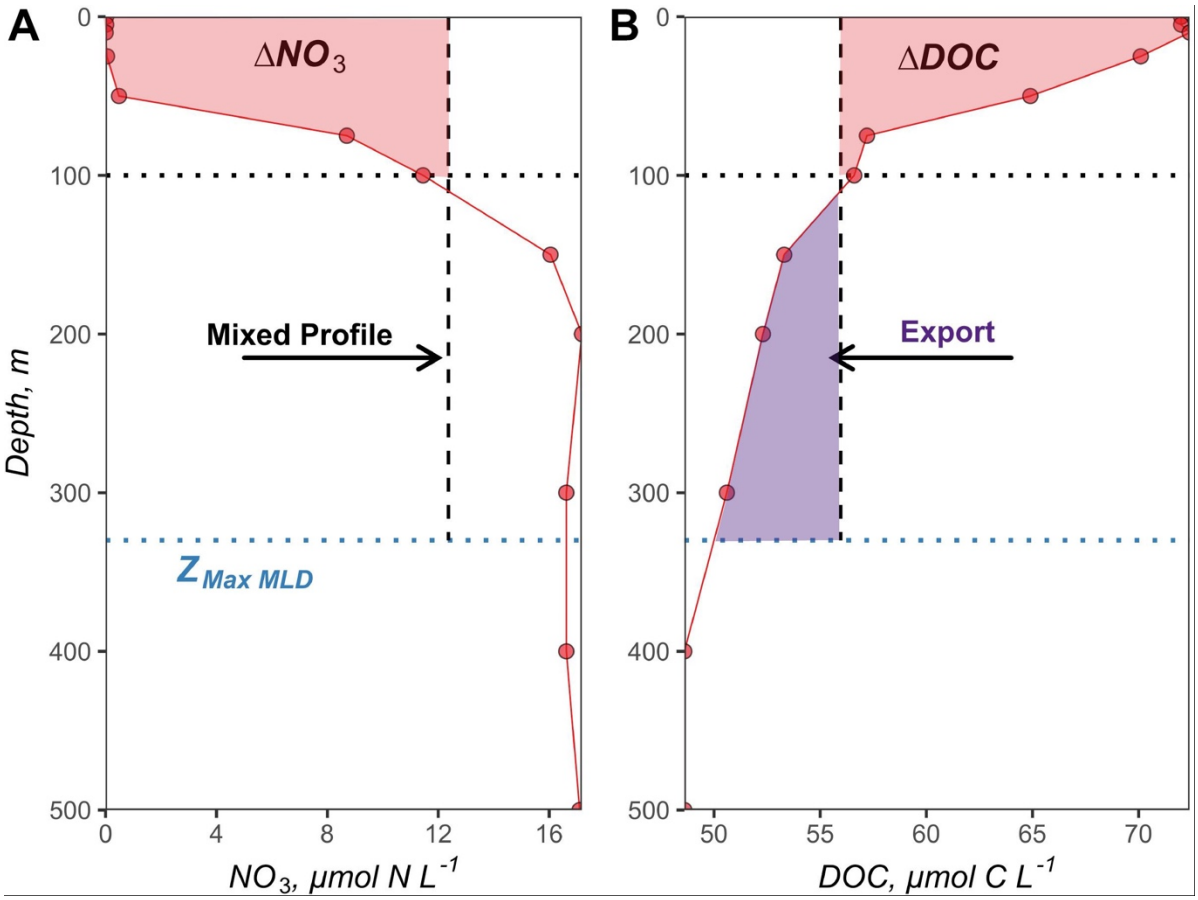

Figure 2.3. Early autumn nitrate (A) and DOC (B) profiles from station 5 at 51.7˚ N and -39.5˚W. The maximum MLD ($Z_{Max\ MLD}$) at the 50˚ latitudinal bin recorded by ARGO floats was 330 m and is shown as the blue dotted line. The black dotted line indicates the 100 m depth horizon, used as a benchmark for the euphotic zone as in previous studies. The vertical black dashed line represents the redistribution of the observed profiles to the maximum MLD (integrated and depth-normalized to maximum MLD), simulating the "mixed" condition reflective of winter / spring deep convection. The red shaded areas within the surface 100 m represents (A) the nitrate drawdown and (B) the accumulation of ΔDOC between the time of mixing to the early autumn stratified period in mol N m^{-2} and mol C m^{-2}, respectively. The purple shaded area below the 100 m depth horizon indicates the magnitude of DOC export in mol C m^{-2}.

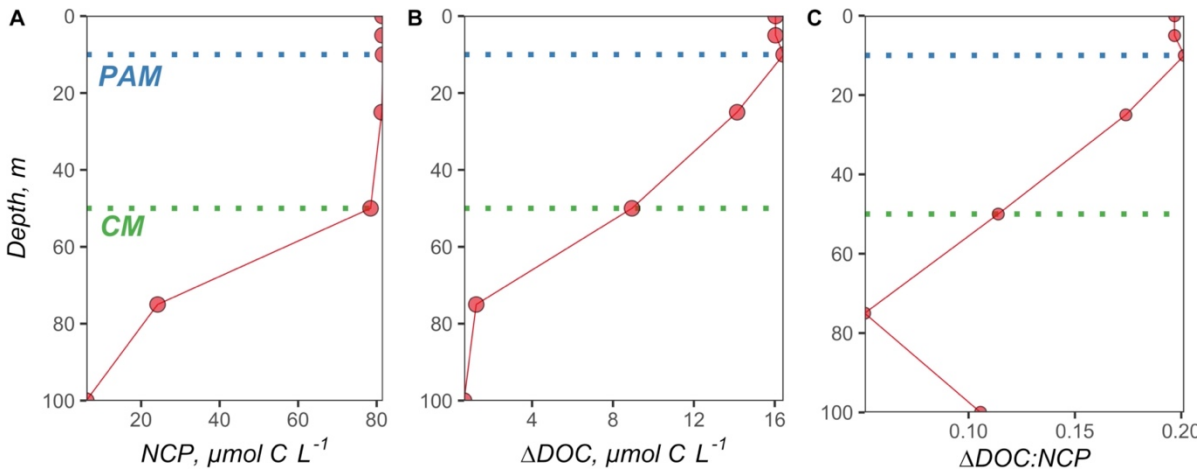

Figure 2.4. Vertical profiles of volumetrically-estimated (A) NCP (difference between NO_3 Mixed and NO_3 Observed at each depth × 6.6, (B) ΔDOC (difference between $DOC_{Observed}$ and DOC_{Mixed} at each depth), and (C) subsequent ΔDOC:NCP. The NO_3 and DOC profiles used to make these estimates were taken from station 5 at 51.7˚ N and -39.5˚W. The green dotted line denotes the chlorophyll maximum (CM), and the blue dotted line demarcates the phytoplankton abundance maximum (PAM).

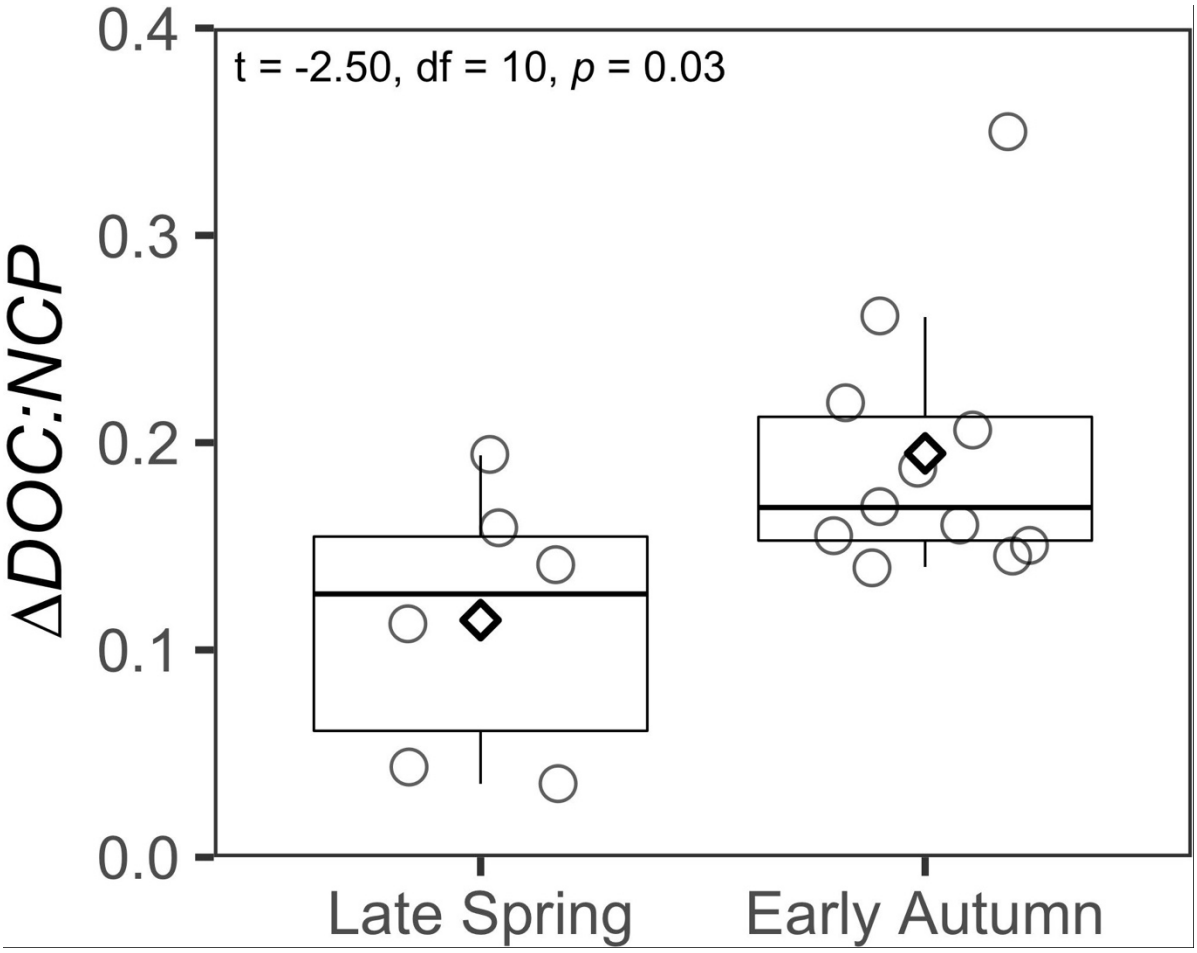

Figure 2.5. Box and whisker plots comparing ΔDOC:NCP integrated over the surface 100 m between the late spring and early autumn. Circles indicate data points. Diamonds represent the mean of the data.

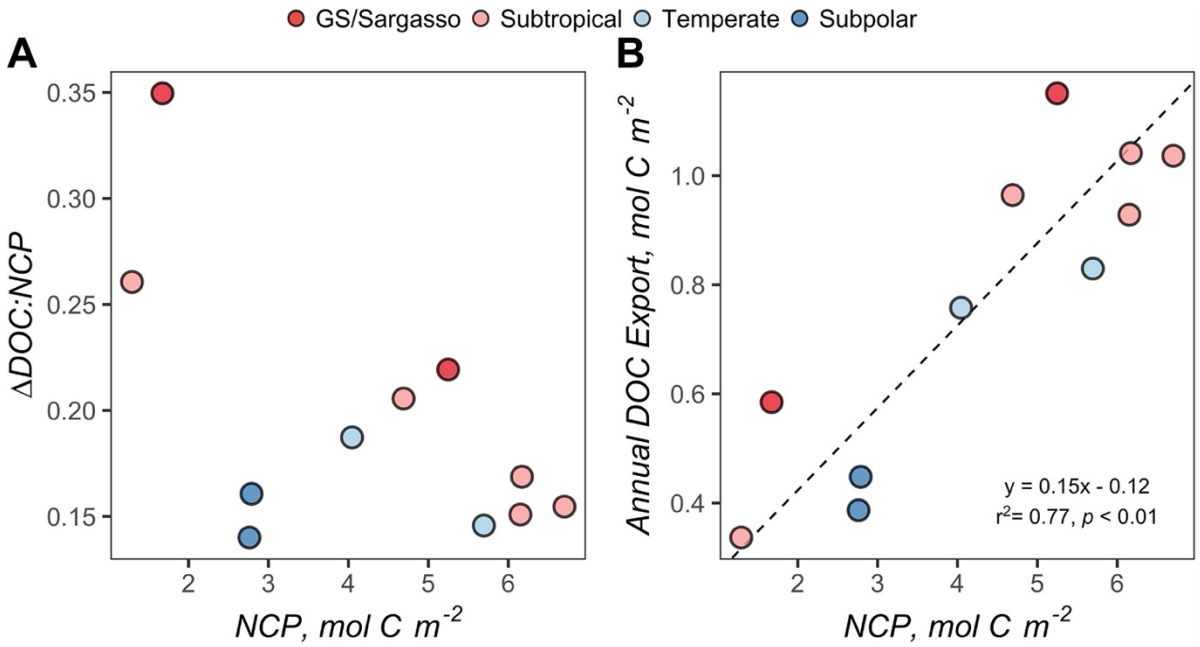

Figure 2.6. (a) Variability of ΔDOC:NCP over the range of seasonal net community production (NCP). (b) Standard major axis model II regressions for NCP and annual DOC export. Each point represents estimates for a station during the early autumn cruise. Points are filled by the subregional classification of the station as described in Figure 1. NCP and ΔDOC:NCP represent values integrated to 100 m. Annual DOC export represents values integrated from 100 m to the maximum mixed layer depth.

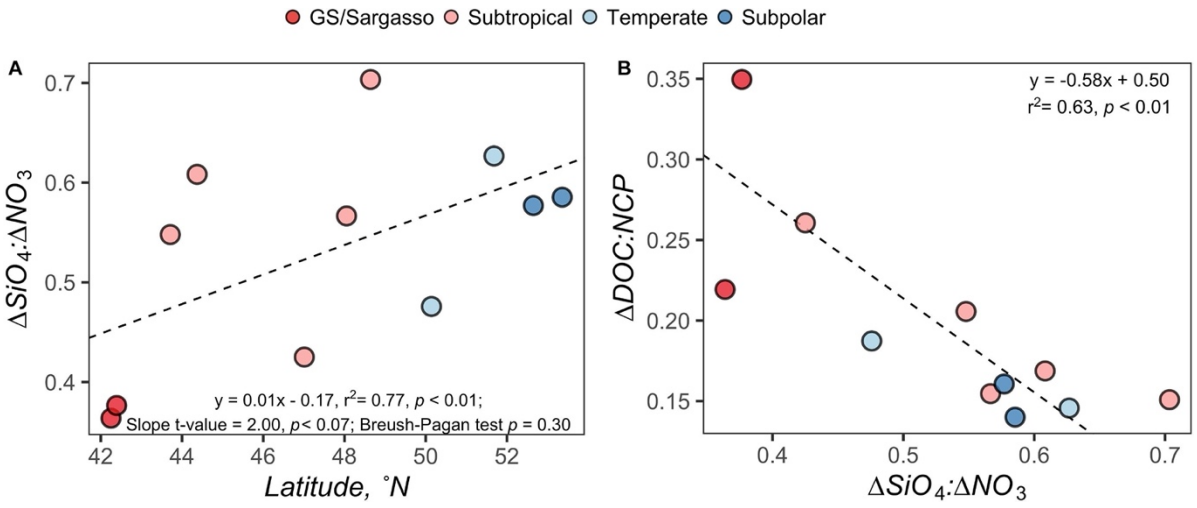

Figure 2.7. Model regressions comparing the ΔDOC:NCP in the surface 100 m; (a) model regression for the ΔSiO_4:ΔNO_3 ratio versus latitude and (b) standard major axis model II regression for ΔDOC:NCP versus ΔSiO_4:ΔNO_3 ratio. Each point represents estimates for a station on the early autumn cruise. Points are filled by the subregional classification of the station as presented in Figure 1.

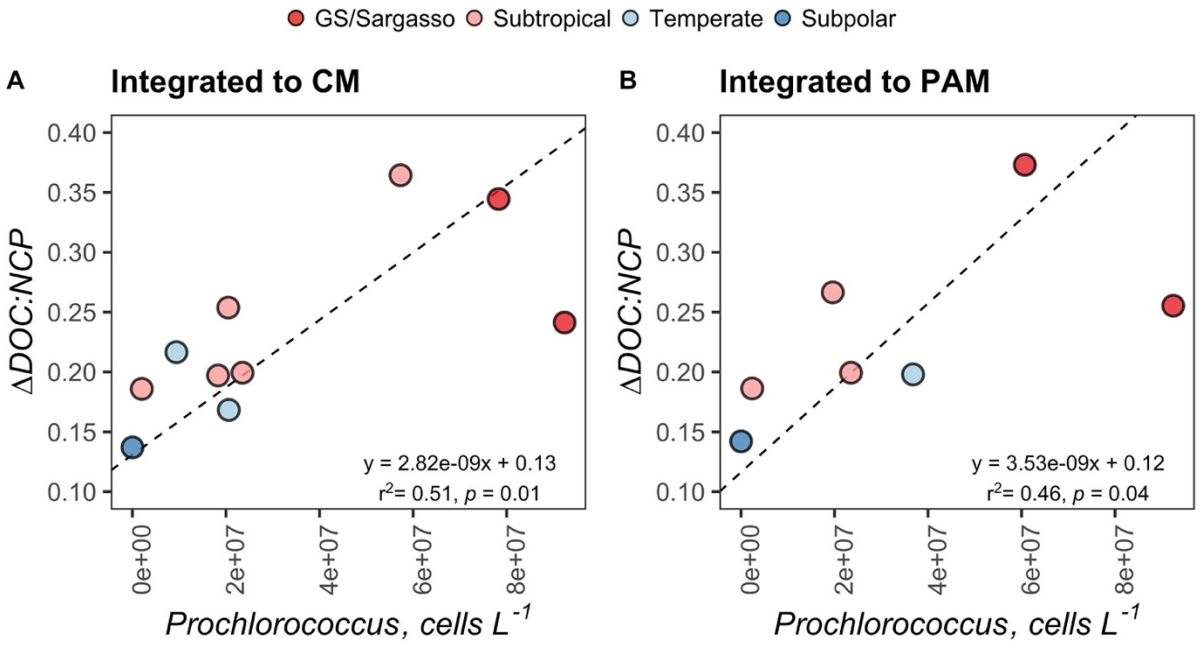

Figure 2.8. Standard major axis model II regressions comparing the ΔDOC:NCP ratio with the absolute abundance of *Prochlorococcus*, integrated to the chlorophyll maximum (CM) (a) and the phytoplankton abundance maximum (PAM) (b) for each station. Each point represents estimates for a station on the early autumn cruise. Points are filled by the subregional classification of the station as presented in Figure 1.

Latitudinal Bin (°N)	ARGO profiles *n*	November-April Argo Profiles *n*	$Z_{Max\ MLD}$ (m)	Latitude of $Z_{Max\ MLD}$ (°N)	Longitude of $Z_{Max\ MLD}$ (°W)	Time of $Z_{max\ MLD}$ (Month-Year)
39	52	52	294	39.2	−40.3	April-2018
40	17	17	484	39.9	−42.1	March-2018
41	49	26	478	41.2	−41.5	March-2018
42	114	61	418	41.6	−41.1	February-2018
42	114	61	418	42.2	−42.2	April-2018
43	66	51	416	42.9	−43.9	April-2018
44	173	89	368	44.4	−43.7	February-2018
45	113	49	404	45.1	−43.0	February-2018
46	78	37	416	45.9	−38.8	February-2016
47	132	9	336	47.2	−39.1	March-2018
48	90	27	508	48.0	−38.8	March-2018
49	92	46	448	48.8	−41.7	February-2017
50	181	159	406	50.4	−40.9	March-2017
51	177	165	386	50.9	−40.5	February-2018
52	348	274	330	51.6	−44.0	February-2018
53	375	223	231	53.4	−40.1	March-2016
54	219	158	223	54.1	−44.1	December-2015
55	39	32	241	54.8	−45.9	January-2016
56	54	11	110	55.6	−44.3	November-2015
57	56	5	284	56.7	−46.7	February-2018

Table 2.1. Annual maximum mixed layer depths ($Z_{Max\ MLD}$), estimated from ARGO profiles.

Station	Latitude (°N)	Longitude (°W)	Bin (°N)	Subregion	Date (yyyy-mm-dd)	CM (m)	PAM (m)	Mixed NO_3 (μmol N L^{-1})	Mixed DOC (μmol C L^{-1})	Mixed SiO_4 (μmol Si L^{-1})	ΔNO_3 (μmol N m^{-2})	NCP (mol C m^{-2})	ΔDOC (mol C m^{-2})	ΔDOC: NCP	DOC Export (mol C m^{-2})	ΔSiO_4 (mol Si m^{-2})	ΔSiO_4: ΔNO_3
1A (0)	42.25	−44.72	42	GS/Sargasso	2017-09-04	75	50	8.5	56.1	3.7	0.80	5.25	1.15	0.22	1.15	0.29	0.36
1	42.39	−42.95	42	GS/Sargasso	2017-09-04	75	50	3.8	54.7	1.7	0.25	1.67	0.58	0.35	0.58	0.10	0.38
2	43.71	−42.90	44	Subtropical	2017-09-05	50	40	10.1	53.6	5.3	0.71	4.69	0.96	0.21	0.96	0.39	0.55
1.5	44.37	−43.37	44	Subtropical	2017-09-06	38 ± 13	0	13.1	55.9	7.8	0.94	6.17	1.04	0.17	1.04	0.57	0.61
3	47.01	−40.11	47	Subtropical	2017-09-08	34 ± 8	16 ± 8	4.7	54.3	2.1	0.20	1.29	0.34	0.26	0.34	0.08	0.43
3.5	48.05	−39.25	48	Subtropical	2017-09-09	25	25	13.9	51.3	7.4	1.02	6.70	1.04	0.15	1.04	0.58	0.57
4	48.64	−39.13	49	Subtropical	2017-09-10	39 ± 13	16 ± 8	13.1	51.6	8.3	0.93	6.15	0.93	0.15	0.93	0.66	0.70
4.5	50.14	−39.26	50	Temperate	2017-09-11	25	o	10.7	52.4	4.7	0.61	4.05	0.76	0.19	0.76	0.29	0.48
5	51.68	−39.51	52	Temperate	2017-09-12	50	10	12.4	56.0	7.5	0.86	5.70	0.83	0.15	0.83	0.54	0.63
5.5	52.65	−39.61	53	Subpolar	2017-09-13	25	10 ± 9	13.0	54.4	7.3	0.42	2.79	0.45	0.16	0.45	0.24	0.58
6	53.36	−39.55	53	Subpolar	2017-09-14	18 ± 7	10 ± 9	12.7	52.7	6.7	0.42	2.76	0.39	0.14	0.39	0.24	0.59

Mixed NO_3, DOC and SiO_4 are estimates of the "mixed" condition reflective of winter / spring deep convection, estimated by redistributing the early autumn observed profiles to the maximum MLD. ΔNO_3, ΔDOC, and ΔSiO_4 are depth-integrated NO_3 drawdown, DOC accumulation, and SiO_4 drawdown over the surface 100 m from the time of deep convection to the time of observation. DOC Export refers to DOC export out of the surface 100 m, calculated as the difference in the integrated DOC stocks (100 m to the maximum MLD for each station) between the mixed and the early autumn stratified condition.

Table 2.2. Seasonal net community production (NCP) and its partitioning into DOC in the upper 100 m as well as DOC export out of the upper 100 m for the early autumn campaign. CM refers to the chlorophyll maximum and PAM refers to the phytoplankton abundance maximum. Mixed NO_3, DOC and SiO_4 are estimates of the "mixed" condition reflective of winter / spring deep convection, estimated by redistributing the early autumn observed profiles to the maximum MLD. ΔNO_3, ΔDOC, and Δ SiO_4 are depth-integrated NO_3 drawdown, DOC accumulation, and SiO_4 drawdown over the surface 100 m from the time of deep convection to the time of observation. DOC Export refers to DOC export out of the surface 100 m, calculated as the difference in the integrated DOC stocks (100 m to the maximum MLD for each station) between the mixed and the early autumn stratified condition.

Station	Latitude (°N)	Longitude (°W)	Bin (°N)	Subregion	Date (yyyy-mm-dd)	CM (m)	PAM (m)	Mixed NO_3 (μmol N L^{-1})	Mixed DOC (μmol C L^{-1})	Mixed SiO_4 (μmol Si L^{-1})	ΔNO_3 (μmol N m^{-2})	NCP (mol C m^{-2})	ΔDOC (mol C m^{-2})	ΔDOC: NCP	ΔSiO_4 (mol Si m^{-2})	ΔSiO_4: ΔNO_3
5	44.15	–43.58	44	Subtropical	2016-05-29	25	0	11.6	54.7	6.5	0.81	5.35	0.23	0.04	0.56	0.69
4	47.44	–38.67	48	Subtropical	2016-05-25	20 ± 13	3 ± 4	13.9	51.3	7.4	0.90	5.92	0.21	0.04	0.63	0.70
3	50.11	–43.88	50	Temperate	2016-05-22	18 ± 8	0	10.7	52.4	4.7	0.31	2.06	0.29	0.14	0.04	0.12
0	54.43	–46.14	54*	Subpolar	2016-05-17	25	0	14.8	49.8	8.1	0.13	0.89	0.17	0.19	0.04	0.30
2	53.54	–42.25	54*	Subpolar	2016-05-20	10	0	12.8	50.4	7.5	0.22	1.48	0.17	0.11	0.06	0.27
1	56.34	–46.05	56*	Subpolar	2016-05-18	18 ± 8	0	13.2	51.2	8.0	0.01	0.03	0.01	0.16	0.00	0.00

CM refers to the chlorophyll maximum and PAM refers to the phytoplankton abundance maximum. Mixed NO_3, DOC and SiO_4 are estimates of the "mixed" condition reflective of winter / spring deep convection, estimated by redistributing the early autumn observed profiles to the maximum MLD. Stars (*) indicate latitudinal bins where only late spring data were available. In those cases, mixed conditions were estimated from the late spring profiles. ΔNO_3, ΔDOC, and ΔSiO_4 are depth-integrated NO_3 drawdown, DOC accumulation, and SiO_4 drawdown over the surface 100 m from the time of deep convection to the time of observation.

Table 2.3. Seasonal net community production (NCP) and its partitioning into DOC in the upper 100 m as well as DOC export out of the upper 100 m for the late spring campaign. CM refers to the chlorophyll maximum and PAM refers to the phytoplankton abundance maximum. Mixed NO_3, DOC and SiO_4 are estimates of the "mixed" condition reflective of winter / spring deep convection, estimated by redistributing the early autumn observed profiles to the maximum MLD. Stars (*) indicate latitudinal bins where only late spring data were available. In those cases, mixed conditions were estimated from the late spring profiles. ΔNO3, ΔDOC, and ΔSiO_4 are depth-integrated NO_3 drawdown, DOC accumulation, and SiO4 drawdown over the surface 100 m from the time of deep convection to the time of observation.

Season	Station	Latitude	Longitude	NCP (100 m, mol C m^{-2})	NCP (CM, mol C m^{-2})	NCP (PAM, mol C m^{-2})	ΔDOC (100 m, mol C m^{-2})	ΔDOC (CM, mol C m^{-2}	ΔDOC (PAM, mol C m^{-2}	ΔDOC: NCP (100 m)	ΔDOC: NCP (CM)	ΔDOC: NCP (PAM)
Late Spring	5.0	44.15	-43.58	5.35	1.87	NA	0.23	0.16	NA	0.04	0.08	NA
Late Spring	4.0	47.44	-38.67	5.92	1.23	0.18	0.21	0.05	0.01	0.04	0.04	0.04
Late Spring	3.0	50.11	-43.88	2.06	0.62	NA	0.29	0.08	NA	0.14	0.13	NA
Late Spring	2.0	53.54	-42.25	1.48	0.37	NA	0.17	0.05	NA	0.11	0.15	NA
Late Spring	0.0	54.43	-46.14	0.89	0.58	NA	0.17	0.09	NA	0.19	0.15	NA
Late Spring	1.0	56.34	-46.05	0.03	0.10	NA	0.01	0.02	NA	0.16	0.19	NA
Early Autumn	0.0	42.25	-44.72	5.25	4.20	2.80	1.15	1.01	0.72	0.22	0.24	0.26
Early Autumn	1.0	42.39	-42.95	1.67	1.61	1.25	0.58	0.56	0.46	0.35	0.34	0.37
Early Autumn	1.5	43.71	-42.90	4.69	3.19	2.62	0.96	0.81	0.70	0.21	0.25	0.27
Early Autumn	2.0	44.37	-43.37	6.17	3.26	NA	1.04	0.64	NA	0.17	0.20	NA
Early Autumn	3.0	47.01	-40.11	1.29	0.96	0.48	0.34	0.35	0.20	0.26	0.36	0.41
Early Autumn	3.5	48.05	-39.25	6.70	2.28	2.28	1.04	0.45	0.45	0.15	0.20	0.20
Early Autumn	4.0	48.64	-39.13	6.15	3.31	1.38	0.93	0.62	0.26	0.15	0.19	0.19
Early Autumn	4.5	50.14	-39.26	4.05	1.74	NA	0.76	0.38	NA	0.19	0.22	NA
Early Autumn	5.0	51.68	-39.51	5.70	4.03	0.82	0.83	0.68	0.16	0.15	0.17	0.20
Early Autumn	5.5	52.65	-39.61	2.79	2.12	0.85	0.45	0.29	0.13	0.16	0.14	0.15
Early Autumn	6.0	53.36	-39.55	2.76	1.31	0.73	0.39	0.18	0.10	0.14	0.14	0.14

Appendix Table 1. NCP, ΔDOC, and ΔDOC estimated for the 100 m, chlorophyll maximum (CM), and phytoplankton abundance maximum (PAM) depth horizons at each station for the late spring and early autumn campaigns.

Phytoplankton Group	*Depth of Integration*	*Slope*	*Intercept*	r^2	*p*
Synechococcus	CM	-2.31e-09	0.31	0.09	0.41
Synechococcus	PAM	-3.3e-09	0.35	0.24	0.22
Picoeukaryotes	CM	-1.06e-08	0.31	0.37	0.06
Picoeukaryotes	PAM	-1.21e-08	0.35	0.57	0.03
Nanoeukaryotes	CM	-4.69e-08	0.31	0.37	0.06
Nanoeukaryotes	PAM	-5.12e-08	0.35	0.45	0.07

Appendix Table 2. Results from standard major axis model II regressions comparing ΔDOC:NCP with the absolute abundances of *Synechococcus*, pico- (< 3 μm), and nanoeukaryotes (3 - 10 μm), integrated to either the chlorophyll maximum (CM) or the phytoplankton abundance maximum (PAM) during the early autumn.

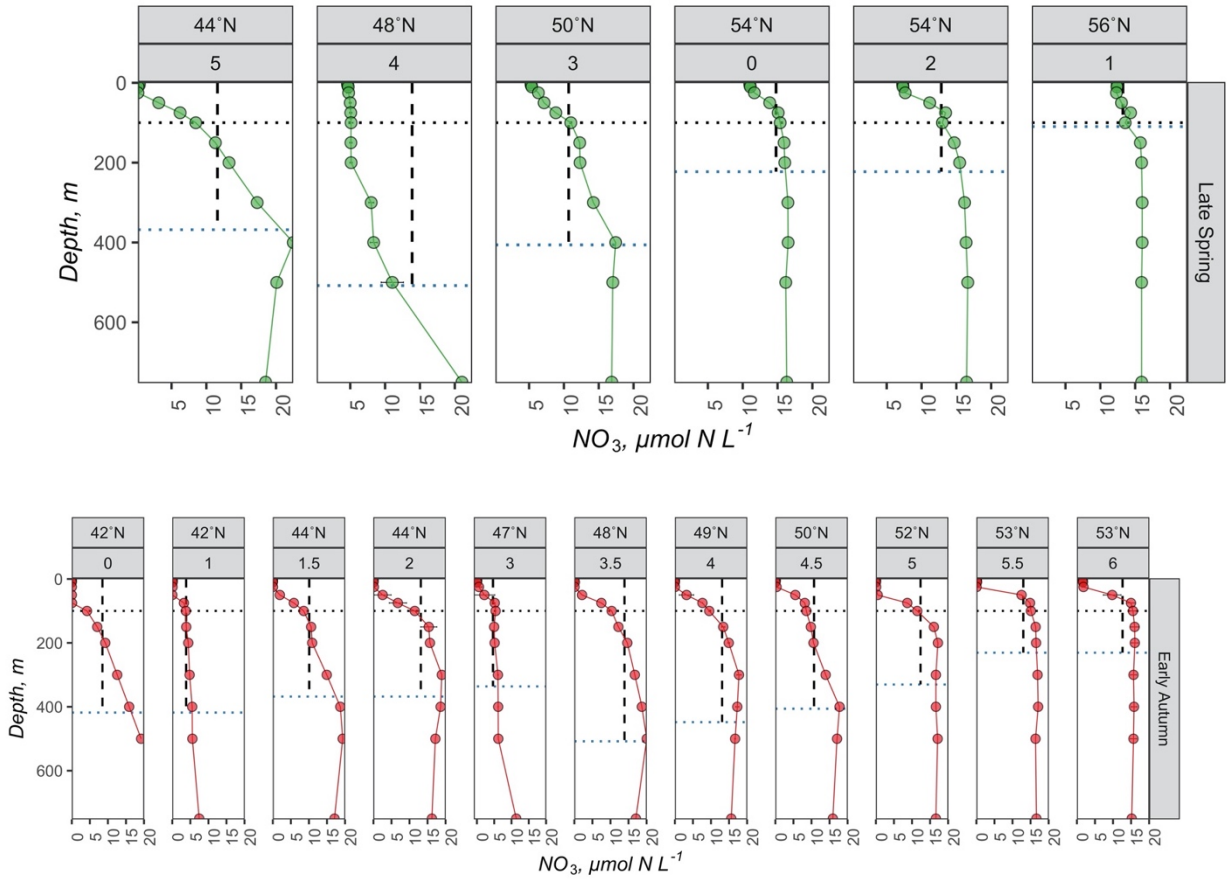

Appendix Figure 1. Average nitrate profiles for each station the late spring (top) and early autumn (bottom) campaigns. Error bars indicate the standard deviations. The upper label of each facet denotes the latitudinal bin in which the profile was observed and the lower label indicates the station number. Horizontal black dotted lines indicate the depth of 100 m and the horizontal blue dotted lines indicate the maximum mixed layer depth. Vertical dashed lines represent the simulated mixed condition.

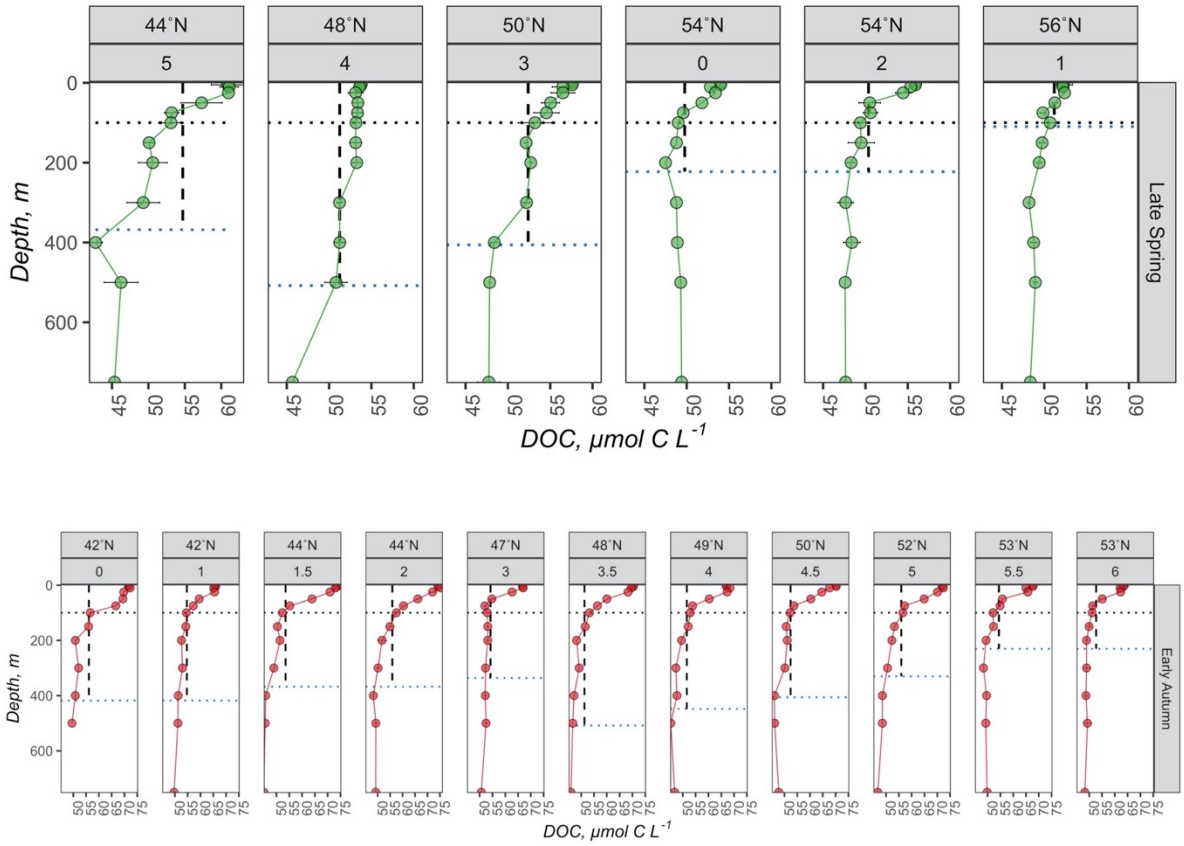

Appendix Figure 2. Average DOC profiles for each station the late spring (top) and early autumn (bottom) campaigns. Error bars indicate the standard deviations. The upper label of each facet denotes the latitudinal bin in which the profile was observed and the lower label indicates the station number. Horizontal black dotted lines indicate the depth of 100 m and the horizontal blue dotted lines indicate the maximum mixed layer depth. Vertical dashed lines represent the simulated mixed condition.

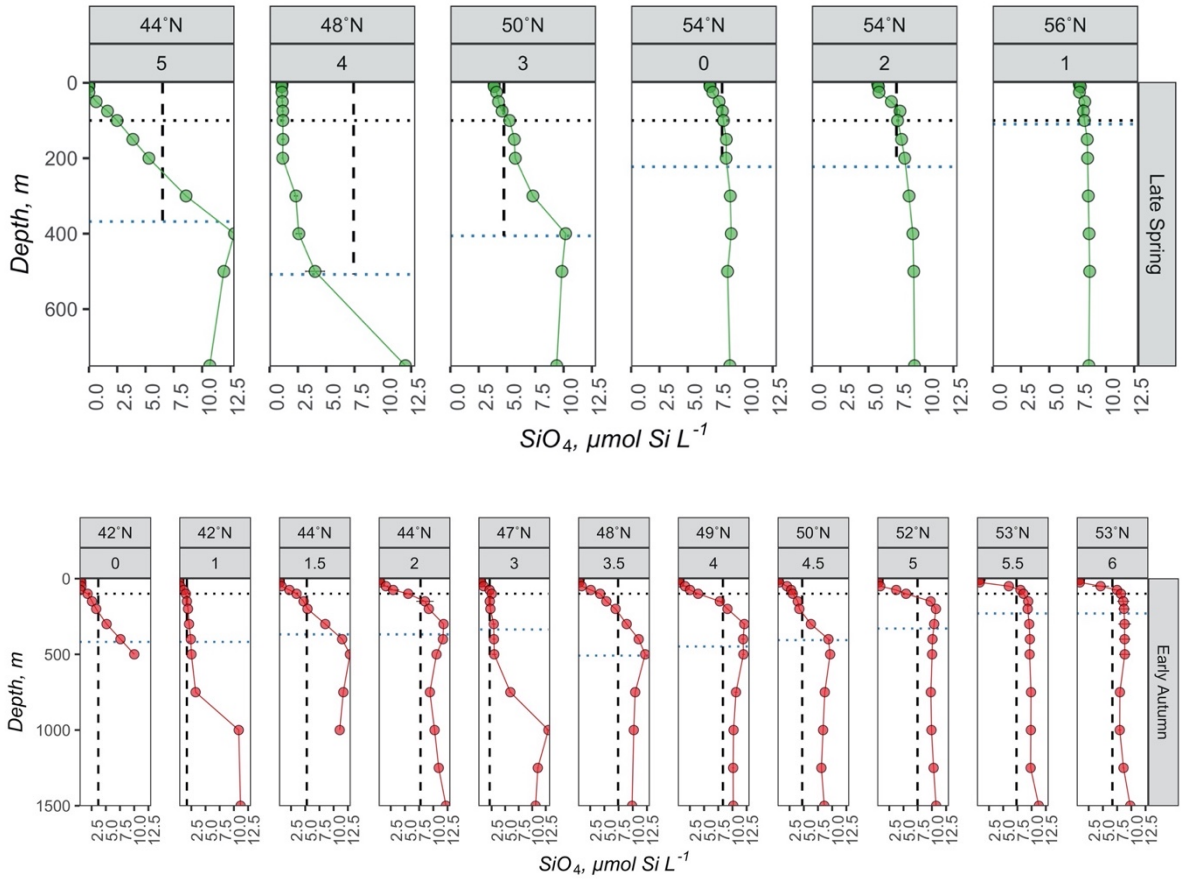

Appendix Figure 3. Average silicate profiles for each station the late spring (top) and early autumn (bottom) campaigns. Error bars indicate the standard deviations. The upper label of each facet denotes the latitudinal bin in which the profile was observed and the lower label indicates the station number. Horizontal black dotted lines indicate the depth of 100 m and the horizontal blue dotted lines indicate the maximum mixed layer depth. Vertical dashed lines represent the simulated mixed condition.

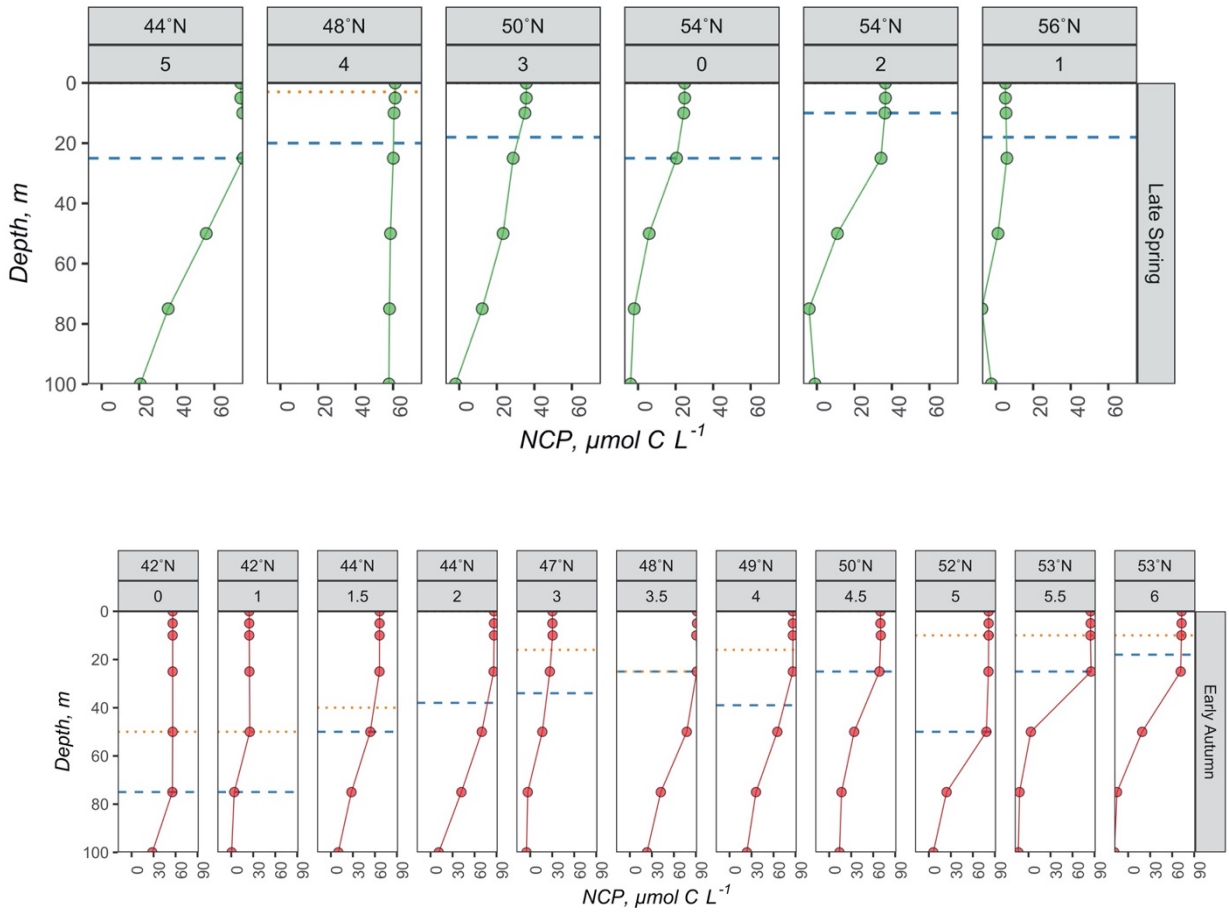

Appendix Figure 4. NCP profiles for each station the late spring (top) and early autumn (bottom) campaigns. The upper label of each facet denotes the latitudinal bin in which the profile was observed and the lower label indicates the station number. Horizontal blue dashed lines indicate the depth of chlorophyll maximum (CM) and the horizontal orange dotted lines indicate the depth of the phytoplankton abundance maximum (PAM).

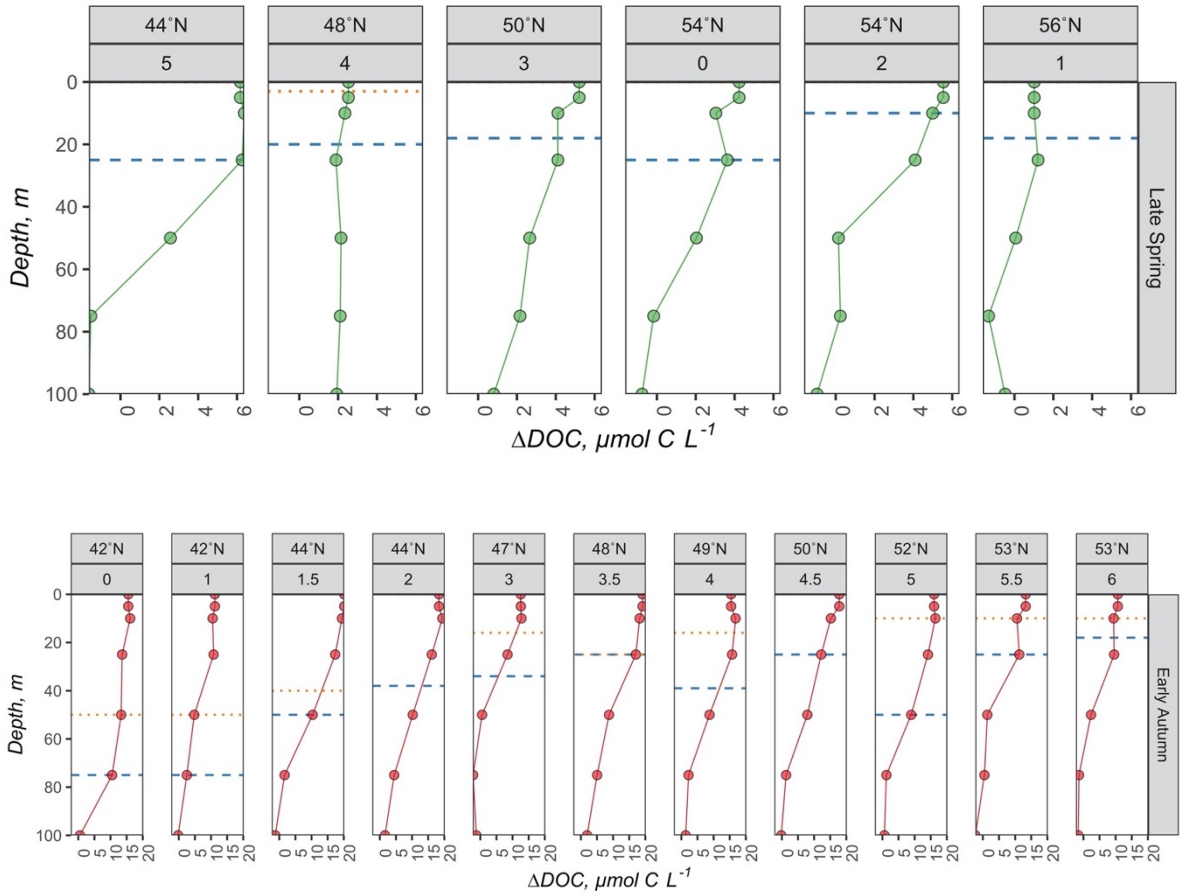

Appendix Figure 5. ΔDOC profiles for each station the late spring (top) and early autumn (bottom) campaigns. The upper label of each facet denotes the latitudinal bin in which the profile was observed and the lower label indicates the station number. Horizontal blue dashed lines indicate the depth of chlorophyll maximum (CM) and the horizontal orange dotted lines indicate the depth of the phytoplankton abundance maximum (PAM).

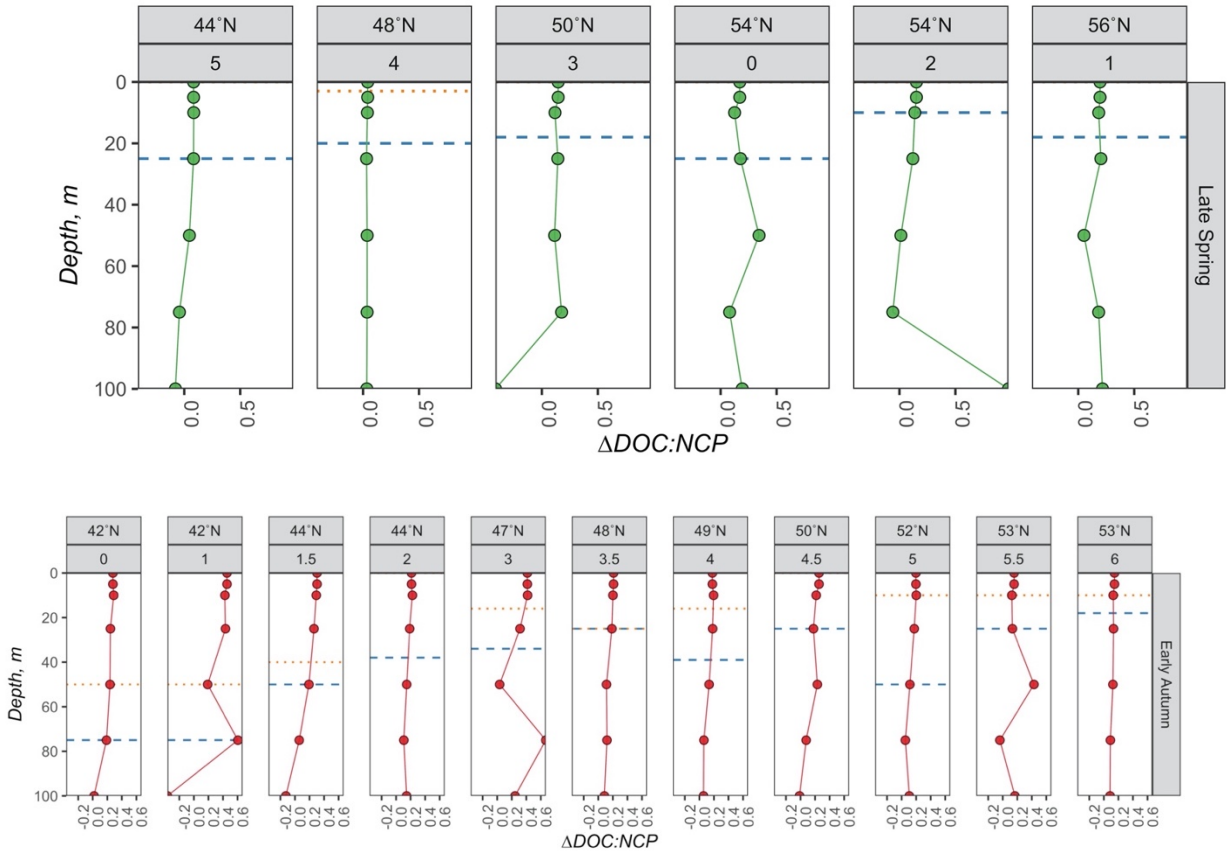

Appendix Figure 6. Δ*DOC:NCP* profiles for each station the late spring (top) and early autumn (bottom) campaigns. The upper label of each facet denotes the latitudinal bin in which the profile was observed and the lower label indicates the station number. Horizontal blue dashed lines indicate the depth of chlorophyll maximum (CM) and the horizontal orange dotted lines indicate the depth of the phytoplankton abundance maximum (PAM).

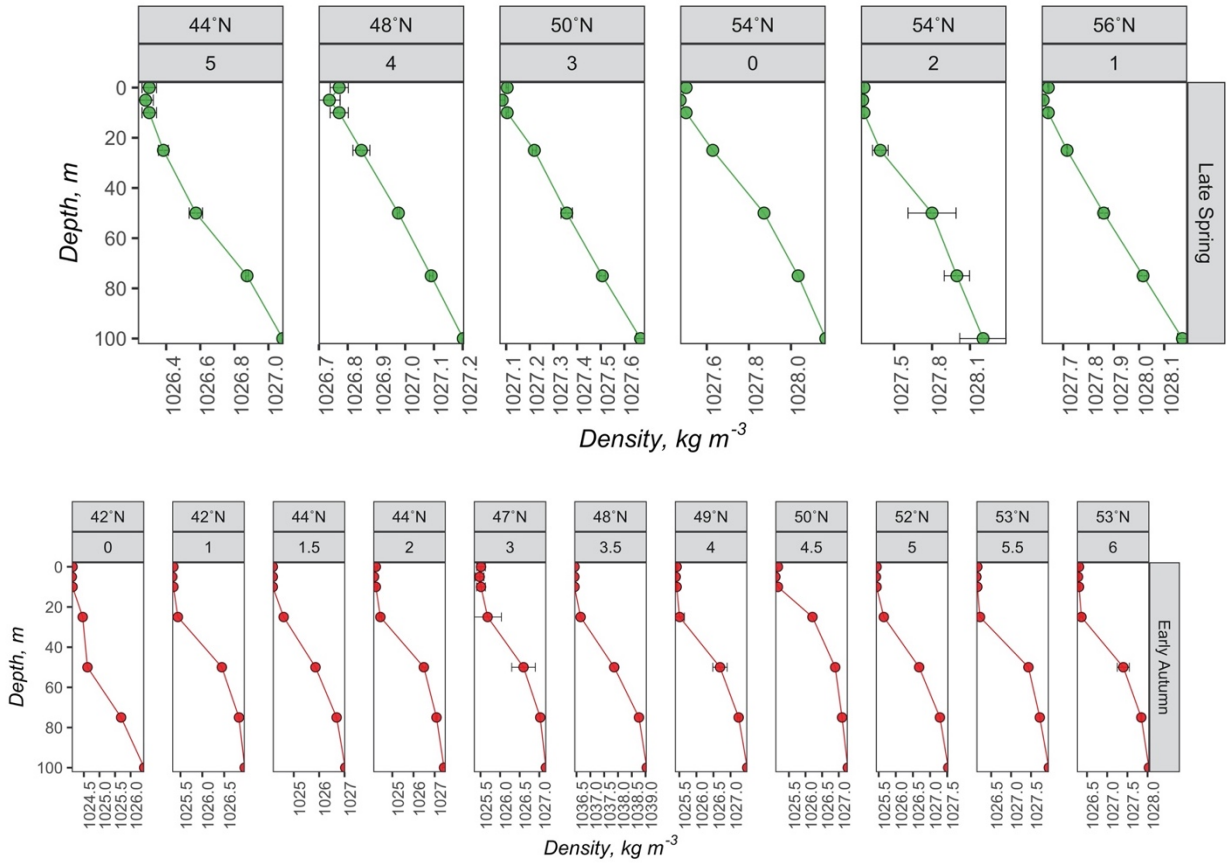

Appendix Figure 7. Density profiles for each station the late spring (top) and early autumn (bottom) campaigns. The upper label of each facet denotes the latitudinal bin in which the profile was observed and the lower label indicates the station number. Error bars indicate the standard deviations.

Comparisons of Derived Estimates with Publicly Available Datasets

Methods

NAAMES ARGO-based estimates of maximum mixed layers were contextualized with the mixed layer climatology and database described by Holte et al (2017), available online (http://mixedlayer.ucsd.edu). Maximum mixed layer climatology was restricted to the months of November to April, the months in which the NAAMES ARGO-based maximum mixed layers were observed (Table 1). Standard deviations of the climatological maximum mixed layers for those months provided insight into interannual variability of maximum MLD estimates.

The $NO_{3\ Mixed}$ and $SiO_{4\ Mixed}$ profiles as well as $\Delta NO_{3\ 100\ m}$ and $NCP_{100\ m}$ estimates were validated against constituent and climatological data provided by the freely available World Ocean Atlas 2018 (WOA18, https://www.nodc.noaa.gov/OC5/woa18/, last access: January 10, 2020) and the Global Ocean Data Analysis Project version 2 2019 (Gv2_2019, https://www.nodc.noaa.gov/ocads/oceans/GLODAPv2_2019/, last access: January 10, 2020) data products. Any wintertime (January-March) NO_3 and SiO_4 profiles from Gv2_2019 as well as constituent and climatological data from WOA18 (1˚ grid, statistical mean and objectively analyzed mean, respectively) that were co-located in the NAAMES study region were compared with the $NO_{3\ Mixed}$ and $SiO_{4\ Mixed}$ profiles generated in this study.

NO_3 and temperature climatology (objectively analyzed mean, 1˚ grid) from the WOA18 data product were used to calculate seasonal nitrate drawdown and subsequently NCP from the winter (January-March) to the spring (April-June) and summer (July-September). To do so, the temperature climatology was used to estimate a

mixed layer depth climatology using the Δ0.2˚C criteria defined by de Boyer Montégut et al (2004). Climatological winter nitrate concentrations over these mixed layer depths were assumed to be representative of the mixed NO_3 condition. Depth-integrated NO_3 drawdown (mol N m^{-2} t^{-1}) over the surface 100 m from the time of deep convection to the spring or summer were calculated for each 1˚ latitudinal bin within the NAAMES region using equation 2. Seasonal depth-integrated nitrate drawdown was then converted to seasonal depth-integrated NCP by employing the Redfield C:N ratio using equation 3.

Additionally, direct calculations of $NCP^{100\ m}$ were computed using TCO_2 and temperature data from GLODAPv2_2019 using the same approach described for the WOA18 climatological data.

Maximum Mixed Layer ARGO Climatology

ARGO-climatology maximum mixed layer depths between the months of November and April in the NAAMES study region were also shallower relative to $Z_{Max\ MLD}$, with monthly means ranging between 10 and 122 m and medians ranging between 10 and 108 m (Appendix Figure 2.10). Standard deviations around the ARGO-climatology monthly maximum mixed layer depths, an indication of interannual variability, ranged on average around 10 – 40 m, but could be as great as 336 m (Appendix Figure 2.10).

Mixed Conditions and NCP

Reconstructed mixed nitrate and silicate profiles were validated against profiles available from the GLODAPv2_2019 (Gv2_2019) data product as well as against constituent (statistical mean) and climatological (objectively analyzed mean) data from the World Ocean Atlas 2018 (WOA2018) data product. Mixed layer nitrate

concentrations from reconstructed profiles ($NO_{3\ Mixed}$) from the current study moderately but significantly correlated with those calculated from the Gv2_2019 and WOA18 data products. $NO_{3\ Mixed}$ values were, however, largely elevated, differing from the Gv2_2019 and WOA18 winter mixed layer concentrations by a mean of 31% (range 0.3 – 74%, median 29%, Appendix Figure 2.11). Similar results were attained for mixed layer silicate concentrations ($SiO_{4\ Mixed}$), with a mean and median observed difference of 43% and 18%, respectively (range 1 – 319%, Appendix Figure 2.11). The elevated $NO_{3\ Mixed}$ and $SiO_{4\ Mixed}$ concentrations in the reconstructed profiles likely reflects the predominantly deeper maximum mixed layers recorded by the NAAMES ARGO floats relative to both cruise and climatological datasets (Figure 2.2, Appendix Figure 2.10).

Comparison of seasonal NCP estimates between the NAAMES, Gv2_2019, and the WOA18 datasets reveals that the NAAMES estimates are generally elevated, with notable exceptions of estimates generated using Gv2_2019 TCO_2 data (Appendix Figure 2.12).

Discussion

We sought to compare $NO_{3\ Mixed}$ and $SiO_{4\ Mixed}$ concentrations in our reconstructed profiles against wintertime (January – March) data from two publicly available data products, the Global Ocean Data Analysis Project version 2 2019 (Gv2_2019) and the World Ocean Atlas 18 (WOA18). Unfortunately, these two data products contained limited wintertime data for the NAAMES study region. The Gv2_2019 data product, encompassing 840 scientific cruises in the global ocean between 1972 and 2019, only included two nutrient profiles within the NAAMES study region, one of which was omitted from the present analysis because it displayed a mixed layer uncharacteristic of deep convection (32 m)

(Olsen et al., 2016, Appendix Figure 2.8). The WOA18 statistical mean data product included just four nitrate values within the NAAMES study region, all of which were at 0 m (García-Martín et al., 2019). Because the WOA18 objectively analyzed climatology nitrate product for the NAAMES study region are interpolated based on these four nitrate values, conclusions drawn from comparisons with the WOA18 product should be taken with caution.

Mixed layer depths for both WOA18 data products were shallower relative to the maximum mixed layer depths estimated from the NAAMES ARGO floats (Appendix Figure 2.9), leading to lower wintertime mixed layer nutrient concentrations than those reported in this study. Seasonal NCP estimates calculated from WOA18 climatology-based nitrate drawdown were also reduced relative to those calculated using NAAMES data, likely due to differences in wintertime mixed layer depths (Appendix Figures 2.9, 2.10). Comparatively, a seasonal NCP estimate calculated from Gv2_2019 TCO_2 uptake was enhanced by as much as 456% relative to estimates calculated using both WOA18 and NAAMES data (Appendix Figure 2.12). While the reason for this discrepancy is unclear, the separation of time between the Gv2_2019 data used may play a role: winter TCO_2 profiles were taken in 2004 while the summer profiles were taken in 1972 and 1999. It is also possible that the NCP estimates based on nitrate drawdown are underestimates as the ratio of carbon and nitrogen fixation by autotrophs could be in excess of the Redfield ratio (Laws, 1991). Regardless, the lack of wintertime data and the relatively shallow winter mixed layer depths in both the Gv2_2019 and WOA18 data products for the NAAMES region are problematic to constraining the conditions under deep convection, rendering comparisons with this study's data equivocal.

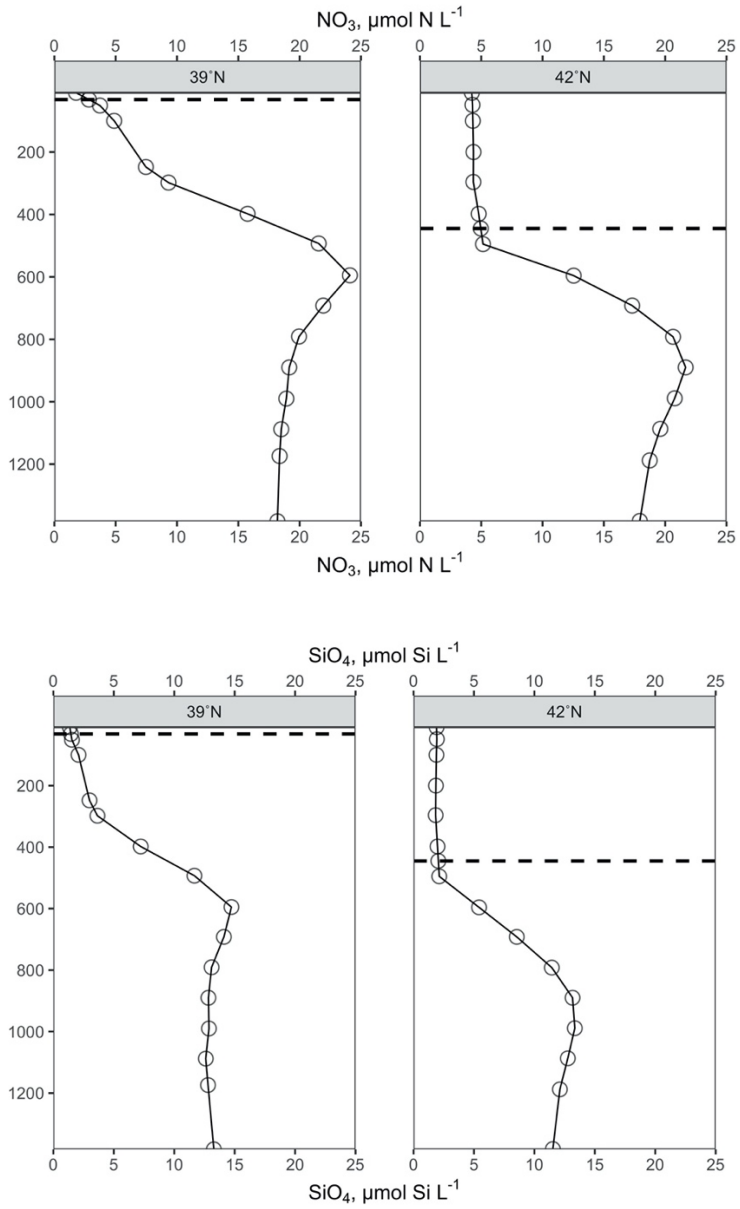

Appendix Figure 8. All Global Ocean Data Analysis Project (Gv2_2019) winter profiles of nitrate (top) and silicate (bottom) from the NAAMES region. The upper label of each facet denotes the latitudinal bin in which the profile was observed. Both profiles originated from a cruise conducted in 2004. Mixed layer depths were calculated to be 32 m and 445 m for the profile taken at 39˚N and the profile taken at 42˚N, respectively.

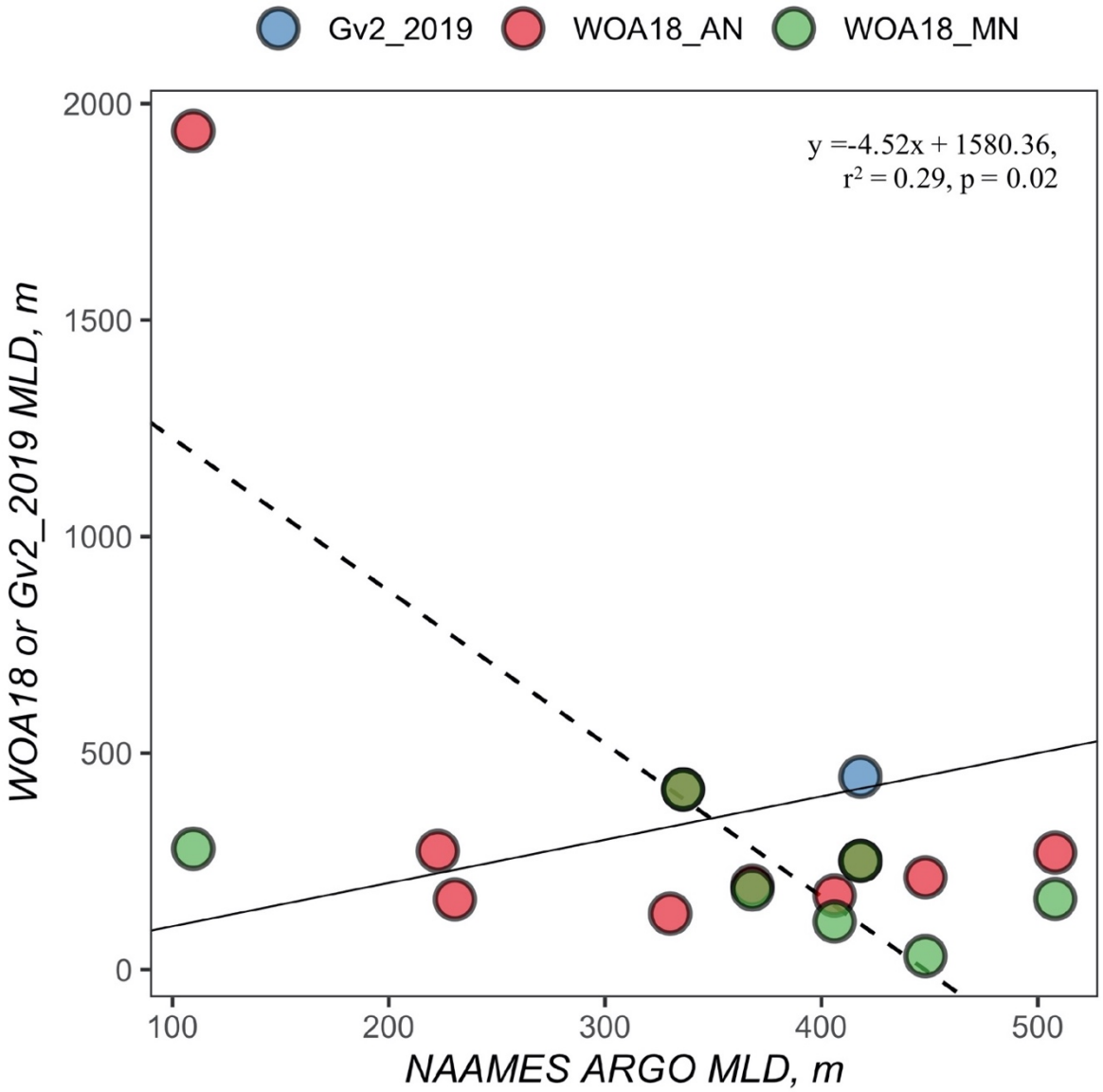

Appendix Figure 9. Standard major axis model II regression for NAAMES ARGO maximum mixed layer depths compared to winter mixed layer depths from the Global Ocean Data Analysis Project (Gv2_2019), the World Ocean Atlas 2018 constituent data (statistical mean, WOA18_AN), and the World Ocean Atlas 2018 climatological data (objectively analyzed mean, WOA18_MN). The solid black line indicates the 1:1 line.

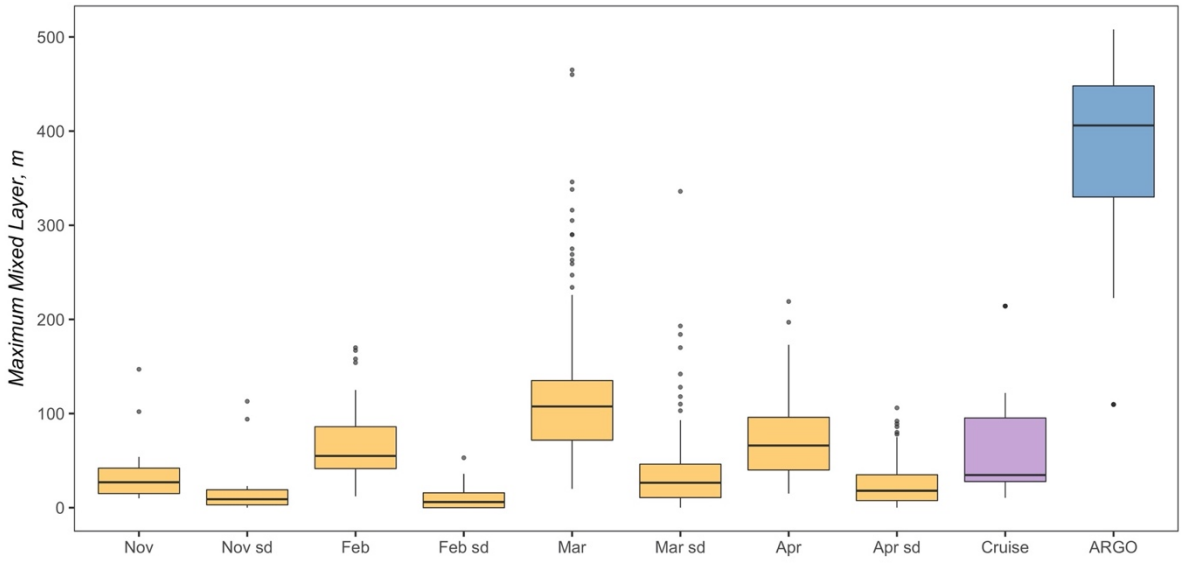

Appendix Figure 10. Box and whisker plots comparing maximum mixed layer depths estimated from ARGO climatological data (yellow), NAAMES cruise data (purple), and NAAMES ARGO data (blue).

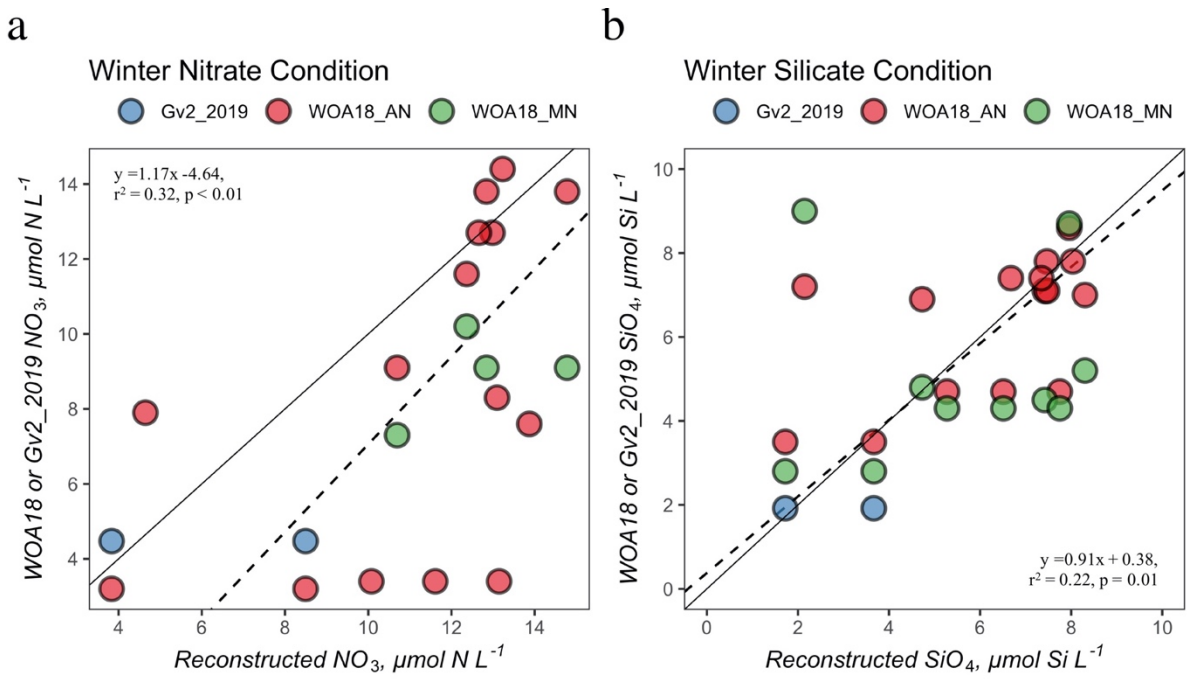

Appendix Figure 11. Standard major axis model II regression for NAAMES reconstructed mixed conditions compared to those estimated from the from the Global Ocean Data Analysis Project (Gv2_2019), the World Ocean Atlas 2018 constituent data (statistical mean, WOA18_AN), and the World Ocean Atlas 2018 climatological data (objectively analyzed mean, WOA18_MN). Solid black lines indicate the 1:1 line.

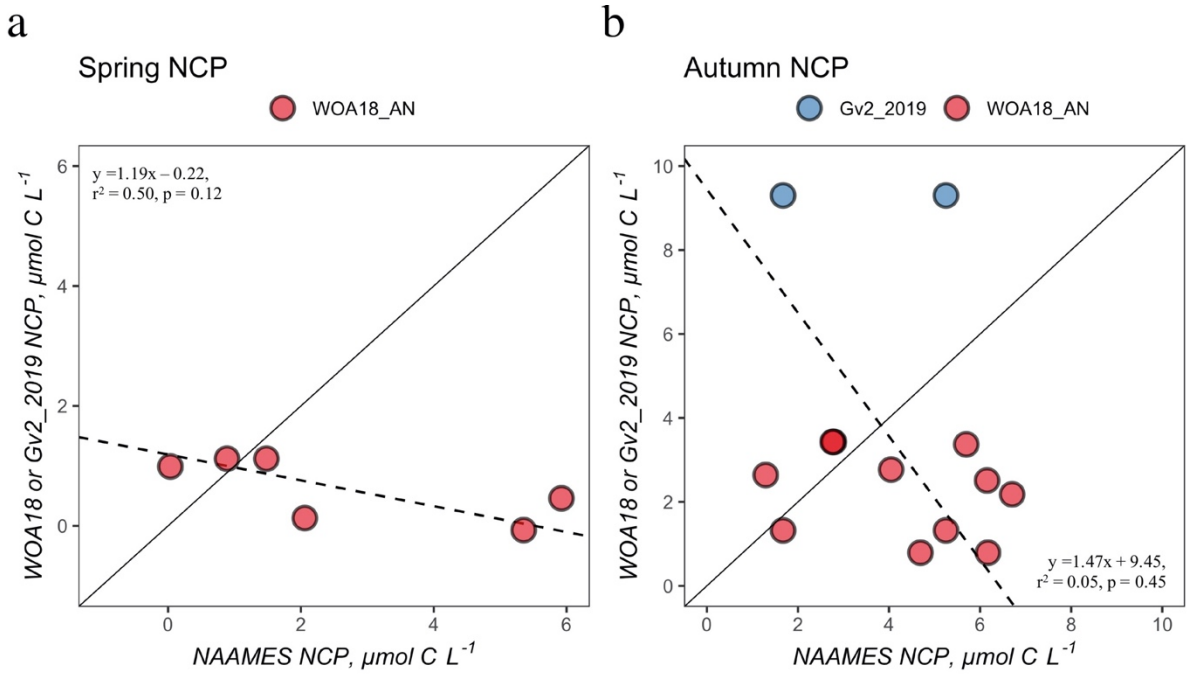

Appendix Figure 12. Standard major axis model II regression for NAAMES late spring and early autumn NCP estimates compared to those estimated using TCO_2 data from the Global Ocean Data Analysis Project (Gv2_2019) and nitrate data from the World Ocean Atlas 2018 constituent (statistical mean, WOA18_AN) dataset. Solid black lines indicate the 1:1 line.

III. The Seasonal Flux and Fate of Dissolved Organic Carbon through Bacterioplankton in the Western North Atlantic

Reprinted from: **N Baetge**, MJ Behrenfeld, J Fox, KH Halsey, KD Mojica, A Novoa. BM Stephens, CA Carlson. 2021. The Seasonal Flux and Fate of Dissolved Organic Carbon through Bacterioplankton in the Western North Atlantic. Frontiers in Microbiology. DOI: 10.3389/fmicb.2021.669883

Abstract

The oceans teem with heterotrophic bacterioplankton that play an appreciable role in the uptake of dissolved organic carbon (DOC) derived from phytoplankton net primary production (NPP). As such, bacterioplankton carbon demand (BCD), or gross heterotrophic production, represents a major carbon pathway that influences the seasonal accumulation of DOC in the surface ocean and subsequently, the potential vertical or horizontal export of seasonally accumulated DOC. Here, we examine the contributions of bacterioplankton and DOM to ecological and biogeochemical carbon flow pathways, including those of the microbial loop and the biological carbon pump, in the Western North Atlantic Ocean (~39 – 54˚N along ~40˚W) over a composite annual phytoplankton bloom cycle. Combining field observations with data collected from corresponding DOC remineralization experiments, we estimate the efficiency at which bacterioplankton utilize DOC, demonstrate seasonality in the fraction of NPP that supports BCD, and provide evidence for shifts in the bioavailability and persistence of the seasonally accumulated DOC. Our results indicate that while the portion of DOC flux through bacterioplankton relative to NPP increased as seasons transitioned from high to low productivity, there was a fraction of the DOM production that accumulated and persisted. This persistent DOM is potentially an important pool of organic

carbon available for export to the deep ocean via convective mixing; thus, representing an important export term of the biological carbon pump.

Introduction

Phytoplankton are prolific in the world's oceans and are recognized to be a critical source of fresh organic matter for marine food webs and subsequently play a key role in the biogeochemical cycling of elements. Despite representing less than 0.2% of Earth's photosynthetic biomass, marine phytoplankton have rapid turnover times and consequently are responsible for nearly half of the planet's annual net primary production (NPP), consuming CO_2 and elemental nutrients while generating oxygen and new organic matter (Field et al., 1998). The organic matter that is produced is partitioned as particulate organic matter (POM) and dissolved organic matter (DOM). This partitioning has a profound impact on the fate and contribution of organic matter to the biological carbon pump.

The biological carbon pump represents a combination of processes that spatially separate organic matter (particulate and dissolved) production from its remineralization (Passow and Carlson, 2012; Boyd et al., 2019), including the passive sinking flux of particulate organic matter (McCave, 1975), physical deep mixing of DOM (Copin-Montégut and Avril, 1993; Carlson et al., 1994) or suspended POM (Dall'Olmo et al., 2016; Lacour et al., 2019), and zooplankton-mediated transport by vertical migration (Steinberg et al., 2000). These three export pathways can transport organic carbon to depths where a portion remains sequestered from the atmosphere for decades to centuries (Ducklow et al., 2001b).

Food web processes that control the production of DOM include direct extracellular release by phytoplankton, viral-induced or auto-lysis of phytoplankton cells, grazing activity (i.e., sloppy feeding, excretion, and egestion by microzooplankton grazers), and

solubilization of organic particles (see review in Carlson and Hansell, 2015). Heterotrophic bacterioplankton production (BP) is the primary conduit for the uptake of bioavailable DOM and its passage to higher trophic levels or remineralization, processes key to defining the microbial loop as an important carbon-flow pathway that can modify the ocean carbon cycle (Azam et al., 1983; Azam, 1998).

The cumulative organic carbon flux through heterotrophic bacterioplankton, or gross bacterioplankton production [also termed bacterioplankton carbon demand (BCD)], can be estimated as the sum of net bacterioplankton production (BP) and the carbon that is respired as CO_2 (Del Giorgio and Cole, 1998; Ducklow et al., 2000; Carlson and Hansell, 2015). Comparing BCD to NPP provides a useful index for evaluating the degree to which NPP can support BCD (BCD:NPP) (Cole et al., 1988). Reported values of BCD:NPP have been as low as 0 (Pomeroy and Deibel, 1986; Pomeroy and Wiebe, 2001) and have also exceeded 1 (Duarte and Agustí, 1998; Hoppe et al., 2002). The BCD:NPP ratio is an important index that can be used to identify regions of net heterotrophy, where the net out-gassing of CO_2 can occur (Hoppe et al., 2002), and it can also serve as a harbinger of DOC accumulation on diel to seasonal time scales. For instance, the enhanced primary production during a phytoplankton bloom in the Antarctic Ross sea was matched by an increase in BCD, which limited DOC accumulation during the phase of the bloom when phytoplankton division outpaced loss rates (Carlson and Hansell, 2003). Conversely, over three bloom seasons in the Sargasso sea, nearly half of the seasonally-produced DOC escaped rapid microbial degradation (i.e. low BCD:NPP), resulting in DOC accumulation (Carlson et al., 1998).

The condition where BCD:NPP is low (i.e., DOC consumption is unable to match the rate of DOC release) has been termed the “malfunctioning microbial loop” (Thingstad et al.,

1997). This ‘malfunctioning’ can arise for a number of reasons. It can result from phytoplankton growth exceeding the metabolic capacity of heterotrophic consumption (Ducklow et al., 1993), the production of recalcitrant compounds (Aluwihare et al., 1997) or precursors to recalcitrant compounds (Arakawa et al., 2017), or the inability of a bacterioplankton assemblage to grow on specific types of organic matter due to community composition or gene expression (Teeling et al., 2012). It can also result from bacterioplankton-phytoplankton competition leading to nutrient limitation on BCD (Zweifel et al., 1995; Cotner et al., 1997; Church, 2008) or from predation limiting bacterioplankton production (Thingstad et al., 1997). It is also possible that BCD may more closely track grazer or viral-mediated release of DOM instead of instantaneous phytoplankton production (Kirchman et al., 1994). Lastly, some BCD may be supported by volatile organic compounds which are not captured in estimates of NPP measured by contemporary methods (Davie-Martin et al., 2020; Moore et al., 2020). A disconnect between BCD and NPP can arise from the combined effects of any or all of these mechanisms and can lead to the seasonal accumulation of DOC in the surface waters; i.e., the accumulation of DOC in the euphotic zone that is greater than the annual minimum concentration observed during deep winter mixing. If the fraction of accumulated DOC that is produced as, or transformed into, recalcitrant compounds persists long enough to be vertically exported to depth during the next winter’s convective mixing event, it can represent an important pathway of the biological carbon pump in systems that experience deep convective mixing or subduction (Carlson et al., 1994).

The Western North Atlantic Ocean is a region characterized by both massive seasonal phytoplankton blooms (Behrenfeld, 2010) and deep convective overturning events that can

physically deliver dissolved and suspended organic matter to depth (Carlson et al., 1994; Dall'Olmo et al., 2016; Baetge et al., 2020). The bloom conditions in the Western North Atlantic provide an ideal system to explore the cumulative influence of microbial processes on the accumulation, bioavailability, and persistence of DOC, and ultimately, on the biogeochemical role of DOC in the biological carbon pump. Here we present data collected over a seasonal cycle as a part of the NASA North Atlantic Aerosols and Marine Ecosystems Study (NAAMES). We combined observations from *in situ* bacterioplankton measurements and experimental DOC remineralization experiments with estimates of NCP partitioned as DOC (Baetge et al., 2020): (1) examine the efficiency at which bacterioplankton use DOC, (2) examine seasonal variability in the fraction of NPP supporting BCD, (3) assess the bioavailability of the seasonally accumulated DOC, and (4) evaluate how export potential of seasonally accumulated DOC varies over a bloom cycle in the Western North Atlantic.

Materials and Methods

Study Region

The NAAMES program, detailed in Behrenfeld et al (2019), was comprised of four field campaigns in the Western North Atlantic involving ship transects between 39˚N and 56˚N latitude and -38˚W to -47˚W longitude all aboard the R/V *Atlantis*. NAAMES was designed to resolve the dynamics and drivers of the annual phytoplankton bloom and their subsequent impacts on the atmosphere. Each cruise accordingly took place at a different time of the year at four different phases of the annual phytoplankton bloom cycle. NAAMES 1 occurred in the early winter ("winter transition": November - December 2015), NAAMES 2 in the late spring ("climax transition": May 2016), NAAMES 3 in the early autumn

("depletion phase": September 2017), and NAAMES 4 in the early spring ("accumulation phase": April 2018). Station locations for all cruises are overlayed on a map of 8-day composite chlorophyll data from NASA's Moderate Imaging Spectroradiometer (MODIS) collected during May 2016 (Figure 3.1). These data (ID: erdMH1chla8day) were retrieved from NOAA's ERDDAP servers (https://upwell.pfeg.noaa.gov/erddap/info/erdMH1chla8day/index.html) using the package *rerddap* (v 0.7.4) in R (v.0.4.0).

In situ Environmental Data

All processed data, analyses, and code presented here are available on GitHub (https://github.com/nbaetge/naames_bioav_ms). NAAMES field cruise data are available through NASA's SeaWiFS Bio-optical Archive and Storage System (SeaBASS; https://seabass.gsfc.nasa.gov/naames) and the Biological & Chemical Oceanography Data Management Office (BCO-DMO, DOI: 10.26008/1912/bco-dmo.824623.1). All seawater samples were collected on the R/V *Atlantis* from 24 10-L Niskin bottles affixed to a Sea-Bird Scientific SBE-911+ Conductivity-Temperature-Depth rosette.

Bacterioplankton Abundance

BA (cells L^{-1}) were determined over 4 – 8 depths throughout the euphotic zone, which ranged from 52 m to 236 m. Cells were enumerated via flow cytometry on NAAMES 1 and via epifluorescence microscopy on the remaining cruises. Whole seawater was collected into sterile conical centrifuge tubes. Flow cytometry samples (2 mL) were preserved with 40 µL of 8% paraformaldehyde (Electron Microscopy Sciences) added to each sample to a final concentration of 0.2%. Samples were then mixed by inversion, flash frozen with liquid nitrogen, and stored at -80˚C until analysis (Halewood et al., 2012). Microscopy samples

were preserved with certified ACS formalin to a final concentration of 1% (vol:vol) and stored at 4˚C until slide preparation within 36 hours of collection. These preserved samples were filtered under gentle vacuum (~34 kPa) onto 25 mm 0.2 µm polycarbonate (PC) membrane filters stained with Acid Black 107 (Irgalan Black) (Hobbie et al., 1977). Cells were stained with 4',6-diamidino-2-phenylindole dihydrochloride (5 mg mL^{-1}, DAPI) under minimal lighting according to Porter and Feig (1980). Filters were mounted onto slides with high viscosity immersion oil (Thermo Scientific Richard-Allan Scientific Resolve) and stored at –20˚C until enumeration at sea and at a shore-based laboratory. An Olympus BX51epifluorescence microscope with ultraviolet excitation at 1000X magnification was used to enumerate bacterioplankton cell abundances following Parsons et al. (2012). Briefly, 12 fields-of-view were counted for each slide and, on average, 50-60 cells were counted for each field-of-view.

Flow cytometry was performed following Halewood et al (2012) using an LSR II equipped with a 488 nm blue laser and a high throughput sampler (Becton Dickinson (BD) Biosciences). Upon analysis, the LSR II was prepared according to the manufacturer's guidelines. Spherotech Rainbow calibration beads (RCP-30-5) were used according to manufacturer's recommendations to diagnose cytometer laser detection performance. Samples were processed in batches of 45, which were thawed, vortexed, transferred to a 96-well plate and stained with SYBR-Green (100x dilution of commercial stock, Molecular Probes, Inc.) to a final concentration of 1:10,000 (vol:vol). To ensure complete staining of bacterioplankton cells, the plate was incubated for 15-30 minutes in darkness prior to analysis on the LSR II. Each well was analyzed for up to 90 seconds, with the minimum green FITC (fluorescin isothiocyanate) threshold set to 200 nm. The population of

bacterioplankton cells (events) on the flow cytograms was interactively defined with a gate based on the relationship between side-scatter and FITC fluorescence using FACSDiva software (BD Biosciences). Bacterioplankton abundance was calculated from the volume analyzed and the number of events in the gate. Internal references, consisting of a 5-point serial dilution (dilution factor of 0.5) of surface Santa Barbara Channel seawater, were used to diagnose machine performance prior to staining NAAMES samples. This dilution series was prepared using whole seawater and 0.2 µm filtrate and each dilution was enumerated via both flow cytometry and microscopy at the time of preparation, Several hundred 2 mL aliquots of the dilution series were fixed with 40 µl 8% paraformaldehyde and frozen at -80˚C. Enumeration of these archived samples provided a means to assess daily machine performance such that large deviations between cell counts of original and archived samples indicated potential issues with machine fluidics or lasers. The slope (0.8) between the flow cytometry counts of these internal references at the time of sample analysis and the corresponding microscopy counts attained at the time of collection were used as a correction factor to align counts from the two enumeration methods. BA was integrated and normalized to the depth of the euphotic zone (i.e., 1% light level) for each station to obtain mean volumetric values.

Net Bacterioplankton Production

Net BP rates were estimated by ^{3}H-leucine (^{3}H-Leu) incorporation using a modified version of the microcentrifuge method (Smith and Azam, 1992). For each depth, a killed control (killed immediately with 100 µL of 100% TCA) and replicate 1.6 mL seawater samples were spiked with ^{3}H-Leu (20 nM; specific activity 50.2-52.6 Ci/mmol; Perkin Elmer, Boston, MA) and incubated for 2-3 h in the dark at ± 2°C of *in situ* temperature.

Incubations were terminated by adding 100 µL of cold 100% trichloroacetic acid (TCA) and were subsequently spun on a microcentrifuge at 20,800 g for 7 min. Supernatant from each incubation tube was decanted, leaving a pellet that was then resuspended in 1.6 mL of 5% TCA. A second 7 min centrifugation step was performed, the supernatant again decanted, the remaining pellet resuspended in 1.6 mL of 80% ethanol (vol/vol), and centrifuged a final time as described in Ducklow et al. (2001a). Ethanol was decanted and 1.6 mL of Ultima Gold scintillation cocktail added to each tube. Radioactivity was measured using a Hidex 300 Scintillation Analyzer and was corrected for quenching using an external gamma source and a quench curve. The coefficient of variation (CV) of assays performed following this protocol were generally 1-15% for replicate incubations, however the deep samples generally had lower incorporation rates and CVs were often between 20-30%. ^{3}H-Leu incorporation rates were converted to carbon units (µmol C L^{-1} d^{-1}) using a conversion factor of 1.5 kg C (mol leucine incorporated)$^{-1}$ (Simon and Azam, 1989). BP was integrated and normalized to the depth of the euphotic zone for each station to obtain mean volumetric values.

Net Primary Production

NPP values (µmol C L^{-1} d^{-1}) were determined using the Photoacclimation Productivity Model (PPM) as reported in Fox et al (2020). The PPM is based on quantitative understanding of shifts in phytoplankton chlorophyll synthesis in response to available light and nutrients (Behrenfeld et al., 2016). These photoacclimation responses were used to estimate depth-resolved phytoplankton growth rates and NPP at each NAAMES station. The PPM results exhibited strong agreement with 24 h ^{14}C-uptake measurements of NPP determined at all stations occupied during the NAAMES campaign (Fox et al., 2020). NPP was integrated and

normalized to the depth of the euphotic zone for each station to obtain mean volumetric rate values.

DOC Remineralization Experiments

At each station, experiments were conducted to determine the magnitude and rate of DOC remineralization using water collected from within the surface 10 m (see Figure 3.2 for experimental design and sampling scheme). Data from DOC remineralization experiments are available from BCO-DMO (DOI: 10.26008/1912/bco-dmo.824623.1). Water was gently gravity-filtered through 142 mm PC filtration cartridges (Geotech Environmental Equipment, Inc.) loaded with either a 1.2- or a 0.2-µm mixed cellulose ester membrane filter (EMD Millipore). The 1.2 µm filtrate was retained as a bacterioplankton inoculum and the 0.2 µm fraction was retained as particle-free media. The 1.2 µm filtrate retained on average 78 ± 16% of the bacterioplankton population in whole seawater (Appendix Table 3.1). When possible, the filter cartridge was attached directly to Niskin bottles with platinum-cured silicone tubing and the filtrate was collected into PC carboys. Otherwise, unfiltered water from the Niskin was first drawn into an acid-washed (10% HCl) and sample-rinsed PC carboy and then filtered into another acid-washed and sample-rinsed PC carboy. Each experiment was initiated by combining the 1.2 µm filtrate (inoculum) with the 0.2 µm filtrate at a 3:7 ratio. A pair of acid-washed PC incubation bottles (modified 5 L Nalgene Biotainer, Appendix) were then rinsed with this water and subsequently filled. All carboys, tubing, and filtration rigs were rinsed with 10% HCl, then with Nanopure water, and finally with sample water three times before use. Membrane filters were flushed with a minimum of 1 L of Nanopure water followed by 0.5 L of sample water prior to collecting filtrate to minimize DOC leaching from the filters.

Experiments incubated in the dark and within ± 1.5°C of *in situ* temperatures using refrigerated incubators (Fisherbrand Isotemp BOD). On NAAMES cruises 3 and 4, pre-combusted (4 hours at 450˚C) 40 mL and 60 mL borosilicate glass incubation vials (Thermo Scientific) were also rinsed and filled with initial incubation water and served as parallel incubations to monitor changes in organic carbon. After returning to port, the vials were shipped overnight in coolers to UC Santa Barbara, transferred to incubators at *in situ* temperatures, and periodically sampled for up to 110 days (T_{End}) after the initiation of the experiment.

Throughout the duration of each experiment, samples for BA, bacterioplankton organic carbon (BOC), total organic carbon (TOC), and dissolved organic carbon (DOC), were collected using positive pressure displacement system (Supplementary Material; Liu et al., 2020). While at sea, Bacterioplankton abundance samples were monitored daily, BOC samples were collected at the initiation time for each experiment (T_0) and during the stationary phase ($T_{Stationary}$) of the bacterioplankton growth curve, and TOC and DOC samples were collected three to six times within the first 14 days. DOC samples were also collected after returning to port from NAAMES 2 and 4 at the one-, two-, and three-month marks. TOC samples were collected at the one-, two-month marks after returning to port from NAAMES 3 and after the one-, two-, and three- month marks after NAAMES 4. Bacterioplankton abundance and BOC were not collected after returning to port from the different cruises.

For each experiment, BOC samples were collected from the 1.2 µm filtrate (inoculum) at T_0 and from each incubation bottle at $T_{Stationary}$ of the bacterioplankton growth curve. T_0 BOC samples were collected from the 1.2 µm filtrate instead of from the mixed

experimental water (3:7 inoculum: particle free water) to ensure that enough cellular material was collected for later CHN analysis, described below. Thus, T_0 BOC in the incubation bottles was estimated as 30% of the BOC measured from the 1.2 µm filtrate. For each BOC sample, one liter of seawater was drawn from a Biotainer and filtered through a polypropylene inline filter cartridge (Cole-Parmer) loaded with two combusted Advantec Grade 25 mm 0.3 µm glass fiber filters (GF75) (Stephens et al., 2020). Two filters were used to increase cell retention (mean 78 ± 9%). Each filter was folded twice, with the sample material on the inside, placed into separate pre-combusted (450˚C for 4 h) 20 mL borosilicate glass vials (Wheaton) and frozen at -20˚C. Filters were analyzed on a Costech ECS 4010 CHNS-O elemental analyzer by Bigelow Analytical Services, which has a detection limit of 0.1 µg C (Bigelow Laboratory for Ocean Sciences, Maine). At each station of NAAMES 2 and 4, 1 L of either 0.2 µm or 30 kDa tangential flow filtration (TFF, EMD Millipore) 10 m seawater filtrate was also filtered through a pair of stacked GF75s. The TFF filtrate did not contain any particles greater than 30kDa; thus, any organic matter retained on the GF75 filter after passing 1 L of TFF filtrate through it was considered absorbed DOC. There was no significant difference between absorbed DOC estimates from filters treated with 0.2 µm or 30 kDa TFF seawater (Wilcoxon $p = 0.1$). The average absorbed DOC estimate, 2.7 µg, was used as a universal blank. For reference, the average carbon value on the second (i.e., bottom) GF75 filter of the experimental samples was 5.1 ± 3.5 µg, indicating the utility of using two GF75 filters to increase the retention of cell carbon.

Both a filtered DOC and a TOC sample, were collected to monitor changes in organic carbon over the course of each experiment. TOC samples were corrected by the contribution of BOC at T_0 and $T_{Stationary}$, hereafter referred to as DOC* (Stephens et al., 2020; Wear et al.,

2020). BA was observed to fall to low densities by T_{End} (Appendix Figure 3.1) so we considered TOC and DOC to be interchangeable by T_{End}. In the absence of BOC collections after $T_{Stationary}$, we did not calculate DOC* at T_{End} because doing so may have artificially enhanced estimates of DOC removal. On NAAMES 2, filtered DOC samples were displaced by positive pressure from each 5 L Biotainer through an inline set of two pre-combusted GF75 filters and into two pre-combusted 40 mL borosilicate glass vials. The collected volume was then immediately fixed by adding 50 µL of DOC-free 4N HCl to a pH of ~3. We observed relatively clean sampling of DOC filtered directly from the Biotainers during NAAMES, but also found greater variability in the temporal trends of DOC concentration when the incubation water volume was less than half of the original incubation volume, after large volumes were removed for DNA and BOC samples at $T_{Stationary}$ (Appendix Figure 3.2). In order to address this issue and reduce potential contamination by handling on subsequent cruises (NAAMES 3 and 4), parallel 40 and 60-mL borosilicate glass incubation vials were added to monitor changes in bulk TOC and DOC. Not only did the adoption of these vials help address potential contamination from handling, it also permitted the long-term monitoring of DOC removal as vials were sampled periodically until T_{End} (Stephens et al., 2020). A direct comparison conducted on both NAAMES 3 and 4 indicated that the filtered DOC concentrations and corresponding DOC* estimates were within 10% of one another, with a systematic positive bias of the filtered DOC measurements relative to DOC* (Appendix Figure 3.3). On NAAMES 4, bacterioplankton abundance and DOC estimates from the large-volume Biotainer and the parallel vials at corresponding timepoints were within 7% and 5% of one another, respectively, indicating that both incubation containers tracked similar microbial dynamics

(Appendix Figure 3.4). Thus, all analyses described below used filtered DOC for NAAMES 2 experiments and DOC* for NAAMES 3 and 4 experiments.

Organic carbon concentrations were determined via the high temperature combustion method using modified Shimadzu TOC-V or TOC-L analyzers as described in Carlson et al. (2010). Concentrations were quantified using standard solutions of glucose and ultra-pure (low carbon) water. All samples were systematically referenced against surface (5m) and deep (<2000 m) Atlantic seawater that were calibrated against consensus reference material (Hansell SSR Lot#08-18) and run every 6 - 8 samples (Hansell and Carlson, 1998b). Typical run sizes were kept under 35 samples to reduce salt accumulation and instrument drift. The precision of the Shimadzu analyzers for surface samples was within 2% CV.

Calculations of Derived Variables

Seasonally Accumulated DOC Bioavailability and Persistence

The microbial dynamics and DOC bioavailability detailed in this manuscript are placed in the context of seasonally accumulated DOM for each station and cruise. The magnitude of DOC that accumulated in excess of the annual DOC minimum that corresponded to the maximal deep winter mixing was determined for each station and is referred to as seasonally accumulated DOC (DOC_{SA}). The annual DOC minimum was approximated for each 1˚ latitudinal bin of the NAAMES study region according to and as reported by Baetge et al (2020). Briefly, observed profiles of DOC concentration at each station were redistributed over their corresponding local maximum MLD that were retrieved from ARGO float observations between 5 May 2014 and 2 December 2018 (Table 3.1). For each DOC remineralization bioassay, DOC_{SA}, μmol C L^{-1} was then calculated as the difference between the initial DOC concentration and the annual DOC minimum. Bioavailable DOC (ΔDOC) for

each DOC remineralization experiment was calculated as the total removal of DOC_{SA} over the short-term ($T_0 - T_{Stationary}$) and long-term ($T_0 - T_{End}$), expressed as both concentration (μmol C L^{-1}) and percentage of initial DOC_{SA}. ΔDOC removal rates (μmol C L^{-1} d^{-1}) for the DOC remineralization experiments were calculated as ΔDOC divided by the number of elapsed days. DOC_{SA} that persists was calculated as concentration (μmol C L^{-1}) and percent of DOC_{SA} remaining at T_{End}. It is important to note that DOC_{SA} may be comprised of DOC compounds that had accumulated in previous seasons. Thus, DOC removal observed in the early autumn experiments may have reflected the removal of DOC that had accumulated earlier in the spring, not necessarily solely DOC produced in the autumn.

Bacterioplankton Growth Efficiencies

Bacterioplankton growth efficiency was determined by assessing changes in BOC from T_0 to $T_{Stationary}$ relative to the drawdown of DOC over the same time frame in each DOC remineralization experiment. Bacterioplankton growth efficiency (BGE) was determined by the following equation:

$$\mathrm{BGE} = \frac{\mathrm{BOC_{Stationary}} - \mathrm{BOC_{Initial}}}{\mathrm{DOC_{Initial}} - \mathrm{DOC_{Stationary}}} \quad (1)$$

where the difference in BOC between the T_0 and $T_{Stationary}$ (ΔBOC) was calculated as the change in the total carbon concentration captured on the GF75 filters divided by the simultaneous change in DOC or DOC* (ΔDOC). The change in BOC (ΔBOC) was not calculated for experiments conducted at Station 3 in the late spring because of a lack of a BOC sample at $T_{Stationary}$. BGEs are highly sensitive to changes in DOC and can be artificially inflated when ΔDOC is small, thus we chose to be conservative by only calculating BGEs for experiments where the removal of DOC was greater or equal to 2 μmol C L^{-1}.

Bacterioplankton Carbon Demand

For each cruise, BCD (μmol C L^{-1} d^{-1}) was calculated as integrated, depth-normalized *in situ* BP divided by the campaign-wide mean BGE (0.26) calculated from all cruises. The fraction of *in situ* NPP that can potentially support *in situ* BCD is expressed as BCD:NPP.

Statistics

All statistical analyses were performed using packages in R (v 4.0.0). Bland-Altman/Tukey Mean-Difference) analyses were used to assess the agreement between corresponding experimental measurements of DOC and DOC* as well as the dynamics between experimental incubation containers. Agreement statistics were computed using the function *blandr.statistics* from the package *blandr* (v 0.5.1). The correlation between these measurements was also evaluated using standardized (reduced) major axis model II linear regressions. Standardized (reduced) major axis model II linear regressions were also used to explore the relationship between BCD and NPP. Regressions were computed using the function *lmodel2* from the package *lmodel2* (v 1.7-3). Model fits with *p*-values > 0.05, ≤ 0.05, or ≤ 0.01 are described as 'not significant', 'significant' and 'highly significant', respectively.

A non-parametric Kruskal-Wallis test (one-way ANOVA on ranks) was performed on each bacterioplankton growth metric, as well as on NPP, to assess if means across all seasons were equivalent. If they were not equivalent, a non-parametric Wilcoxon tests was then performed *post hoc* to assess whether means between two seasons were equal. Kruskal-Wallis and Wilcoxon tests were both performed using the *compare_means* function in the package *ggpubr* (v 0.3.0). For both tests, group means that were likely equal, significantly

different, or highly significantly different are indicated by p-values > 0.05, ≤ 0.05 to 0.01, and ≤ 0.01, respectively.

Results

Bacterioplankton and DOM Dynamics in the Remineralization Experiments

Bacterioplankton generally followed the logistic model of growth (Figure 3.3a). While bacterioplankton cell production was highly variable within each season, the general trend indicated a greater change in cell abundance in late spring relative to the other seasons. It is notable, however, that the change in BOC measured from $T_0 - T_{Stationary}$ was not statistically different between seasons (Table 1, $p = 0.44$). This may result from differences in cell size (not measured) or carbon per cell between different seasons.

DOC remineralization was also variable within each season and between seasons (Figure 3.3b). Total short-term DOC removal, between T_0 and $T_{Stationary}$ (5 – 10 days of incubation) in each experiment, was limited to a range of 2.1 – 4.3 μmol C L^{-1} across all seasons (Figure 3.3b), with no statistical difference in the mean magnitude of DOC removed between seasons (Figure 3.3b, Table 3.1, Kruskal-Wallis $p = 0.13$).

The Bioavailable Fraction of Seasonally Accumulated DOC from DOC Remineralization Experiments

On average, the magnitude of DOC above annual surface minimum DOC concentration (i.e., DOC_{SA}) increased as stratification of the water column intensified from the early spring (2.9 ± 1.4 μmol C L^{-1}), to late spring (6.3 ± 2.9 μmol C L^{-1}), and to early autumn (13.3 ± 3.6 μmol C L^{-1}) (Table 3.1). Here, we used the DOC removal from remineralization experiments to assess the bioavailable fraction of this surface accumulated pool (ΔDOC, Figure 3.3b). Over the spatial extent of the NAAMES study region and the

temporal period between the early spring and early winter, the magnitude of short-term ΔDOC (i.e., short-term DOC removal within 10 days) lacked any clear seasonal trends, as noted above. Latitudinal trends in short-term ΔDOC were also absent within individual seasons (Kruskal-Wallis $p = 0.22$ [early spring], $p = 0.68$ [late spring], $p = 0.19$ [early autumn]). Long-term ΔDOC ($T_0 - T_{End}$, 13 – 110 days) for the spring averaged 3.4 ± 0.9 and 4.8 ± 1.0 μmol C L^{-1} for early autumn (Table 3.1). The long-term ΔDOC was not significantly different from spring to autumn; however, there were large seasonal differences in proportion of the ΔDOC relative to the amount of accumulated DOC ($\Delta DOC:DOC_{SA}$). ΔDOC in the short-term was greatest in the early spring, representing on average 211 ± 197% of the DOC_{SA} pool, before decreasing to 50 ± 24% in the late spring and then to 29 ± 10% in the early autumn. Over the long-term, a similar trend was observed in the incubations whereby the percentage of DOC_{SA} that was bioavailable was greatest in early spring (>140%) and lowest (~40%) in early autumn (Table 3.1). ΔDOC greater than 100% in our experiments indicated that the responding heterotrophic bacterioplankton community was not only able to degrade all of DOC_{SA}, but was also able to remove some fraction of the presumably lower quality background DOC pool represented by the annual DOC minimum. It should also be noted that, DOC contamination during post-cruise sampling in several of the late spring (NAAMES 2) experiments precluded accurate resolution of long-term DOC removal in four of the six sets of experiments for that cruise (Table 3.1). The source of DOC contamination in the long-term incubations remains unclear but may be related to the increase in container surface area to seawater volume ratio as incubation volume was drawn below 50% of initial volume (Appendix Figure 3.2). Regardless, the trend of decreasing $\Delta DOC:DOC_{SA}$ from the early spring to the early autumn

is evident from both the short-term and long-term estimates of DOC removal within the remineralization experiments.

The seasonal progression of the relative percentage of DOC_{SA} that was bioavailable or that persisted was best exemplified at latitude 44°N, which was occupied for each of the early spring, late spring, and early autumn cruises (Figure 3.4). The initial condition of these experiments demonstrates the increasing magnitude of the total DOC_{SA} pool as well as the ΔDOC fraction from spring to early autumn. As described above, however, the relative contribution of ΔDOC was greatest in early spring and decreased by late spring and early autumn. Conversely, the fraction of the DOC_{SA} pool persisting after ~ 60 days increased from spring to early autumn. In many cases, all of the DOC_{SA} determined in the spring was bioavailable on the time scales of the remineralization experiment, whereas up to 73% of the DOC_{SA} pool determined for early autumn persisted over the experimental incubation period. (Table 3.1).

Bacterioplankton Growth Efficiencies

The ratio of the change in BOC from T_0 to $T_{Stationary}$ to the corresponding change in DOC over the time frame of the short-term incubations was used to derive estimates of bacterioplankton growth efficiencies (BGE) for each experiment (Figure 3.5, Table 3.1). Although there was considerable variability in BGE within and between seasons, ranging from 0.13 to 0.52 with a mean of 0.26, no significant difference in BGE was found between seasons (Kruskal-Wallis $p = 0.37$) or latitudinal range (Kruskal-Wallis $p = 0.15$).

In Situ Net Primary Production and in situ Bacterioplankton Growth Metrics

Average net primary production rates estimated over the euphotic zone, ranged from 0.11 – 3.34 μmol C L^{-1} d^{-1} and declined significantly from late spring to early winter (Figure

3.6, Table 3.2). Metrics of bacterioplankton abundance and production over the euphotic zone demonstrated similar seasonal trends, such that the range of variability and the magnitude of rates or cell densities were greatest in late spring and lowest in autumn/winter. Significant temporal differences in each of the bacterioplankton growth metrics were primarily driven by the decline of those parameters from the spring to the early autumn. Bacterioplankton abundance ranged from $3.04 \times 10^8 - 2.12 \times 10^9$ cells L^{-1}, increasing from the early to late spring before decreasing in early autumn (Figure 3.6). Net BP, ranging from 0.015 – 0.155 μmol C L^{-1} d^{-1}, never exceeded NPP and overall net BP represented 3 – 25% of NPP (Figure 3.6, Table 3.2).

BCD was calculated for each station by dividing measurements of net bacterioplankton production by the campaign-wide mean BGE of 0.26. The seasonal change in the magnitude of BCD rates exhibited similar patterns as NPP where rates were greatest and most variable in the spring compared to autumn/winter (Table 3.2, Figure 3.7, 3.8). BCD ranged from 0.06 – 0.60 μmol C L^{-1} d^{-1} and never exceeded NPP (0.11 – 3.34 μmol C L^{-1} d^{-1}). However, BCD:NPP significantly differed between seasons (Kruskal-Wallis $p < 0.01$), being driven by significant decreases from the maximum of 70 ± 14% in early winter to 19 ± 5% in early spring (Wilcoxon $p = 0.05$) and to 22 ± 10% in the late spring (Wilcoxon $p = 0.01$).

Discussion

This work evaluates both the ecological and biogeochemical contribution of DOM over the progression of a composite annual phytoplankton bloom cycle in the Western North Atlantic. Of ecological interest is the instantaneous flux and fate of the most labile constituents of DOM through the bacterioplankton community, whether incorporated into

new biomass with potential for trophic transfer or respired into inorganic constituents. Of biogeochemical interest is the portion of DOM that is produced as or transformed into more recalcitrant compounds that can persist and potentially be exported via mixing or subduction. Many previous studies have investigated either the instantaneous flux of DOC (e.g. Teira et al., 2003; Alonso-Sáez et al., 2007) or the seasonal accumulation of a persistent pool of DOC (e.g. Copin-Montégut and Avril, 1993; Carlson et al., 1994; Børsheim and Myklestad, 1997). This study is unique in that it evaluates both fluxes in order to better elucidate and link how heterotrophic bacterioplankton mediate carbon cycling in the NAAMES study region.

Assessment of Bacterioplankton Growth Efficiency in the Western North Atlantic

After DOC is assimilated by bacterioplankton, a fraction is used to fuel anabolism while the rest is catabolized used to generate the ATP necessary for the remaining cellular energetic demands, such as membrane transport, cellular maintenance, and motility. The efficiency by which natural bacterioplankton assemblages repackage DOC into cells and transfer energy to higher trophic levels is partially controlled by BGE (Del Giorgio and Cole, 1998; Carlson and Hansell, 2015). The greater the BGE, the greater the trophic link, the lower the BGE, and the greater the energetic sink within the microbial food web (Ducklow et al., 1986)

BGEs used to estimate gross bacterioplankton production are either empirically determined as changes in DOC and cell biomass (e.g., Carlson et al., 1999; Lønborg et al., 2011; Halewood et al., 2012; Wear et al., 2015) or from measures of bacterioplankton production and respiration (e.g., Reinthaler and Herndl, 2005; Alonso-Sáez et al., 2008; Del Giorgio et al., 2011; Lønborg et al., 2011), adopted from the literature (Marañón et al.,

2007), or derived from empirical models (Del Giorgio and Cole, 1998; Rivkin and Legendre, 2001; Hoppe et al., 2002). Empirically determined BGE calculations often necessitate the use of carbon conversion factors (CCFs) to express changes in bacterioplankton cell abundance as changes in cell carbon or O_2 consumption as CO_2 production. Converting cell abundance to biomass CCFs previously reported for open ocean bacterioplankton range from 5 – >20 fg C cell^{-1} (Lee and Fuhrman, 1987; Fukuda et al., 1998; Gundersen et al., 2002). The calculation of BGE is sensitive to the CCF chosen to estimate cell carbon (Alonso-Sáez et al., 2007) and it can be problematic to apply a single CCF across all data within a DOC remineralization experiment, such as those presented here, as cell sizes can change with cell growth (e.g., Liu et al., 2020; Stephens et al., 2020). Thus CCFs are a significant source of uncertainty for budgets of ocean carbon flux that rely on constrained estimates of BGEs (Lochte et al., 1993; Burd et al., 2010). Here we circumvent the need for CCFs by directly measuring the change in bacterioplankton carbon (BOC) collected on GF75 (nominal 0.3 μm cutoff, mean cell retention 78 ± 9%) between the initiation of the experiment (T_0) and stationary phase ($T_{Stationary}$) of growth in each of the DOC remineralization experiments.

The BGEs empirically determined here occupied a small range, with a mean of 26 ± 10% across three different seasons and the broad spatial range of the NAAMES study region (Table 3.1). These BGEs fall within the range reported for the open ocean (1 – > 60%, Del Giorgio and Cole, 1998) and from previous phytoplankton bloom studies (5 – 62%, (Carlson and Hansell, 2003; Wear et al., 2015a). In the Ross Sea, Carlson and Hansell (2003) reported that BGEs increased from ~5% during the early phase of a phytoplankton bloom to 30 – 40% in the late stage of phytoplankton bloom senescence, leading the authors to

hypothesize that the bioavailable fraction of DOM near the end of the bloom is of a quality that readily meets the metabolic demands of the responding *in situ* bacterioplankton community. Comparatively, BGEs in the southern North Sea were reported to decrease from 25% in the spring and summer to 14% in the fall and 5% in winter (Reinthaler and Herndl, 2005). The authors hypothesized that the corresponding decreases in BGE and NPP was due to a coincident decrease in DOM lability from spring to winter. BGEs in the NW Mediterranean, ranged from 3 – 42% and were highest in the winter and spring when chlorophyll *a* concentrations and rates of NPP were elevated, suggesting that relatively high primary productivity was a source of sustained flux of bioavailable DOM (Alonso-Sáez et al., 2008). Wear et al. (2015a) also observed a similar relationship between the physiological state of a phytoplankton bloom and BGE variability in the coastal upwelling system of the Santa Barbara Channel (CA, USA). BGEs were observed to be low (min 17%) in early bloom and then increase later (max 62%) as phytoplankton became Si stressed. Over the same time period, *in situ* DOC concentrations, DOC bioavailability, and DOC persistence increased.

In contrast to the previous studies discussed above, our estimates of BGE over the entire study region in the Western North Atlantic did not reveal a statistically significant seasonal pattern (i.e., early spring [27 ± 5%], late spring [22 ± 1%] and early autumn [30 ± 15%]; Figure 3.5, Table 3.1). It is possible that the heterogeneity of the physical and chemical environment over the large geographical realm of the NAAMES region obscured linkages between BGE dynamics and phytoplankton bloom stages and their associated processes. In other words, the spatial heterogeneity of the NAAMES region may overwhelm seasonal differences. Thus, seasonality in BGE may have been more pronounced if the

empirical determinations were focused on temporal dynamics within narrower geographic regions, each of which may be characterized by differences in DOM availability and bioavailability, community composition (both phytoplankton and bacterioplankton), and nutrient availability. We were not able to resolve significant seasonality in BGE at ~44˚N (21%), the one station occupied in early spring, late spring, and early autumn. Due to logistical limitations, we do not have a similar seasonal DOM remineralization experiments at other latitudinal regions. Thus, there are insufficient data in this study to directly assess seasonal changes in BGEs for other localized regions or mesoscale features (e.g., eddies) of the Western North Atlantic, a topic for future investigation.

Seasonality in BCD and BCD:NPP Reflect Changes in the Accumulated DOM Pool

Due to the narrow range of empirically derived BGE estimates during the NAAMES cruises, we adopted a universal campaign mean BGE of 26% to estimate BCD. We acknowledge that the application of a universal BGE oversimplifies estimates of BCD and can affect the interpretation of ocean carbon cycling and budgets (Ducklow et al., 2002; Marañón et al., 2007; Burd et al., 2010). Furthermore, our use of a theoretical leucine-to-carbon conversion factor to estimate BP also neglects variability in the fate of incorporated leucine in bacterioplankton cells, whether used for biomass production or respiration (del Giorgio et al., 1997). Despite these caveats, we consider our estimates of BCD to be conservative yet realistic of the flux of the most labile DOM required to support gross bacterioplankton production for the NAAMES campaign.

Over the composite annual cycle of the broad NAAMES study region, bacterioplankton abundance, production, and BCD were positively correlated with seasonal variability in NPP (Figure 3.6, 3.7b, 3.7c, 3.8; Table 3.2). However, while the rates of NPP

and BCD were each greatest in the spring, a relatively smaller fraction of NPP was diverted to labile DOM flux compared to autumn, as revealed by the lower BCD to NPP ratio in the spring (Figure 3.7b, 3.7c, 3.7d; Table 3.2). Interestingly, the spatial variability in the scaling of BCD:NPP showed a marked decrease as NPP increased northward in the early autumn (Figure 3.7c, 3.7d; Table 3.2). This pattern may be due to a general timing phenomenon where blooms peak and decline earlier in southern latitudes than northern latitudes (Bolaños et al., 2021). Living phytoplankton cells can release up to 80% of their primary production as DOM via direct extracellular release, though most studies report that extracellular release ranges between 5 – 20% of NPP (Nagata, 2008; Carlson and Hansell, 2015). If extracellular release truly falls between 5 – 20%, then food web interactions and DOM production processes other than direct phytoplankton release are sources of organic matter that support heterotrophic demand on rapid timescales. Thus, although the organic carbon available for heterotrophic bacterioplankton production was largely constrained by NPP, it is important to recognize that there are many food web processes that result in the production of DOC (Carlson and Hansell, 2015) and volatile organic compounds (Buchan et al., 2014); thus, instantaneous measures of BCD may lag the instantaneous measures of NPP (Billen, 1990; Ducklow et al., 2002).

The greater overall rates of net BP and BCD as well as the elevated bacterioplankton abundances observed in the spring periods indicate that there was a greater flux of labile DOM to bacterioplankton at that time. However, the corresponding low BCD:NPP suggests that a greater fraction of bloom produced organic matter was either partitioned as POM or was exported from the euphotic zone with a smaller fraction accumulating as DOM. During post-bloom periods (autumn/winter), both NPP and BCD rates decreased yet the ratio of

BCD:NPP increased, indicating that the flux of the most labile DOC became more strongly coupled to NPP.

Seasonality in DOC_{SA} Bioavailability and its Implications

The fraction of primary production partitioned as DOC that is not readily available for rapid consumption by the existing heterotrophic community can accumulate and persist over time. The seasonal accumulation of this DOC, termed DOC_{SA}, represents a portion of net community production (NCP, i.e., export production) and as such, represents the DOC that is potentially available for vertical or horizontal transport (Hansell et al., 1997b; Carlson et al., 1998; Hansell and Carlson, 1998b). As previously described for the NAAMES study region, the fraction of NCP represented as DOC_{SA} increased from late spring to early autumn. This seasonal change in DOC_{SA}:NCP indicates that a smaller fraction of NCP is partitioned as DOC during the bloom condition (~11%) and becomes greater under the non-bloom condition (~20%) (Baetge et al., 2020).

The successional pattern from bloom to non-bloom states demonstrates that while there was a consistent flux of labile DOM to fuel heterotrophic bacterioplankton production, there were other components of the bulk DOC pool that were produced but remineralized on longer timescales, and subsequently accumulated over time. The present study shows that as DOC_{SA}:NCP increased from the "climax transition" to the "depletion phase" of the phytoplankton bloom cycle in the NAAMES study region (Baetge et al., 2020), the proportion of $\Delta DOC:DOC_{SA}$ decreased and led to the buildup of a semi-labile DOC pool (Figure 3.4, Table 3.1). From a biogeochemical perspective, it is this semi-labile DOC pool that resists or escapes microbial degradation on short time scales and persists long enough to be mixed or subducted from the epipelagic to the mesopelagic during annual deep

convective mixing at some latitudes that represents a DOC export pathway of the biological carbon pump (Copin-Montégut and Avril, 1993; Carlson et al., 1994; Børsheim and Myklestad, 1997; Hansell and Carlson, 2001a; Baetge et al., 2020).

The factors that regulate DOC accumulation and its persistence remain elusive in DOM biogeochemistry (Benner and Amon, 2015; Carlson and Hansell, 2015). One hypothesized factor is the "malfunctioning microbial loop" in which heterotrophic DOC consumption is unable to match DOC release due to inorganic nutrient limitation/competition or from predation (Cotner et al., 1997; Thingstad et al., 1997). The production and release of recalcitrant DOM compounds that are intrinsically resistant to heterotrophic utilization by eukaryotes (Aluwihare and Repeta, 1999; Mitra et al., 2014) and prokaryotes (e.g. McCarthy et al., 1998; Kawasaki and Benner, 2006) is another way that DOC can accumulate. The microbial carbon pump posits that as labile DOC compounds are utilized by heterotrophic bacterioplankton, recalcitrant DOM byproducts are produced and accumulate (Jiao et al., 2010; Benner and Herndl, 2011). However, DOC may accumulate not just because of its intrinsic resistance to biological uptake and oxidation, but also because the "economics" of oxidizing a compound may vary depending on the community structure of the heterotrophic community (Carlson et al., 2009; Treusch et al., 2009; Giovannoni, 2017; Landry et al., 2017; Saw et al., 2020) and the growth factors required to optimize hydrolytic enzyme production or transport regulation (Reintjes et al., 2020; Arnosti et al., 2021). The alternative "molecular diversity hypothesis" proposes that it is not the inherent stability of a DOC compound that results in its accumulation but rather that any one of the millions of DOM compounds is maintained at a concentration too low for a microbe to detect or invest in uptake mechanisms for, consequently allowing the compound to

accumulate (Arrieta et al., 2015). The vast diversity of DOM molecules may control the accumulation of otherwise bioavailable compounds, precluding any individual molecule from approaching the chemoreceptive threshold of prokaryotes (Kattner et al., 2011), facilitating low encounter rates between substrate and bacteria via molecular diffusion (Stocker, 2012), and/or demanding more energy from heterotrophs to acquire a particular substrate than they may receive from that substrate (thermodynamic inhibition) (LaRowe et al., 2012). Whatever the mechanisms, $\Delta DOC:DOC_{SA}$ for the NAAMES campaign decreased from spring to early autumn and resulted in the accumulation of a DOC pool that persisted, potentially becoming available for vertical export during deep winter convective mixing (Baetge et al., 2020) and episodic deep mixing events (Omand et al., 2015; Lacour et al., 2019).

Conclusions

This study allowed us to resolve the fate of DOM production in in the western North Atlantic over various temporal scales. By combining field observations of net BP and DOC variability (Baetge et al., 2020) with DOC remineralization experiments, we demonstrated seasonality in the BCD:NPP ratio as well as changes in the magnitude and bioavailability of the seasonally accumulated DOC pool. On shorter timescales, the flux of the most labile DOC compounds that supported instantaneous BCD rates was greatest in the spring despite a lower BCD:NPP ratio. During periods of low productivity (i.e., early autumn "depletion phase" and early winter "winter transition"), rates of NPP and BCD decreased yet a greater fraction of the daily NPP supported BCD. Our results also demonstrated that during the high productivity periods (i.e., early spring "accumulation phase" and late spring "climax transition") of the phytoplankton bloom, a relatively smaller fraction of NCP was partitioned as DOC_{SA}.

However, the DOC that did accumulate had a larger bioavailable fraction than the DOC_{SA} present during periods of low productivity.

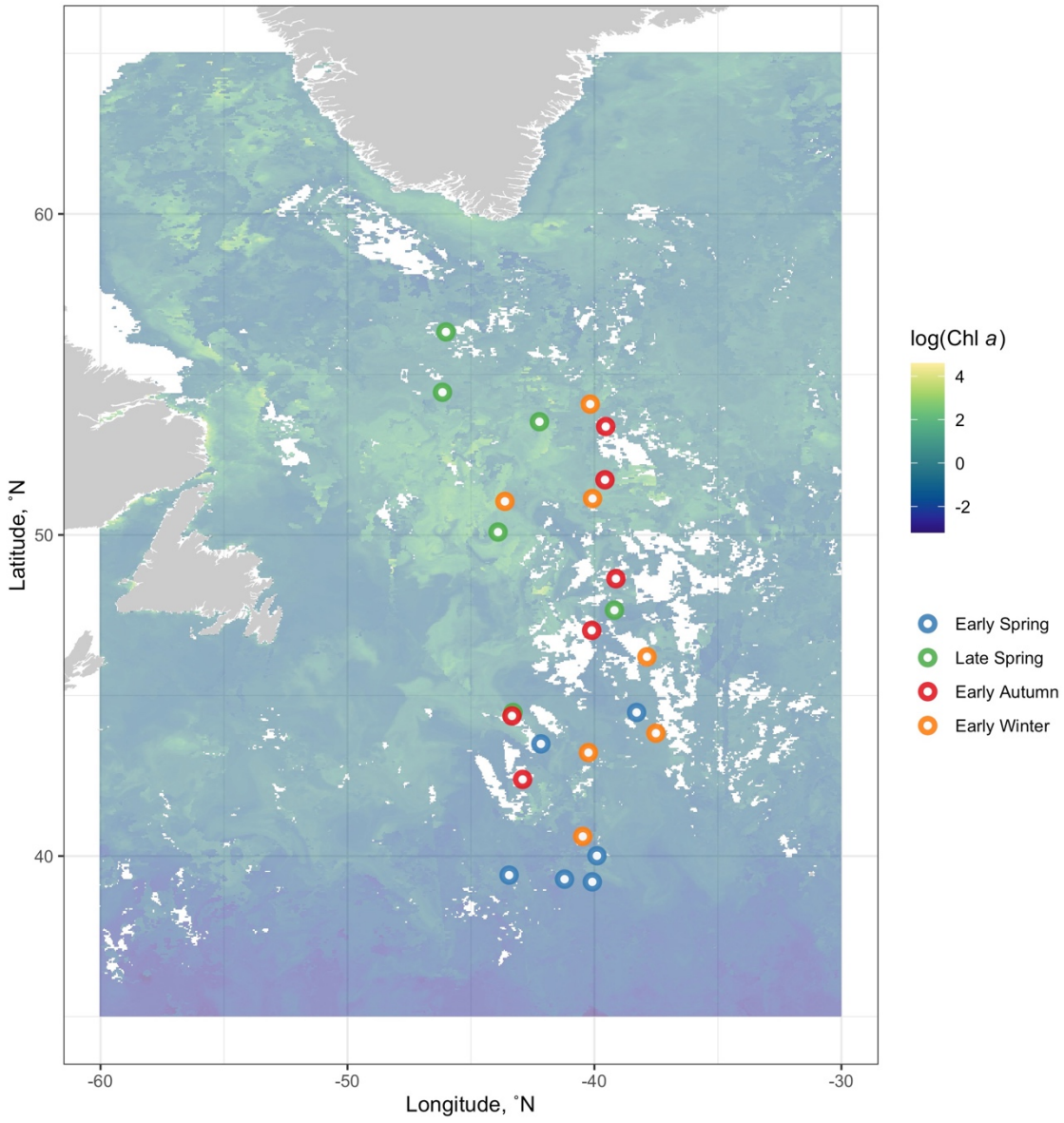

Figure 3.1. Station locations for all cruises are overlain on a map of 8-day composite log-transformed chlorophyll data from NASA's Moderate Imaging Spectroradiometer (MODIS) collected during May 2016. NAAMES 1 occurred in the early winter ("winter transition": November - December 2015, orange points), NAAMES 2 in the late spring ("climax transition": May 2016, green points), NAAMES 3 in the early autumn ("depletion phase": September 2017, red points), and NAAMES 4 in the early spring ("accumulation phase": April 2018, blue points).

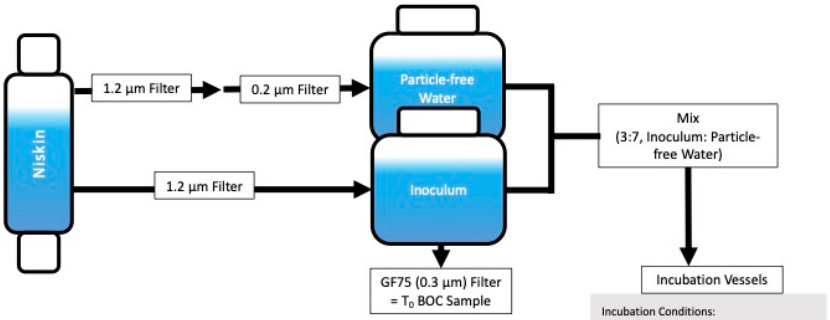

Variable Sampling Frequency

Cruise	Bottle BA	Vial BA	BOC	Bottle TOC	Bottle DOC	Vial TOC	Vial DOC
NAAMES 2 (Late Spring)	Shipboard Daily	-	$T_{Stationary}$	-	~Days 0, 1, 3, 7, 10, 14, 30, 60, 90	-	-
NAAMES 3 (Early Autumn)	Shipboard Daily	-	$T_{Stationary}$	~Days 0, 7, 14	~Days 0, 7, 14	~Days 0, 7, 14, 30, 60	-
NAAMES 4 (Early Spring)	Shipboard Daily	~Day 7	$T_{Stationary}$	~Days 0, 7, 14	~Days 0, 7, 14	~Days 0, 7, 14, 30, 60, 90	~Days 0, 7, 14, 30, 60, 90

Figure 3.2. Schematic of the initiation and incubation conditions of the DOC remineralization experiments conducted on NAAMES 2 – 4, detailed in section "DOC Remineralization Experiments". Also included is a table of the sampling frequency for the incubations, in which bacterioplankton abundance is denoted by "BA", bacterioplankton organic carbon by "BOC", total organic carbon by "TOC", and dissolved organic carbon by "DOC". "T_0" refers to the initial condition of the experiment while "$T_{Stationary}$" refers to the stationary phase of cell growth determined by the bacterioplankton abundance curve. Note that T_0 BOC was collected from the inoculum while $T_{Stationary}$ BOC was collected from the bottle incubations.

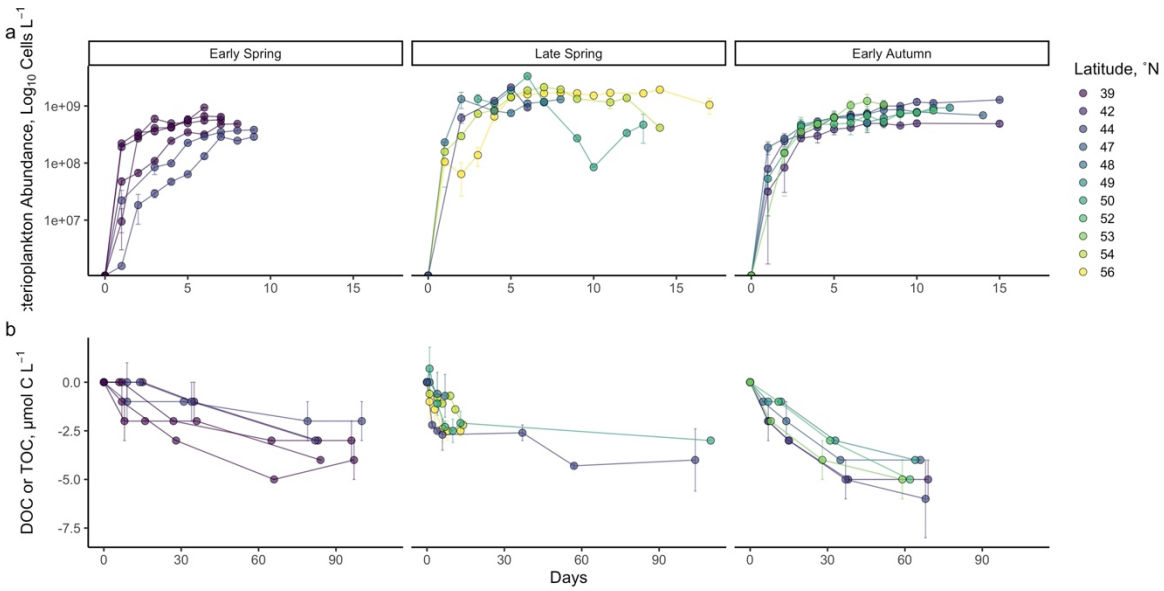

Figure 3.3. Time series of station mean $\log_{10}$ cell abundance (a) and DOC/TOC (b) from DOC remineralization experiments. Data represent the change in bacterioplankton $\log_{10}$ cell abundance from T_0 up to 17 days or change in DOC concentration throughout the long-term incubation of up to 110 days. Late spring organic carbon data are from filtered DOC samples, while early spring and early autumn organic carbon data are from unfiltered TOC samples. Error bars indicate the standard deviation between the means of replicated experiments.

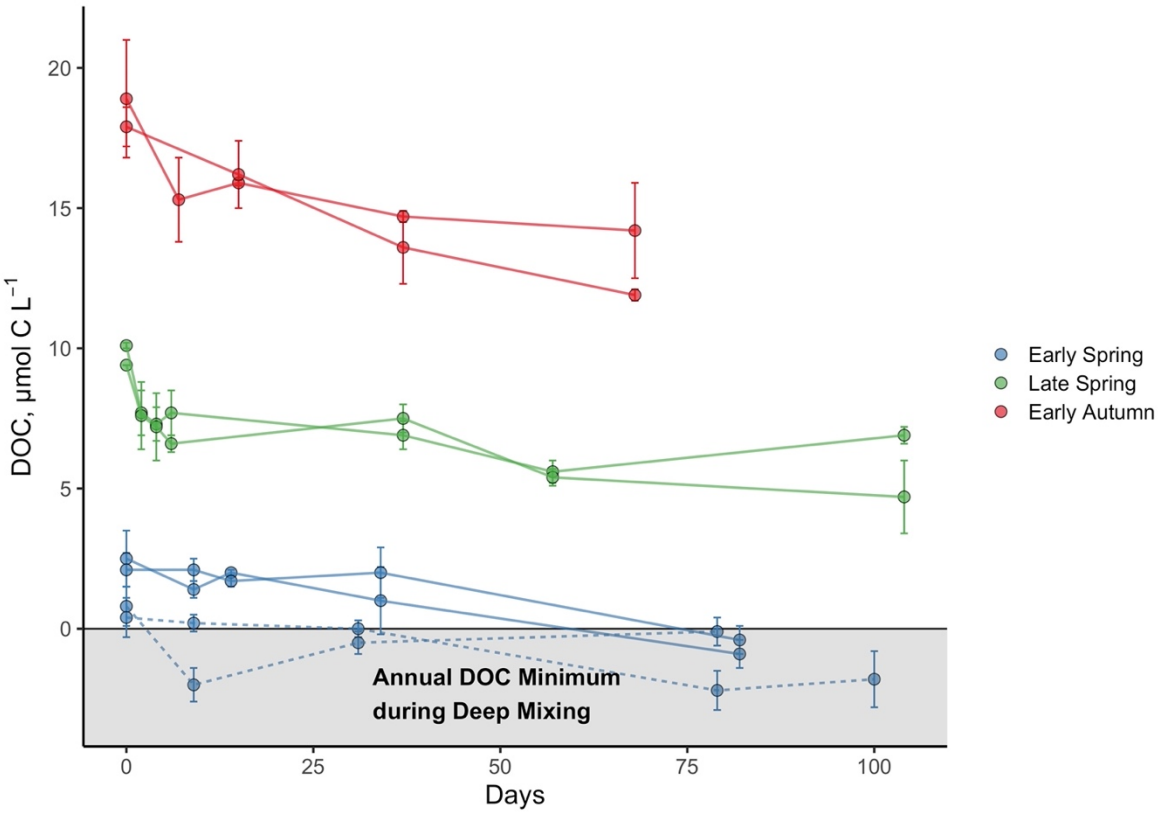

Figure 3.4. Bioavailability and persistence of seasonally accumulated DOC (DOC_{SA}) at the 44˚N latitudinal bin of the NAAMES study region based on DOC remineralization experiments. Experiments were conducted at two different stations corresponding to 44˚N in the early spring and are denoted by the solid (station 3) and dashed lines (station 4). Data represent measurements for each incubation bottle, with error bars representing the standard deviations. The horizontal line intersecting the y-axis at 0 represents the baseline after the annual minimum DOC concentration corresponding to the maximal deep winter mixing (Baetge et al. 2020) has been subtracted from the measured surface DOC concentration for each season.

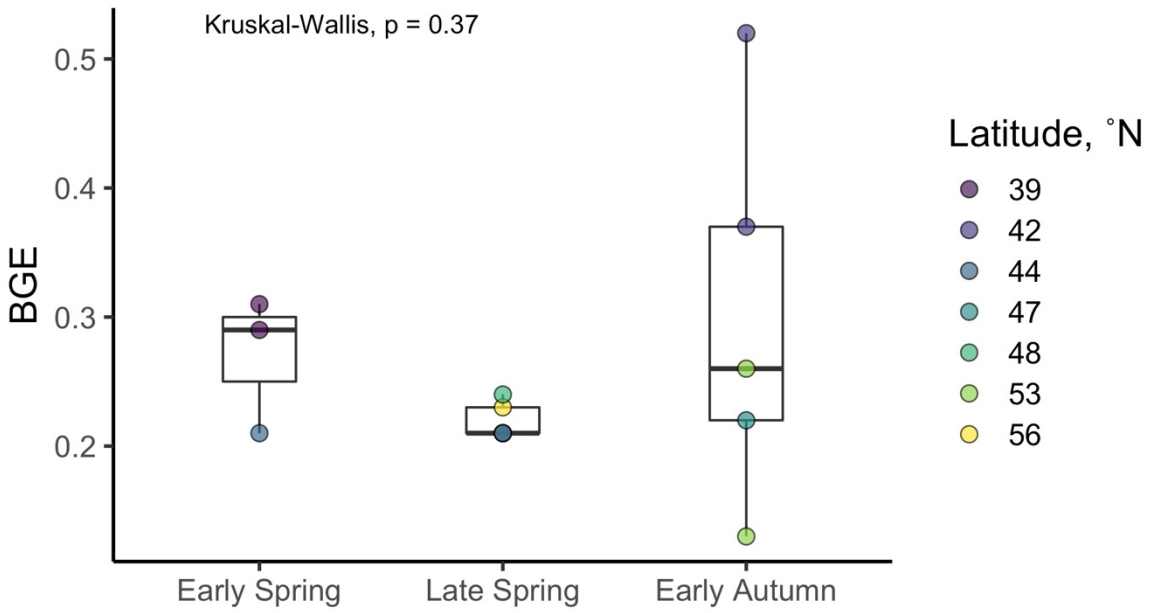

Figure 3.5. Bacterioplankton growth efficiency (BGE) estimates derived from the DOC remineralization experiments. Filled circles represent individual incubations and fill color represents station where experiment was conducted (see Table 1 for corresponding station latitudes). Boxes represent the 1.5 interquartile range, with the internal solid line representing the median. *p*-values are reported for the non-parametric Kruskal-Wallis test (one-way ANOVA on ranks), which tests if the means of all groups are equal.

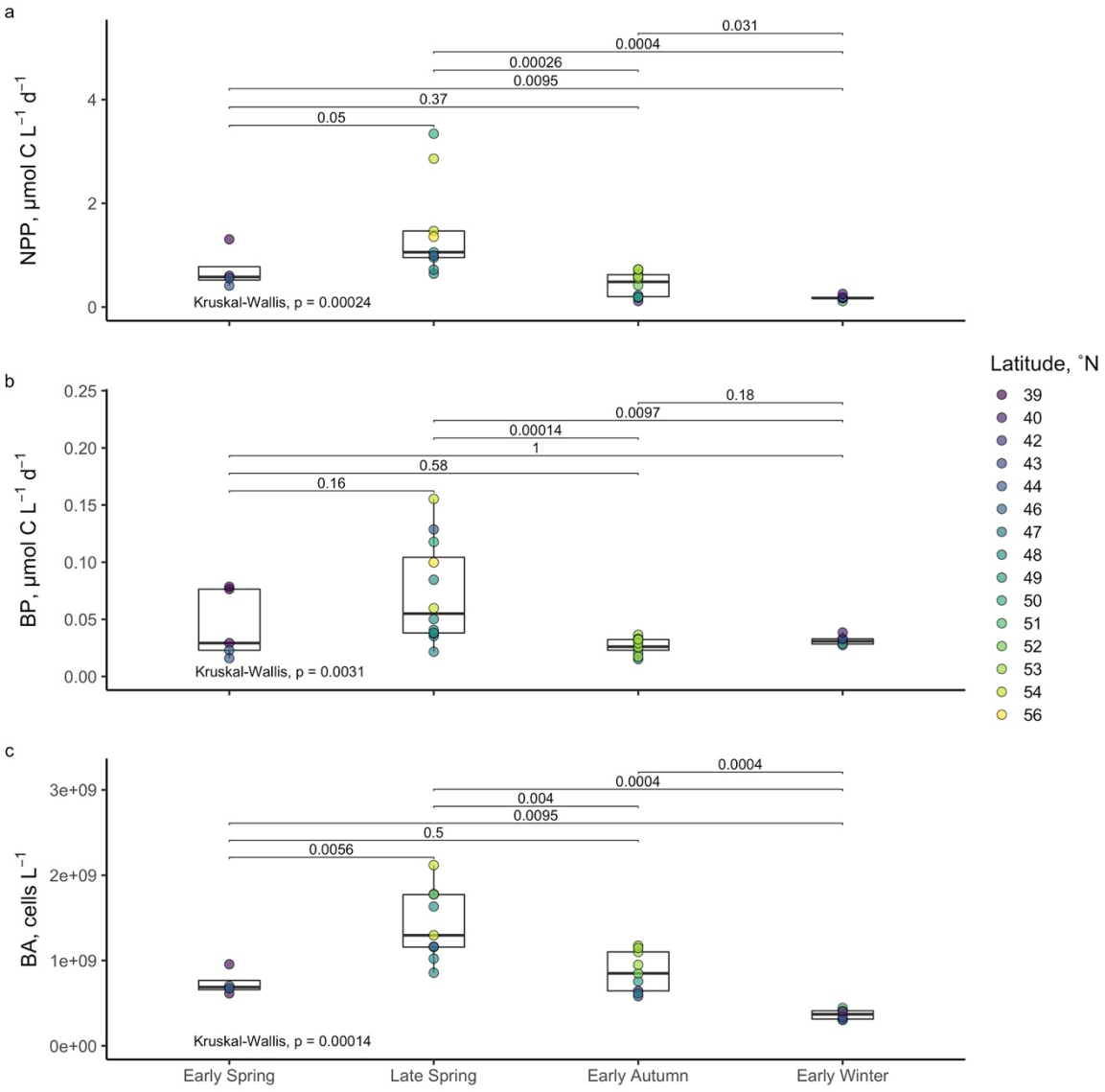

Figure 3.6. Averages of net primary production (NPP, a), bacterioplankton production (BP, b), and bacterioplankton abundance (c) within the euphotic zone for each station. Boxes represent the 1.5 interquartile range, with the internal solid line representing the median. Circles represent data points. *p*-values are reported for the non-parametric Kruskal-Wallis test (one-way ANOVA on ranks), which tests if the means of all groups are equal. Level of significance is also reported for the non-parametric two sample Wilcoxon test, which tests whether the means between two groups are equal.

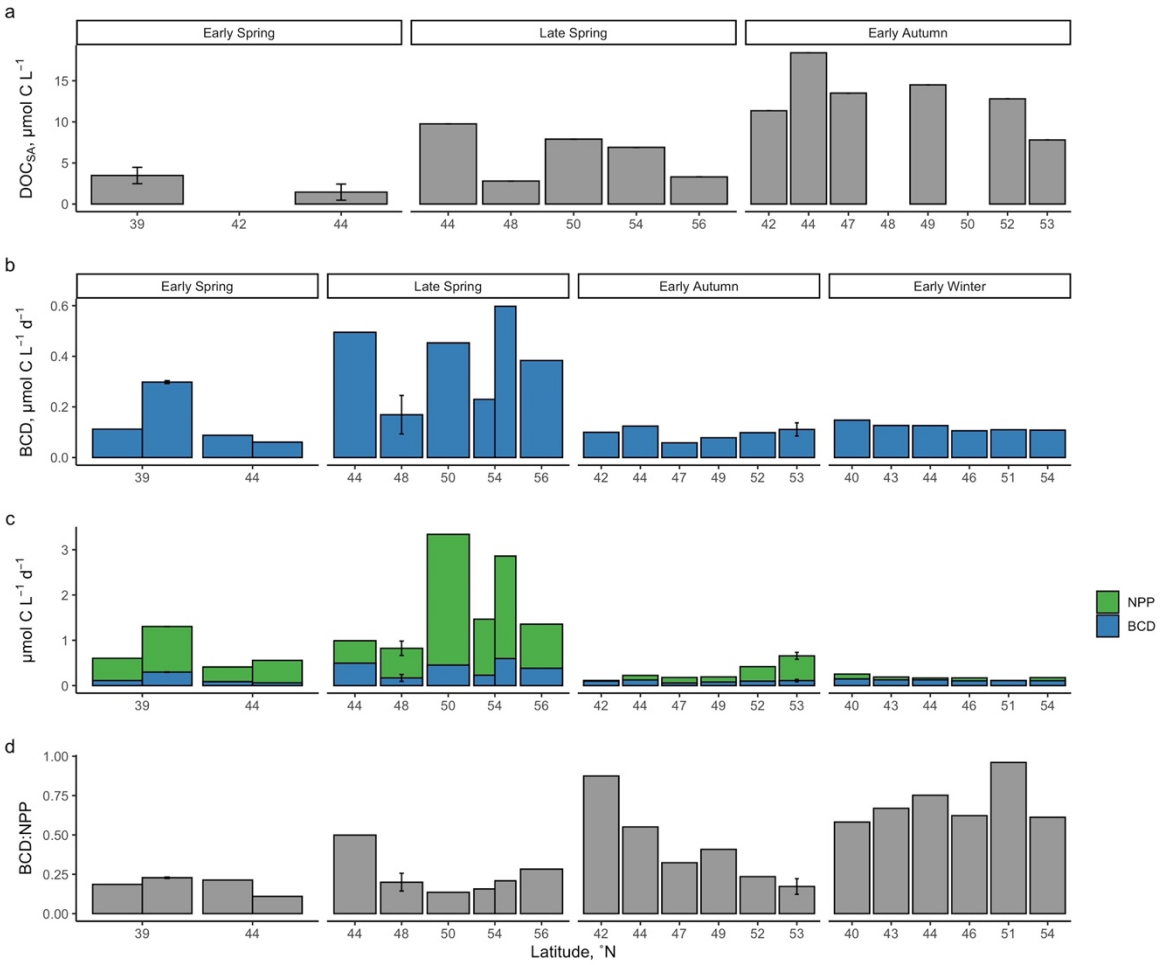

Figure 3.7. Seasonally accumulated DOC from the initial condition of the DOC remineralization experiments, which were conducted using water from the surface 10 m (a). BGEs were applied to *in situ* measurements of net bacterioplankton production to estimate bacterioplankton carbon demand (BCD, b) and the fraction of NPP it represents (c, d). Error bars represent standard deviations.

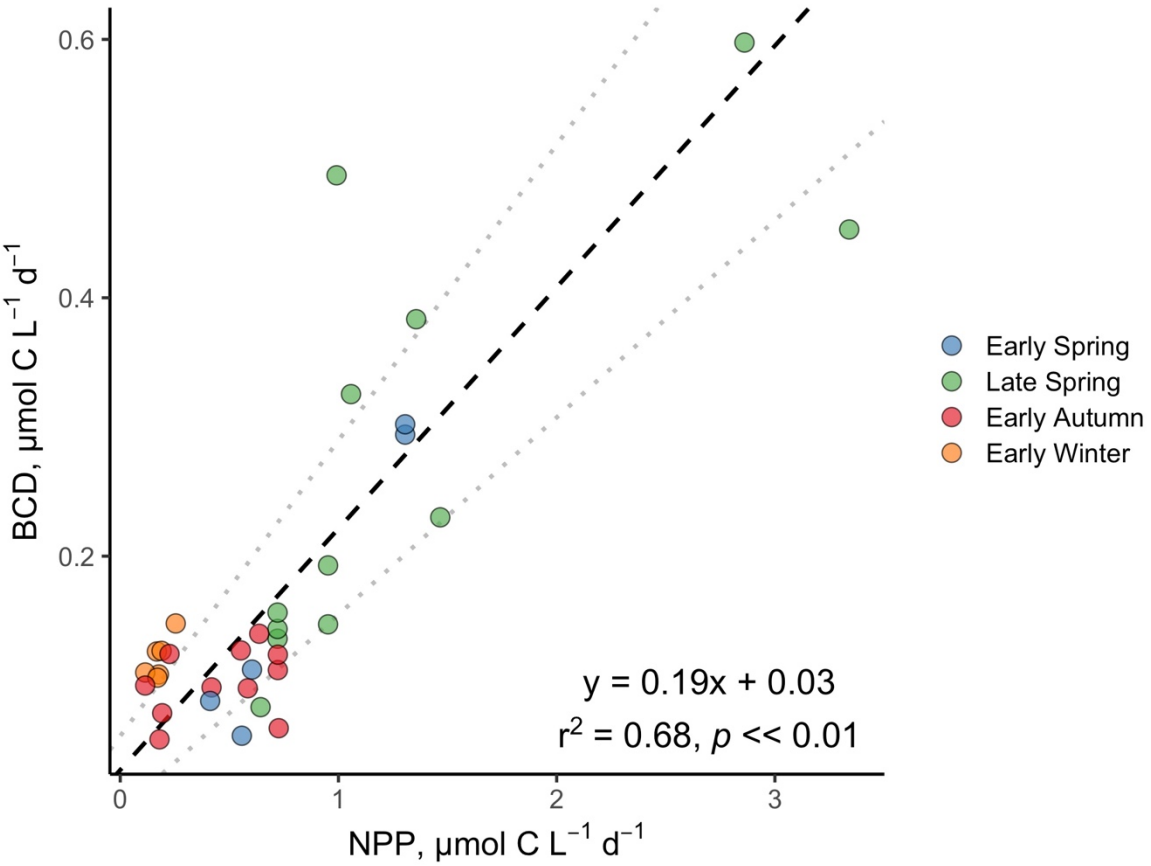

Figure 3.8. Standardized (reduced) major axis model II linear regression between NPP and BCD. Dotted grey lines indicate the 2.5% and 97.5% confidence intervals.

Station	Latitudinal Bin (°N)	Longitudinal bin (°W)	Max MLD (m)	Annual DOC Minimum (µmol C L^{-1})	T_0 DOC (µmol C L^{-1})	T_0 DOC_{SA} (µmol C L^{-1})	$T_{Stationary}$ (days)	T_{end} (days)	T_0 BOC (µmol C L^{-1})	$T_{Stationary}$ BOC (µmol C L^{-1})	ΔBOC (µmol C L^{-1})	$T_{Stationary}$ DOC (µmol C L^{-1})	Short-term ΔDOC (µmol C L^{-1})	BGE	Short-term %ΔDOC (µmol C L^{-1})	Short-term ΔDOC Removal Rate (µmol C L^{-1} d^{-1})	T_{end} DOC_{SA} (µmol C L^{-1})	Long -term ΔDOC (µmol C L^{-1})	Long-term %ΔDOC (µmol C L^{-1})	Long-term ΔDOC Removal Rate (µmol C L^{-1} d^{-1})	Persistent DOC_{SA} (µmol C L^{-1})	% Persistent DOC_{SA}
Early Spring (April 2018): "Accumulation Phase"																						
1	39	-44	294	55.5	60.3 ± 0.6	4.8	8	84	0.1	1.1 ± 0.0	1.0 ± 0.0	56.9 ± 0.9	3.4 ± 0.2	0.30 ± 0.01	71 ± 5	0.4 ± 0.0	55.6 ± 0.2	4.7 ± 0.8	99 ± 18	0.06 ± 0.01	0	0
2	39	-41	294	55.5	58.3 ± 0.1	2.8	6	83	0.2	0.8 ± 0.1	0.6 ± 0.1	57.6 ± 0.3	NR	NR	NR	NR	55.4 ± 0.1	3.1 ± 0.0	111 ± 0	0.04 ± 0.0	0	0
2RD	39	-40	294	55.5	59.5 ± 0.1	4.0	7	97	0.2	1.7 ± 0.1	1.5 ± 0.4	57.0 ± 0.5	NR	NR	NR	NR	55.8 ± 0.6	3.8 ± 0.8	95 ± 20	0.04 ± 0.01	0	0
2RF	39	-40	294	55.5	58.5 ± 0.0	2.4	7	96	0.1	1.2 ± 0.0	1.1 ± 0.0	56.7 ± 0.3	NR	NR	NR	NR	54.5 ± 0.1	4.0	167	0.04	0	0
3	44	-42	368	55.9	58.2 ± 0.3	2.3	9	82	0.1	0.7 ± 0.1	0.6 ± 0.1	57.7 ± 0.5	NR	NR	NR	NR	55.3 ± 0.3	3.1 ± 0.6	132 ± 28	0.04 ± 0.01	0	0
4	44	-38	368	55.9	56.7 ± 0.3	0.8	9	100	0.1	0.6 ± 0.1	0.5 ± 0.1	53.9 ± 0.6	2.8	0.21	350	0.3 ± 0.1	54.1 ± 0.7	2.3	288	0.02	0	0
Overall (Mean, SD)			**319 ± 38**	**55.6 ± 0.2**	**58.6 ± 1.2**	**2.9 ± 1.4**	-	-	**0.1 ± 0.05**	**1.0 ± 0.4**	**0.9 ± 0.4**	**56.6 ± 1.4**	**3.2 ± 0.4**	**0.27 ± 0.05**	**211 ± 197**	**0.4 ± 0.1**	**55.1 ± 0.7**	**3.6 ± 0.9**	**149 ± 73**	**0.04 ± 0.01**	**0**	**0**
Late Spring (May 2016): "Climax Transition"																						
5	44	-43	368	55.9	65.7 ± 0.5	9.8	6	104	0.5	1.1 ± 0.1	0.6 ± 0.1	63.1 ± 0.8	2.6 ± 0.3	0.21	27 ± 7	0.4 ± 0.1	61.7 ± 1.1	4.0 ± 1.1	41 ± 11	0.04 ± 0.01	5.8 ± 1.1	59 ± 11
4	48	-39	508	51.3	54.7 ± 1.1	3.4	7	8	0.2	0.7 ± 0.0	0.5 ± 0.0	52.6 ± 0.0	2.1	0.24	62	0.3	53.4 ± 0.8	NR	NR	NR	NR	NR
3	50	-44	406	52.4	60.3	7.9	10	13, 110	0.4	ND	ND	57.8 ± 0.6	2.5 ± 0.6	NR	32	0.3 ± 0.1	57.3 ± 0.6	3.0	38	0.03	4.9	62
2	54	-42	223	50.4	57.3 ± 0.4	6.9	8	14	0.5	1.5 ± 0.0	1.0 ± 0.0	56.5 ± 0.1	NR	NR	NR	NR	55.0 ± 0.1	2.6	38	0.2	4.3	62
1	56	-46	110	51.2	54.5 ± 1.0	3.3	8	17	0.4	1.0 ± 0.1	0.6 ± 0.1	51.9 ± 0.5	2.6 ± 0.5	0.22 ± 0.02	77 ± 15	0.3 ± 0.1	51.2 ± 0.6	3.3 ± 0.2	98 ± 6	0.20 ± 0.01	0	0
Overall (Mean, SD)			**323 ± 157**	**52.0 ± 2.1**	**58.5 ± 4.7**	**6.3 ± 2.9**	-	-	**0.4 ± 0.1**	**1.1 ± 0.3**	**0.6 ± 0.2**	**56.3 ± 4.6**	**2.5 ± 0.4**	**0.22 ± 0.01**	**50 ± 24**	**0.3 ± 0.1**	**55.7 ± 4.0**	**3.3 ± 0.7**	**59 ± 31**	**0.1 ± 0.09**	**3.8 ± 2.6**	**46 ± 31**
Early Autumn (September 2017): "Depletion Phase"																						
1	42	-43	418	55.4	66.8 ± 0.2	11.4	7	69	0.2	2.1 ± 0.4	1.9 ± 0.4	62.5 ± 0.1	4.3 ± 0.1	0.45 ± 0.11	37 ± 1	0.6 ± 0.0	62.2 ± 0.7	4.8 ± 1.2	42 ± 11	0.07 ± 0.02	6.6 ± 1.2	58 ± 11
2	44	-43	368	55.9	74.3 ± 0.7	18.4	7	68	0.5	2.5 ± 0.1	2.0 ± 0.0	73.7 ± 0.6	NR	NR	NR	NR	68.9 ± 1.2	5.8 ± 0.8	32 ± 5	0.09 ± 0.01	12.6 ± 0.8	68 ± 5
3	47	-40	336	54.2	68.8 ± 0.8	14.6	5	66	0.7	1.6 ± 0.4	0.9 ± 0.4	66.1 ± 1.9	2.7	0.22	18	0.5	64.0 ± 0.2	4.5 ± 1.3	31 ± 10	0.07 ± 0.02	101 ± 1.3	69 ± 10
4	49	-39	448	51.6	66.1 ± 0.4	14.5	7	64	0.6	1.0 ± 0.1	0.4 ± 0.1	64.8 ± 0.4	NR	NR	NR	NR	62.9 ± 0.2	3.8 ± 0.7	26 ± 5	0.06 ± 0.01	10.7 ± 0.7	73 ± 5
5	52	-40	330	56.0	68.8 ± 0.6	12.8	7	62	1.4	1.4 ± 0.2	0.1 ± 0.2	68.0 ± 0.2	NR	NR	NR	NR	65.0 ± 0.4	5.3 ± 1.1	41 ± 8	0.08 ± 0.02	7.6 ± 1.1	59 ± 8
6	53	-40	231	52.7	60.5 ± 0.3	7.8	8	59	1.1	1.6 ± 0.3	0.5 ± 0.3	57.9 ± 0.1	2.6 ± 0.2	0.20 ± 0.09	33 ± 3	0.3 ± 0.0	56.6 ± 1.0	5.0 ± 1.1	64 ± 15	0.08 ± 0.02	2..8 ± 1.1	35 ± 15
Overall (Mean, SD)			**355 ± 76**	**54.2 ± 1.8**	**67.9 ± 4.5**	**13.3 ± 3.6**	-	-	**0.8 ± 0.4**	**1.7 ± 0.5**	**1.0 ± 0.8**	**65.5 ± 5.3**	**3.2 ± 0.9**	**0.30 ± 0.15**	**29 ± 10**	**0.4 ± 0.1**	**63.2 ± 4.0**	**4.8 ± 1.0**	**40 ± 15**	**0.08 ± 0.02**	**8.4 ± 3.5**	**60 ± 14**

Table 3.1. BGEs and DOC Bioavailability from DOC Remineralization Experiments. Station: where experiments were conducted; **Latitudinal bin**: stations were binned to the nearest degree based on latitudinal coordinates; **Longitudinal bin**: binned to the nearest degree; Max MLD: maximum mixed layer depth identified from ARGO profiling data between 2014 and 2018 for each latitudinal bin, detailed in Baetge et al. (2020); **Annual DOC minimum**: DOC concentration corresponding to the maximal deep winter mixing, which was determined for each station as detailed in Baetge et al. (2020); DOC_{SA}: Seasonally accumulated DOC, magnitude of DOC that accumulated in excess of annual DOC minimum; **T_0 DOC:** initial DOC concentration in the DOC remineralization experiments; **DOC_{SA}:** seasonally accumulated DOC, calculated as T_0 DOC minus the corresponding annual DOC minimum; **$T_{Stationary}$**: stationary growth phase timepoint where BOC and DOC(*) samples were collected; **T_{End}**: termination of experiments; **T_0 BOC**: BOC at T_0; **$T_{Stationary}$ BOC**: BOC at $T_{Stationary}$; **ΔBOC**: change in BOC from T_0 to $T_{Stationary}$; **$T_{Stationary}$ DOC**: DOC at $T_{Stationary}$; **Short-term** ΔDOC: change in DOC from T_0 to $T_{Stationary}$ equal to bioavailable DOC, expressed as concentration, $\%DOC_{SA}$, and removal rate; **T_{End} DOC**: DOC at T_{End}; **Long-term** ΔDOC: change in DOC from T_0 to T_{End} equal to bioavailable DOC, expressed as concentration, $\%DOC_{SA}$, and removal rate; **Persistent** DOC_{SA}: the fraction of DOC_{SA} remaining at T_{End}, that is DOC_{SA} - Long-term ΔDOC, expressed as concentration and $\%DOC_{SA}$. Data represent means of replicated experiments with error representing standard deviations. **NR** = Not Resolvable due to DOC or TOC removal not meeting criteria of ≥ 2 µmol C L^{-1}; **ND** = No Data.

Station	Latitudinal Bin (°N)	MLD (m)	Euphotic Zone Depth (m)	Temperature (°C)	Chl *a* (mg m^{-3})	NPP (µmol C L^{-1} d^{-1})	BP (µmol C L^{-1} d^{-1})	BP:NPP (%)	BCD (µmol C L^{-1} d^{-1})	BCD:NPP (%)
Early Spring (April 2018): "Accumulation Phase"										
1	39	80	106	18.3	0.67	0.60	0.03	5	0.11	19
2	39	59 ± 7	98	17.0 ± 0.01	0.73 ± 0.26	1.31	0.08 ± 0.001	6	0.30 ± 0.006	23
3	44	214	120	18.2	0.64	0.41	0.02	6	0.09	21
4	44	129	126	13.1	0.57	0.56	0.02	3	0.06	11
Overall (Mean, SD)		**121 ± 69**	**113 ± 13**	**16.7 ± 2.1**	**0.67 ± 0.15**	**0.84 ± 0.43**	**0.05 ± 0.03**	**5 ± 1**	**0.17 ± 0.12**	**19 ± 5**
Late Spring (May 2016): "Climax Transition"										
5	44	34	91	15.8	1.07	0.99	0.13	13	0.50	50
4	48	73 ± 104	116 ± 22	15.5 ± 0.03	0.85 ± 0.30	0.82 ± 0.16	0.04 ± 0.02	5 ± 1	0.17 ± 0.08	20 ± 6
3	50	9	52	8.7	5.74	3.34	0.12	4	0.45	14
0	54	13	87	3.9	0.95	1.47	0.06	4	0.23	16
2	54	23	54	5.5	3.31	2.86	0.16	5	0.60	21
1	56	34	72	3.9	1.49	1.36	0.10	7	0.38	28
Overall (Mean, SD)		**31 ± 23**	**79 ± 24**	**12.2 ± 5.1**	**1.54 ± 1.52**	**1.32 ± 0.88**	**0.07 ± 0.04**	**6 ± 3**	**0.28 ± 0.17**	**22 ± 10**
Early Autumn (September 2017): "Depletion Phase"										
1	42	38	244	18.0	0.18	0.11	0.03	23	0.10	87
2	44	38	207	8.0	0.21	0.23	0.03	14	0.12	55
3	47	17	200	16.6	0.13	0.18	0.02	8	0.06	32
4	49	40	188	10.4	0.17	0.19	0.02	11	0.08	41
5	52	17	157	8.7	0.39	0.42	0.03	6	0.10	24
6	53	35 ± 2	103 ± 6	7.3 ± 0.6	1.38 ± 0.37	0.66 ± 0.08	0.03 ± 0.01	4 ± 1	0.11 ± 0.03	17 ± 5
Overall (Mean, SD)		**30 ± 11**	**183 ± 48**	**9.6 ± 4.0**	**0.85 ± 0.67**	**0.46 ± 0.24**	**0.03 ± 0.01**	**8 ± 6**	**0.10 ± 0.03**	**31 ± 23**
Early Winter (November – December 2015): "Winter Transition"										
7	40	27	98	18.3	0.57	0.25	0.04	15	0.15	58
6	43	7	103	17.1	0.49	0.19	0.03	17	0.13	67
5	44	79	103	16.2	0.48	0.17	0.03	20	0.13	75
4	46	101	126	15.5	0.45	0.17	0.03	16	0.11	62
3	51	64	59	7.2	1.41	0.11	0.03	25	0.11	96
2	54	95	104	5.5	0.87	0.18	0.03	16	0.11	61
Overall (Mean, SD)		**62 ± 38**	**98 ± 22**	**13.3 ± 5.5**	**0.71 ± 0.38**	**0.179 ± 0.045**	**0.03 ± 0.004**	**18 ± 4**	**0.12 ± 0.02**	**70 ± 14**

Table 3.2. NPP, BP, and BCD. **Station:** where experiments were conducted; **Latitudinal Bin**: stations were binned to the nearest degree based on latitudinal coordinates; **MLD:** mixed layer depth; **Euphotic Zone Depth**: 1% light level; **Temperature**: CTD-recorded temperature integrated and normalized to the depth of the euphotic zone; **Chl *a*:** chlorophyll *a* estimated from CTD fluorescence, integrated and normalized to the depth of the euphotic zone; **NPP**: net primary production integrated and normalized to the depth of the euphotic zone; **BP**: net bacterioplankton production integrated and normalized to the depth of the euphotic zone; **BP:NPP**: the ratio of BP to NPP; **BCD**: bacterioplankton carbon demand or gross bacterioplankton production integrated and normalized to the depth of the euphotic zone. **BCD:NPP**: the ratio of BCD to NPP. Data represent means of estimates from multiple profiles with error representing standard deviations.

Appendix

Positive Pressure Incubation Bottles

5 L Nalgene Biotainer PC bottles were used as the incubation vessels. To sample an incubation, a bottle was pressurized using filtered air, displacing the water volume through a sample line.

Bottle caps were modified to accommodate for sampling via positive pressure. Each cap was fitted with two 0.25” (~6.4 mm) Nalgene polypropylene barbed bulkhead fittings, one of which would accommodate a water sample line while the other an air-intake line. A 3.5 mm length of 1/8” ID x 1/4” OD (~3.2- x 6.4 mm) platinum-cured silicon tubing was affixed to the top of each bulkhead fitting.

For the sample line, a 325 mm length of 1/16” ID x 1/8” OD (~0.06- x 3.2-mm) PTFE tubing was passed through one bulkhead fitting to the bottom of the bottle. Another 7.5-mm length of 1/8” ID x 1/4” OD (~3.2- x 6.4-mm) platinum-cured silicon tubing was inserted to the top-end of the PTFE tubing. Inserted between the platinum-cured silicon and PTFE tubing were 1-mm lengths of 1/16” ID x 1/8” OD (~0.06- x 3.2-mm) platinum-cured silicon tubing, which helped to keep the cap air-tight. Attached to the top end of the sample line were both a polypropylene flow-control clamp and a polycarbonate male Luer lock ring x 1/8” (3.2 mm) hose barb adapter. A polycarbonate female Luer lock ring x 1/8” (3.2 mm) hose barb adapter was attached to the second port, which would accommodate the air-intake line.

Positive Pressure Air Manifold and Sampling

Ambient air was pumped at < 24 kPa using a Fluval Q2 aqurium pump through a Restek refillable hydrocarbon trap. A length of 1/8" ID x 1/4" OD (~3.2- x 6.4 mm) platinum-cured silicon tubing and 1/16" ID x 1/8" OD (~0.06- x 3.2 mm) PTFE tubing was used as the airline. At the end of the airline was a polycarbonate male Luer lock ring x 1/8" (3.2 mm) hose barb adapter, which could be connected to the port of an incubation bottle cap.

Bottles to be sampled were first mixed gently by swirling. After being pressurized with filtered air, ~25 mL of sample is passed through the sample line and discarded. Samples were then collected, in order, for bacterioplankton abundance, total organic carbon (TOC), dissolved organic carbon (DOC), bacterioplankton carbon, and bacterioplankton community composition. Samples requiring filtration were filtered inline by attaching a filter holder or cartridge directly to the sample line.

When a bottle was not being sampled, its sample line was connected to its air-intake port, sealing the bottle from atmospheric contamination.

Bacterioplankton Abundances during DOC Remineralization Setup

Cruise	Station	Whole water	Inoculum (1.2 µm filtrate)	Experimental Mix at T_0
		Cells L^{-1}		
NAAMES 2	1*	$1.84 * 10^9$	$1.68 * 10^9$	$0.46 * 10^9$
NAAMES 2	2	$2.34 * 10^9$	$1.78 * 10^9$	$0.49 * 10^9$
NAAMES 2	3	$1.83 * 10^9$	$1.18 * 10^9$	$0.47 * 10^9$
NAAMES 2	4	$1.89 * 10^9$	$1.31 * 10^9$	$0.25 * 10^9$
NAAMES 2	5*	$1.99 * 10^9$	$1.99 * 10^9$	$0.49 * 10^9$
NAAMES 3	2**	$1.30 * 10^9$	$0.42 * 10^9$	$0.12 * 10^9$
NAAMES 3	3	$1.20 * 10^9$	$0.71 * 10^9$	$0.17 * 10^9$
NAAMES 3	4	$1.13 * 10^9$	$0.62 * 10^9$	$0.23 * 10^9$
NAAMES 3	5*	$1.59 * 10^9$	$1.81 * 10^9$	$0.39 * 10^9$
NAAMES 3	6	$1.81 * 10^9$	$1.41 * 10^9$	$0.42 * 10^9$
NAAMES 4	2RD	$0.65 * 10^9$	$0.51 * 10^9$	$0.15 * 10^9$
NAAMES 4	2RF	$0.78 * 10^9$	$0.52 * 10^9$	$0.15 * 10^9$
NAAMES 4	1	$0.66 * 10^9$	$0.49 * 10^9$	$0.13 * 10^9$
NAAMES 4	2	$1.24 * 10^9$	$0.91 * 10^9$	$0.21 * 10^9$
NAAMES 4	3*	$0.67 * 10^9$	$0.64 * 10^9$	$0.14 * 10^9$
NAAMES 4	4	$0.65 * 10^9$	$0.55 * 10^9$	$0.15 * 10^9$

Appendix Table 3.1. Bacterioplankton abundances estimated by epifluorescence microscopy in whole water (*in situ*), inoculum (1.2 µm filtrate), and the 3:7 inoculum: particle free-water experimental mix at the start of each DOC remineralization experiment. On average, 78 ± 16% of the bacterioplankton population in whole seawater passed through the 1.2 µm filter, but in some cases (n = 4, stations marked with "*") was near or above 100% indicative of poor filtration or potentially, errors in the abundance estimates. The whole water bacterioplankton

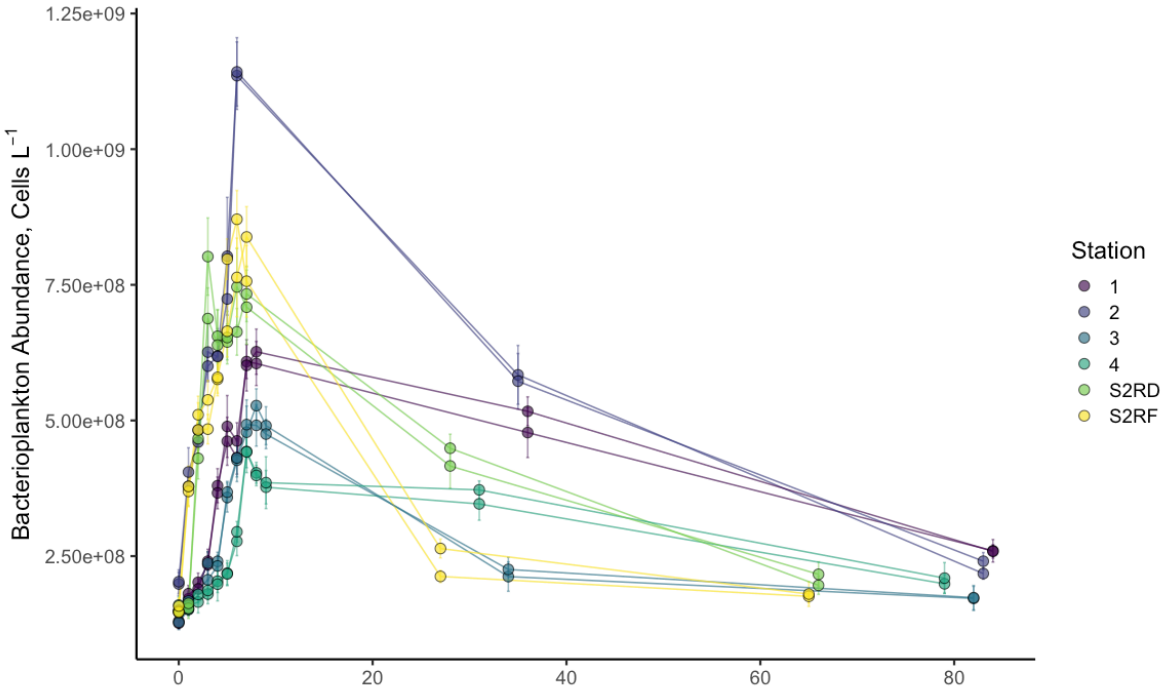

Appendix Figure 3.1. Time series of bacterioplankton abundance in DOC remineralization experiments conducted on all stations of NAAMES 4, displaying marked decrease in abundances after 20 days. Data prior to 20 days represent estimates from incubation bottle samples while data at and beyond 20 days represent estimates from incubation vials.

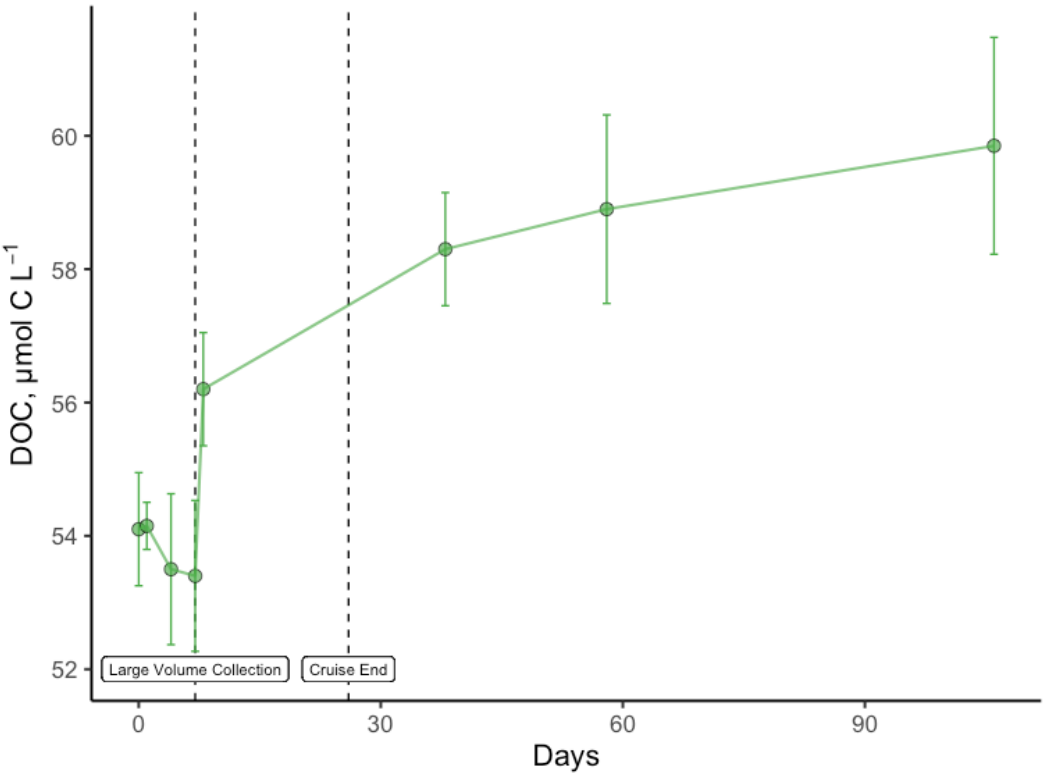

Appendix Figure 3.2. DOC remineralization experiment from NAAMES 2 Station 4 displaying marked increase in DOC from day 7 to 8, following removal of large volumes of incubation water for BOC and DNA sampling. The day after drawing large volume samples, DOC increased 2.8 µmol C L-1 (5.2%) and continued to increase throughout the post-cruise shore-based incubation and sampling period (98 days), casting uncertainty in our ability to observe long-term trends after removing large volumes of incubation water.

DOC versus DOC Comparison*

A direct comparison between filtered DOC concentrations and corresponding DOC* estimates from experiments conducted on both NAAMES 3 and 4 showed that the data were significantly and highly correlated. Filtered DOC concentrations were on average 1.6 μmol C L^{-1} higher than DOC*, a difference near the threshold of analytical resolution, with 95% limits of agreement at 4.1 and -0.9 μmol C L^{-1}. While the stacked GF75 filters retained 78 ± 9% of cells on average, the remainder that passes through the filters may account for some of the systematic positive bias of the filtered DOC measurements relative to DOC*. Because of the observed agreement between the incubation container measurements as well as the availability of data, the present analyses used filtered DOC for NAAMES 2 experiments DOC* for NAAMES 3 and 4 experiments to maximize the use of available data and minimize measurement error due to sample handling.

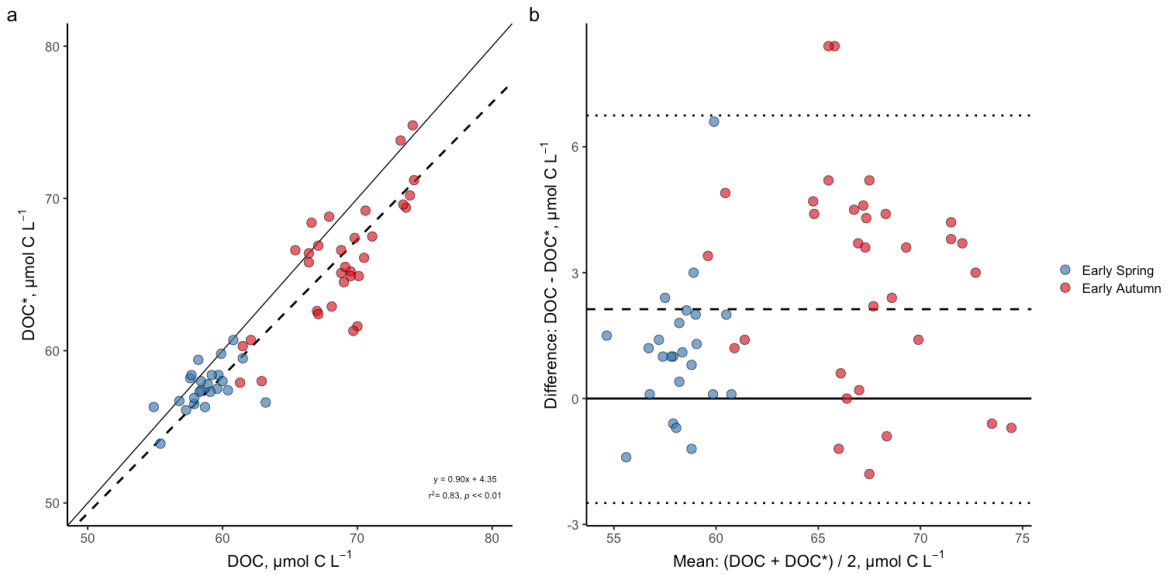

Appendix Figure 3.3. Standardized (reduced) major axis model II linear regression (a) and Bland-Altman/Tukey Mean-Difference plot (b) between DOC concentrations measured filtered samples and estimated by subtracting estimates of bacterioplankton biomass (i.e. BOC) from corresponding measurements of TOC (DOC*). Solid and dashed lines in panels a represents the identity and regression lines, respectively. In panel b, the solid line represents the no-bias line, the dashed line represents the mean-difference or bias line, and the dotted lines represent the 95%

Incubation Vessel Comparison

Single samples for bacterial abundance and replicate DOC samples were drawn over time from both incubation containers over several experiments during NAAMES 4. Measured bacterioplankton abundances and filtered DOC concentrations between the vessel incubations were highly and significantly correlated, with a slight bias towards bottle incubation measurements which were higher by 2.4×10^6 cells L^{-1} and 0.39 µmol C L^{-1} for bacterial abundance and DOC, respectively. The 95% limits of agreement were at 3.4×10^8 and -3.4×10^8 cells L^{-1} for the bacterial abundance measurements and at 2.6 and -1.8 µmol C L^{-1} for the DOC measurements, indicating that both incubation containers tracked similar microbial dynamics.

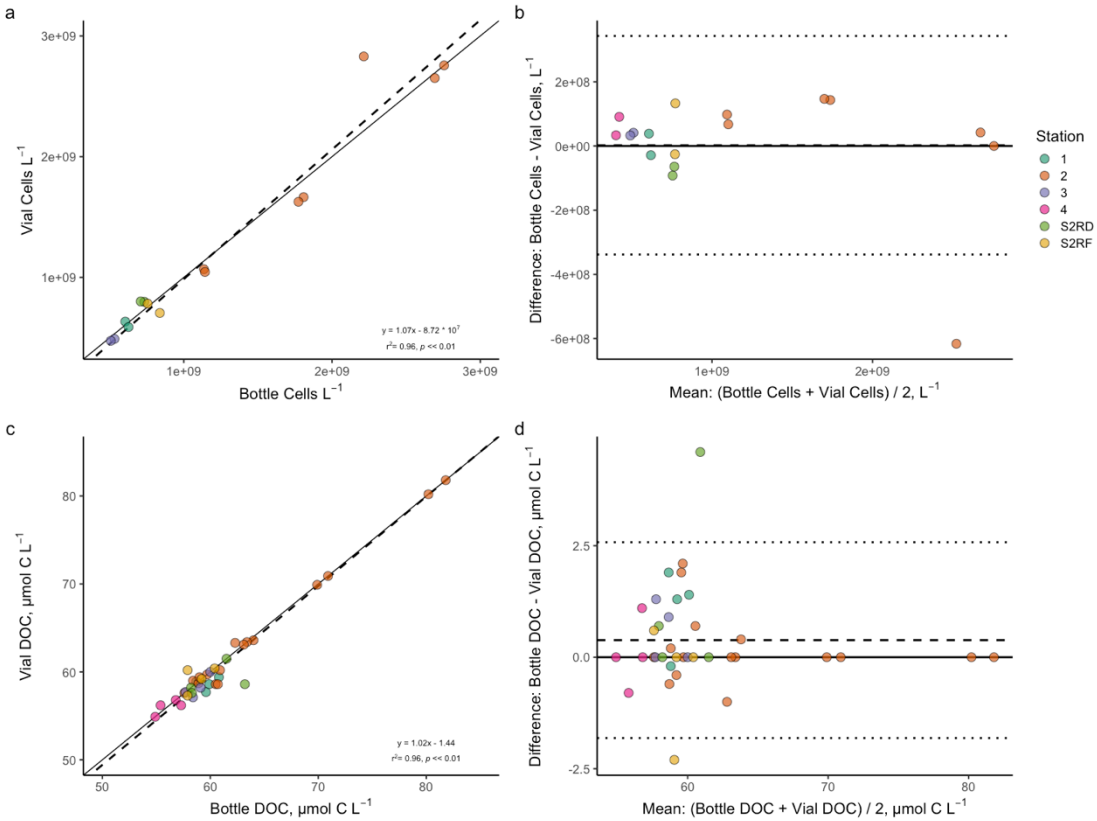

Appendix Figure 3.4. Standardized (reduced) major axis model II linear regression (a, c) and Bland-Altman/Tukey Mean-Difference plots (c, d) between cell abundances (a, b) and DOC concentrations (c, d) measured from bottle and vial incubations conducted on NAAMES 4 (early spring). Solid and dashed lines in panels a and c represent the identity and regression lines, respectively. In panels b and d, the solid line represents the no-bias line, the dashed line represents the mean-difference or bias line, and the dotted lines represent the 95% limits of agreement.

IV. Microbial Response to Physical Stratification following Deep Convection

Abstract

Organic matter produced by primary production in the sunlit ocean can be physically transported to depths within the mesopelagic zone. The mechanisms that drive this export of organic matter include subduction, deep convection, as well as episodic disturbances like passing storms and diel changes in convective mixing. Uncertainty remains around the fate of the organic matter exported to depth by these mechanisms, but a majority is remineralized or respired by heterotrophic microbes. It is rare to have opportunities to observe how microbes respond to organic matter delivery following deep mixing events in situ. Here, we report observations from a three-day occupation of a retentive anticyclonic eddy in the Western North Atlantic in which bacterioplankton growth and community composition responses were tracked as the water column re-stratified following a recent deep convection event. While we observed rapid changes in bacterioplankton carbon and carbon demand throughout the water column, changes in community composition were small and gradual with notable responses by a few mesopelagic bacterioplankton lineages including SAR11 subclade II and SAR202 subclade I.

Introduction

Dissolved organic carbon (DOC) is produced as a result of numerous food web processes (Carlson and Hansell, 2015). However, the magnitude of annual DOC production is ultimately constrained by autochthonous primary production rates. Global net primary production (NPP) produces approximately 53 Pg C y^{-1} (Dunne et al., 2007) and is the main source of dissolved organic carbon (DOC) production (~21 Pg C y^{-1}) in the oceans (Carlson

and Hansell, 2015). The oceanic DOC pool stores approximately 662 Pg C, which is comparable to the inventory of CO_2 in the atmosphere and the amount of carbon in terrestrial biomass (Hansell et al., 2009). Heterotrophic bacterioplankton rapidly recycle DOC for energy generation and biomass synthesis (Azam et al., 1983) and those living in the ocean's surface waters are responsible for remineralizing a majority (~91%) of newly produced DOC (Azam et al., 1993; Carlson and Hansell, 2015). DOC that resists rapid microbial degradation can accumulate in surface waters, generating vertical gradients in DOC (Carlson et al., 1994; Carlson and Hansell, 2015).

Why and how DOC accumulates is not well understood, with a number of hypotheses having been proposed (see reviews in Benner and Amon, 2015; Carlson and Hansell, 2015; Dittmar, 2015). Some DOC compounds accumulate because they are intrinsically resistant to or slowly degraded by heterotrophic utilization (Hansell, 2013; Shen and Benner, 2020). Alternatively, the molecular diversity of organic compounds that comprise the bulk DOC pool can limit unique compounds from existing at detectable concentrations or from encountering microbes with the appropriate uptake mechanisms. Thus, the accumulated DOC pool reflects the sum of these highly diverse but individually low-concentration compounds (Dittmar, 2015). DOC may also accumulate because costs may outweigh the benefits of oxidizing particular compounds, depending on the proximal heterotrophic community structure and its metabolic capabilities (Carlson et al., 2009; Treusch et al., 2009; Giovannoni, 2017; Landry et al., 2017; Saw et al., 2020). It is possible that all of these mechanisms simultaneously contribute to the accumulation of DOC compounds in surface waters, where they are functionally recalcitrant because their supply outpaces microbial consumption (Zakem et al., 2020). However, accumulated DOC that is resistant to rapid

microbial utilization at one geographical location or depth can be readily utilized by heterotrophic bacterioplankton at another (Carlson et al., 2011).

In regions like the Western North Atlantic where annual deep convection occurs, accumulated DOC in surface waters can be physically delivered to the deep ocean. Deep convection obliterates vertical density gradients and redistributes suspended and dissolved organic matter homogenously throughout the mixed layer. The net effect is that DOC is reduced in the epipelagic as lower concentrations from depth are mixed to the surface, and enriched in the mesopelagic as a portion of the accumulated euphotic zone DOC is mixed to depth (Carlson et al., 1994). However, it is estimated that only ~11% of the surface accumulated DOC exported to the deep ocean survives to depths greater than 500 m (Carlson et al., 2010; Hansell et al., 2012), due to its remineralization within the upper mesopelagic. Field and experimental studies have provided evidence for the degradation of surface accumulated DOC by mesopelagic heterotrophic microbes following deep convection. At the Bermuda Atlantic Time-series Study (BATS) site, a portion of the DOC exported out of the euphotic zone following winter deep convection was observed repeatedly to be removed in the upper mesopelagic on the timescales of weeks (Goldberg et al., 2009). At the same time, absolute bacterioplankton abundance in the upper mesopelagic at BATS was observed to increase following deep convection (Carlson et al., 2009), with increases in relative abundance by certain bacterioplankton taxa like SAR11subclade II, OCS116, SAR202, and marine *Actinobacteria* (Morris et al., 2005; Carlson et al., 2009; Treusch et al., 2009; Vergin et al., 2013; Liu et al., 2020a). These observations suggest that some mesopelagic bacterioplankton have the metabolic capability to degrade functionally

recalcitrant DOC that accumulates in surface waters on the timescales of weeks (Morris et al., 2005; DeLong et al., 2006b; Landry et al., 2017).

Metagenomic evidence supports the claim that some mesopelagic microbial lineages are well adapted to utilize compounds that are apparently recalcitrant to epipelagic populations (Saw et al., 2020). Indeed, mixed culture experiments conducted at BATS demonstrated multi-week increases in the relative abundance of slow-growing mesopelagic bacterioplankton (e.g., SAR202, *Methylophaga*, *Hyphomonadaceae*, and *Alcanivoracaceae*) after the introduction of recalcitrant carboxyl-rich alicyclic (CRAM) proxy compounds (Liu et al., 2020b). While these experiments advance understanding about what could happen in the days and weeks following deep convection, measurements of *in situ* microbial responses in the hours to days following deep convection could provide insights regarding the fate of surface accumulated DOC after it is vertically exported from the epipelagic and potentially remineralized in the mesopelagic.

An opportunity to observe microbial responses to deep convection was afforded at a hydrostation occupied in May 2016 during the second of four field campaigns of the North Atlantic Aerosols and Marine Ecosystems Study (NAAMES) (Behrenfeld et al., 2019). Here, we describe changes in the biogeochemistry, bacterioplankton growth, and community structure in the euphotic and upper mesopelagic zones (0 – 75 m and 100 – 200 m, respectively) during the multi-day drifter-following occupation of this hydrostation. We also compare the observations made at this recently and deeply mixed hydrostation (May, 2016) to another hydrostation with strongly contrasting environmental conditions, in which the water column had been stratified for several months (September, 2017). This persistently stratified station was also chosen as it was the only other station that was sampled for

multiple days. This study demonstrates rapid changes in bacterioplankton stocks and rates (particularly in the mesopelagic zone) as a deeply mixed layer shoaled. Interestingly, these dramatic changes only resulted in subtle shifts in bacterioplankton community composition, with noteworthy responses constrained to a few mesopelagic lineages such as SAR11 subclade II and SAR202 subclade I.

Materials and Methods

The two NAAMES campaigns each involved a ship transect aboard the R/V *Atlantis* between 39˚N and 56˚N latitude and -38˚W to -47˚W longitude. In May 2016 (NAAMES 2), the R/V *Atlantis* arrived on a water mass (N2S4, [47.46˚N, -38.72˚W]) that had been recently perturbed by a deep convection event and was subsequently tracked, sampled, and characterized over a period of three days (May 23 [21:46 UTC] - 27 [23:54 UTC]) as the water column re-stratified (Graff and Behrenfeld, 2018). By comparison, in September 2017 (NAAMES 3), the R/V *Atlantis* arrived on a water mass (N3S6, [53.38˚N, -39.54˚W]) that remained strongly stratified over a four-day occupation (September 13 [17:06 UTC] – 17 [18:15 UTC]).

Drifter-following Sample Collection

Surface drifters were deployed from the R/V *Atlantis* upon arrival at each hydrostation and then followed throughout the hydrostation occupation. N2S4 and N3S6 had different physical properties: N2S4 was within the core of a moderately retentive anticyclonic eddy in the dynamic region of the Gulf Stream and North Atlantic Drift while N3S6 was located in a quiescent subarctic region of the northwest Atlantic characterized by large-scale wind-driven circulation and relatively more uniform currents (Della Penna and Gaube, 2019). These differences were reflected in the movement of the deployed drifters. The drifters

deployed at N2S4 moved anticyclonically before being transported outside of the core of the eddy by wind-driven near-surface currents, while those deployed at N3S6 were transported eastward by the wind. Hydrographic data were collected on each day of hydrostation occupation from Sea-Bird Scientific SBE-911+ Conductivity-temperature-depth (CTD) profiler sensors attached to a rosette with 24 x 10 L Niskin bottles. Additional sensors included those for chlorophyll fluorescence (WET Labs ECO-AFL/FL), beam transmission (WET Labs C-Star), turbidity (WET Labs ECO), and oxygen (SBE43). These data are available through NASA's Ocean Biology Distributed Active Archive Center (OB.DAAC) SeaWiFS Bio-optical Archive and Storage System (SeaBASS; https://seabass.gsfc.nasa.gov/naames) and were averaged over 1 m bins for the present analysis. Following previous studies of the NAAMES hydrostations, mixed layer depths for each CTD profile were determined as the depth below 5 m at which the Brunt-Väisälä buoyancy frequency (N^2) was greater than its standard deviation (Graff and Behrenfeld, 2018; Morison et al., 2019). Apparent Oxygen Utilization (AOU, μmol O_2 L^{-1}) is defined as the depletion of oxygen relative to saturation and was calculated for each binned CTD profile (to 1 m) as the difference between the saturation oxygen concentration and the observed oxygen concentration. Oxygen saturation was estimated from potential temperature and salinity following Weiss (1970).

The Niskin bottles collected seawater samples at nominal depths of 5, 10, 25, 50, 75, 100, 150, and 200 m for analysis of chlorophyll *a*, phytoplankton cell abundance, [nitrate + nitrite], bacterioplankton cell abundance, bacterioplankton leucine incorporation rate, DOC, and total dissolved amino acids (TDAA). These data are available through OB.DAAC SeaBASS (https://seabass.gsfc.nasa.gov/naames), as well as the Biological & Chemical

Oceanography Data Management Office (BCO-DMO, DOI: 10.26008/1912/bco-dmo.824623.1). All processed data, analyses, and code presented here are available on GitHub (https://github.com/nbaetge/naames_multiday).

Chlorophyll a, Phytoplankton Cell Abundance, and Net Primary Production

Chlorophyll *a* concentrations (µg L^{-1}) were measured by fluorometric analysis using the acidification technique and a Turner Designs 10AU digital fluorometer (Mueller et al., 2003). For each sample, 500 mL raw seawater were filtered through a 25 mm 0.45 µm (Millipore HA) nitrocellulose filter, which was then extracted in 90% acetone for 48 hours at 0˚C. Fluorescence was measured before and after acidification to determine Chlorophyll *a* concentration. Phytoplankton abundances (cells L^{-1}) for < 64 µm diameter cells were determined within hours of sample collection using a BD Influx Sorting Flow Cytometer and separated into four major groups (*Prochlorococcus*, *Synechococcus*, Picoeukaryotes, Nanoeukaryotes) (see methods in Graff and Behrenfeld, 2018). Total phytoplankton cell abundance was calculated as the sum of the abundances of all the groups. Vertically-resolved net primary production (NPP) (µmol C L^{-1} d^{-1}) was estimated using the Photoacclimation Productivity Model (PPM) from Fox et al (2020), which accounts for physiological adjustments in intracellular chlorophyll concentration in response to light and nutrient availability (Behrenfeld et al., 2016). There was strong agreement between NPP estimates from the PPM and measurements of 24 h ^{14}C-uptake conducted at all NAAMES hydrostations (Fox et al., 2020).

Bacterioplankton Cell Abundance and ^{3}H-leucine Incorporation

Bacterioplankton cell abundances (cells L^{-1}) were determined for whole seawater samples preserved with certified ACS formalin to a final concentration of 1% (vol:vol).

Within 36 hours of collection, cells from each sample were filtered onto a blackened 0.2 μm polycarbonate (PC) membrane filter, stained with DAPI (4',6-diamidino-2-phenylindole dihydrochloride, 5 mg mL^{-1}), mounted onto a slide with high viscosity immersion oil (Thermo Scientific Richard-Allan Scientific Resolve) and stored at –20˚C until enumeration. DAPI-stained cells were manually enumerated using an Olympus BX51epifluorescence microscope with ultraviolet excitation at 1000X magnification. 12 fields-of-view were counted for each slide and, on average, 50-60 cells were counted for each field-of-view (Porter and Feig, 1980).

Bacterioplankton ^{3}H-leucine incorporation rates (pmol ^{3}H-Leu L^{-1} h^{-1}) were estimated using a modified version of the microcentrifuge method (Smith and Azam, 1992). For each depth, a dead control (killed immediately with 100 μL of 100% trichloroacetic acid [TCA]) and replicate 1.6 mL seawater samples were spiked with ^{3}H-Leu (20 nM; specific activity 50.2-52.6 Ci/mmol; Perkin Elmer, Boston, MA). After incubating in the dark for 2-3 hours at ± 2°C of *in situ* temperature, incubations were terminated with 100 μl cold 100% TCA. Cells were pelletized after a series of microcentrifugation steps, washed with 5% TCA, 80% ethanol (vol/vol), and resuspended in Ultima Gold scintillation cocktail as described in Ducklow et al. (2001). Radioactivity was measured using a Hidex 300 Scintillation Analyzer and was corrected for quenching using an external gamma source and a quench curve. The coefficient of variation (CV) between measurements from replicate incubations was generally 1-15%. However, CVs were often between 20-30% for deep samples because of their lower incorporation rates.

Dissolved Nutrients, Dissolved Organic Carbon, and Total Dissolved Amino Acids

Nitrate + Nitrite concentrations (N + N, μmol N L^{-1}) at each depth were determined from samples that were gravity-filtered directly from the Niskin bottles through 47 mm 0.8 μm polycarbonate (Millipore) filters and stored at -20˚C in sterile 50 mL conical centrifuge tubes. Samples were analyzed using a Lachat QuickChem QC8500 automated ion analyzer (University of Rhode Island Graduate School of Oceanography Marine Science Research Facility), which measures N+N with a precision of ∼0.3 μmol L^{-1}.

Replicate DOC samples at each depth were gravity filtered directly from the Niskin bottles through 47 mm 0.7 μm GF/F filters (Whatman, first flushed with 100 mL sample water) into pre-combusted 40 mL EPA borosilicate glass vials. Samples were acidified to a pH of ≤ 3 by adding 50 μL DOC-free 4 N HCl and stored at 14˚C in a volatile organic-free environmental chamber until analysis. DOC concentrations (μmol C L^{-1}) were measured in batches of ≤ 35 samples using the high-temperature combustion method (Carlson et al., 2010) on Shimadzu TOC-V or TOC-L analyzers. Concentrations were quantified using standard solutions of glucose and low carbon ultra-pure water. Samples were systematically referenced against surface and deep seawater calibrated with consensus reference material (Hansell SSR Lot#08-18), which were run every 6-8 samples. Precision of the Shimadzu analyzers was within 2% CV.

Total dissolved amino acids (TDAA) samples were gravity filtered directly from the Niskin bottles through 47 mm 0.7 μm GF/F (Whatman, first flushed with 100 mL sample water) into acid-washed 60 mL high density polyethylene (HDPE) bottles and stored at -20˚C. Samples were processed following Liu et al (2020a), where samples were hydrolyzed in 6N HCl under nitrogen for 20 hours at 110˚C, neutralized using nitrogen evaporation,

derivatized with ortho-phthalaldehyde, and measured using a Dionex ICS5000+ high performance liquid chromatography (HPLC) equipped with a fluorescence detector (excitation = 330 nm, emission = 418 nm). The molecular formula of each amino acid resolved by the HPLC was used to calculate its carbon concentration in μmol C L^{-1}. Thus, TDAA represents the sum of the carbon concentrations of all the individual amino acids. DOC-normalized yields of TDAA were calculated as the percentage of total DOC measured as amino acid carbon.

Derived Variables for NAAMES 2 Station 4 (N2S4)

Net bacterioplankton production (μmol C L^{-1} d^{-1}) was estimated for each depth by applying a Leucine conversion factor of 1.5 kg C (mol Leu incorporated) $^{-1}$ (Simon and Azam, 1989). Bacterioplankton carbon demand (BCD) (μmol C L^{-1} d^{-1}) was calculated as net bacterioplankton production divided by the bacterioplankton growth efficiency (BGE) (0.24) estimated by Baetge et al. (2021) from DOC remineralization experiments conducted at 10 m.

Phytoplankton cell abundance, NPP, AOU, bacterioplankton cell abundance and carbon demand, DOC, and TDAA profiles were all integrated for the euphotic and the upper mesopelagic zones. Here, the euphotic zone is defined as the depth horizon between 0 and 75 m while the upper mesopelagic zone is defined between 100 and 200 m. The integrated stocks and rates of net primary production and bacterial production for both depth horizons were depth-normalized to provide mean volumetric concentrations and rates for the respective depth zones.

Bacterioplankton Community Composition

Nucleic acid sample collection, extraction, purification and 16S rRNA gene amplification, library preparation, sequencing, and amplicon assignment are detailed in Bolaños et al (2021). Samples from each depth were collected by filtering four liters of seawater through a 0.22 µm Sterivex filter (polyethersulfone membrane, Millipore) and preserved in sucrose lysis buffer (SLB, 20 mM EDTA, 400 mM NaCl, 0.75 M sucrose, and 50 mM Tris-HCl, pH 9.0) at -80˚C. Nucleic acids were extracted and purified following the phenol: isoamyl alcohol: chloroform (25:1:24) protocol of Giovannoni et al (1996). The V1-V2 region of the 16S rRNA gene was amplified via polymerase chain reaction (PCR) using the 27F (5'-AGAGTTTGATCNTGGCTCAG-3') forward and 338 RPL (5'-GCWGCCWCCCGTAGGWGT-3') reverse primers, each with respective Illumina overhang adapters (Bolaños et al., 2021). Twenty-five µl PCR reactions consisted of 2.5 µL (5 ng μL^{-1}) of genomic DNA template, 5 µl of each primer (1 µM) 12 µL of 2x KAPA HiFi HotStart ReadyMix, and 5 µL PCR water. Thermocycling conditions of the PCR reactions were 3 minutes at 95˚C, 25 cycles of 30 seconds at 95˚C, 30 seconds at 55˚C, 30 seconds at 72˚C, and 5 minutes at 75˚C. Libraries for each amplicon reaction product were constructed by attaching dual indices and Illumina sequencing adapters with the Nextera XT Index Kit using a second PCR amplification. Purified libraries were pooled in equimolar concentrations and sequenced using the Illumina MiSeq platform (v2, 2x250 PE lane) at the Center for Genome Research and Biocomputing (Oregon State University, Corvallis, OR, USA). Amplicon sequence datasets can be found in the NCBI SRA database under the BioProject identifier PRJNA627189.

Primer sequences were removed from demultiplexed FASTQ files using the CutAdapt algorithm (Martin, 2011). All subsequent sequence analyses were performed using the R software environment (v 4.0.0). Using the package *dada2* (v 1.2.0, Callahan et al., 2016), trimmed FASTQ files were quality filtered, dereplicated, and merged to create an amplicon sequence variant (ASV) table, from which potential chimeras were removed de novo. ASVs were taxonomically assigned using the Silva database (v 123, Quast et al., 2013) and PhyloAssigner (v089, Vergin et al., 2013). Phylogenetic databases are available at https://www.github.com/lbolanos32/NAAMES_2020. Using the function *rarefy_even_depth* in the package *phyloseq* (v 1.32.0, McMurdie and Holmes, 2013), sequence read counts were subsampled to the minimum sample read depth (9702 reads) with replacement to standardize for sampling effort. The Chao1 alpha diversity index was estimated using the *phyloseq* function *estimate_richness*. Pairwise comparisons of the Chao1 index between depth horizons on each day of hydrostation occupation were performed with t-tests using the function *compare_means* of the package *ggpubr* (v 0.3.0). Bray-Curtis dissimilarities were calculated using the *vegdist* function of the package *vegan* (v 2.5-6, Oksanen et al., 2013). NMDS ordinations with Bray-Curtis dissimilarities were computed with the *phyloseq* function *ordinate*. One-way permutational multivariate ANOVA (PERMANOVA) was used to characterize the degree of similarity between community composition across hydrostations, depth horizons, and time using the function *adonis* in the R package *vegan* (v 2.5-6) (Anderson, 2001). Homogeneity of dispersion, or variance, among sample groups was assessed using the *vegan* function *betadisper* (Anderson, 2006). For all statistical analyses, p-values of > 0.05, ≤ 0.05, and ≤ 0.01 are described as not significant, significantly different (*), or highly significantly different (**), respectively. For each the euphotic and upper

mesopelagic zones, the relative abundance of a taxonomic group to the family level was calculated by summing its ASV counts across all depths in the depth horizon and then dividing the summed counts by the total counts in the depth horizon. An approximation of cell abundance for each taxonomic group was estimated using the product between the relative abundance of its sequences and the total cell abundance, normalized to its gene copy number, hereafter termed '16S rRNA-estimated cell abundance'. Bacterial ribosomal RNA copy number information was retrieved from the ribosomal RNA operon copy number database (*rrn*DB) (Stoddard et al., 2015). If copy number information was not available for a phylogenetic order, then the copy number for the next higher taxonomic rank was used.

Results

NAAMES 2 Station 4 (N2S4)

The mixed layer depth in the anticyclonic eddy of N2S4 was greater than 200 m upon occupation on May 24, 2016 and shoaled over the next 4 days to < 20 m, with sustained thermal stratification after the first day (Figure 4.1a, b). On the last day on station the R/V *Atlantis* drifted from the eddy's core to its periphery which had distinct near-surface and mesopelagic acoustic backscattering signatures (Della Penna and Gaube, 2020). The change in physical characteristic indicate that biological distributions and rate process likely varied between the eddy regions. Thus, the data presented here are restricted to those collected within the eddy core over the first three days of hydrostation occupation. On the first day of occupation, biological and chemical parameters, including N+N, chlorophyll *a*, phytoplankton cell abundance, bacterioplankton production, AOU, and DOC, were all homogenously distributed over the surface 200 m, indicating that the eddy had experienced a recent deep mixing event (Figure 4.1c – e, 4.1g, 4.1j).

In the euphotic zone (0 – 75 m), there were clear increases in chlorophyll *a*, phytoplankton cell abundance, and net primary production (NPP) corresponding to decreases in N+N and AOU (Figure 4.1c – g, 4.2a, 4.2b, 4.2e, 4.2f). The relative abundance of prasinophytes and diatoms increased over the station occupation (Bolaños et al., 2021), but so did the growth rates of other picoeukaryotes and cyanobacteria (Morison et al., 2019). Bacterioplankton cell abundance, ^{3}H-Leucine incorporation (i.e., net bacterioplankton production), and carbon demand (BCD) all increased in the euphotic zone over time. As a result of the competing photoautotrophic and heterotrophic processes, we were not able to resolve changes in the bulk DOC concentrations during our station occupation. Although bulk DOC concentrations within the euphotic zone did not change significantly and averaged 53.4 ± 0.2 μmol C L^{-1}, the contribution of total dissolved amino acids (TDAA) to the bulk DOC pool increased by ~9% (Figure 4.1j, 4.1k, 4.2g, 4.2h).

Phytoplankton cell abundance and chlorophyll *a* declined within the upper mesopelagic zone (100 – 200 m), with NPP remaining at near zero (Figure 4.1d – f, 4.2a, 4.2b). While there was a small increase in AOU, there was a clear increase in N+N corresponding to increases in bacterioplankton cell abundance and BCD. Bulk DOC concentrations displayed a decreasing trend within the upper mesopelagic zone, but these changes were not statistically significant and DOC concentrations averaged 53.0 ± 0.4 μmol C L^{-1} over the occupation of station N2S4. The contribution of TDAA to the bulk DOC pool decreased by ~10% (Figure 4.1j, 4.1k, 4.2g, 4.2h).

NAAMES 3 Station 6 (N3S6)

In contrast to N2S4, the water mass occupied at 53.38˚N, -39.54˚W over four days in September 2017 displayed little change in its mixed layer depth (mean of 34 ± 2 m) and

remained thermally stratified throughout the occupation (Figure 4.3a, b). Chlorophyll *a*, bacterioplankton ^{3}H-Leucine incorporation, and DOC did not systematically vary within the euphotic zone (0 – 75 m) over the four-day occupation. Changes in other variables, including N+N, NPP, and phytoplankton and bacterioplankton cell abundances, were also not systematic and were dampened relative to the changes observed at N2S4. Inorganic N+N concentrations were minimal and remained so throughout the occupation, limiting phytoplankton production and cell abundance (Figure 4.3c – j). The phytoplankton community was stable over the course of station occupation and consisted of a diverse array of eukaryotes, including cryptophytes, prymnesiophytes, pelagophytes, and bacillariophytes, and an enhanced abundance of cyanobacteria relative to N2S4 (Bolaños et al., 2021). In general, the upper mesopelagic (100 – 200 m) exhibited little temporal change in measured property profiles, although some minor changes could be discerned for N+N and AOU (Figure 4.3c – j).

Bacterioplankton Community Composition

Bacterioplankton profiles were analyzed over the surface 200 m to assess community composition shifts during rapid re-stratification of the deeply-mixed water column at N2S4 and to compare these dynamics with properties of a persistently stratified system (i.e., N3S6). Bacterioplankton ASV richness at N3S6 was elevated in the upper mesopelagic zone relative to the euphotic zone, whereas it was not significantly different between the depth horizons at N2S4. ASV richness throughout the water column at N2S4 was comparable to that of the upper mesopelagic zone at N3S6 (Figure 4.4). NMDS ordination based on Bray-Curtis dissimilarities (stress = 0.02) showed N2S4 communities clustering distally from

those of N3S6 (PERMANOVA $p << 0.01$), with variances (i.e., dispersions) between the groups being significantly different (ANOVA $p << 0.01$) (Figure 4.5a).

At N2S4, variance was similar between the euphotic and mesopelagic zones (ANOVA $p = 0.24$) and communities were not significantly different (PERMANOVA $p = 0.79$). However, there were significant differences in community structure within the upper mesopelagic zone over time (NMDS Bray-Curtis dissimilarity stress = 0.10, PERMANOVA $p = 0.04$) (Figure 5b). Variance between euphotic and upper mesopelagic zone communities at N3S6 was similar (ANOVA $p = 0.38$). While there was some separation between euphotic and upper mesopelagic zone communities at N3S6 (NMDS Bray-Curtis dissimilarity stress = 0.02), they were not significantly different (PERMANOVA $p = 0.07$). This is likely due to the inclusion of communities below the thermocline (75 m) as a part of the euphotic zone. Variance between groups within the euphotic and upper mesopelagic zones at N3S6 was similar (ANOVA $p = 0.92$ and $p = 0.85$, respectively) and community structure within these depth horizons did not change significantly over time (PERMANOVA $p = 0.78$ and $p = 0.13$ for the euphotic and upper mesopelagic, respectively). (Figure 4.5c).

During the re-stratification of N2S4, subclades (approximately Family-level) of SAR11 dominated in relative abundance. During station occupation, SAR11 increased by ~4% in the euphotic zone and represented ~45% of the bacterial community, whereas in the upper mesopelagic it increased by ~7% to represent ~47% of the community (Figure 6). The relative abundance of SAR 11 subclade 1a was greatest of all SAR11 subclades and increased by ~3% and ~5% to represent ~35% and ~36% of the total community in the euphotic and upper mesopelagic zones, respectively throughout the station occupation (Figure 4.6a). Of the remaining SAR11 subclades (I, IB, II, IV), only subclades IB and II

showed changes (≤ 1%) in relative abundance in the upper 200 m, individually comprising less than 5% of the bacterioplankton community in each the euphotic and mesopelagic zones. All members of the SAR11 clade increased in 16S rRNA-estimated cell abundance as total community abundance increased throughout the surface 200 m of the water column. Members of the Gammaroteobacteria *Oceanospriallales* were the next most relatively abundant members of the total bacterioplankton community, particularly ZD0405, SAR86 and *Oceanospirillaceae*, and together represented 17 – 18% of the community in each the euphotic and mesopelagic zones. While the relative abundance of these families did not change significantly in the euphotic zone, the relative abundance of *Oceanospiralles* decreased by ~4% in the upper mesopelagic zone with families ZD405 decreasing by ~2%, SAR86 decreasing by ~1%, and *Oceanospirillaceae* decreasing by ~1% (Figure 4.6a). However, the total bacterioplankton community abundance increased in the upper mesopelagic (Figure 4.1h); thus, if this this increase in cell abundance is taken into account with the changes in relative abundance of each taxonomic family, 16S rRNA-estimated cell abundances reveal increasing trends in ZD405 and SAR86. *Flavobacteriales* (~8 ± 1%), an unassigned group of Marinmicrobia SAR406 (~5 ± 1%), OCS116 (~5%), *Rhodobacterales* (~4 ± 1%), *Rhodospirillaceae* (~3 ± 1%), and *Acidimicrobiales* (~2%) were the next most relatively abundant orders across both depth horizons, contributing to greater than or equal to ~2% of the total bacterioplankton community. These bacterial lineages showed little change in relative abundance over time but did increase in estimated 16S rRNA-estimated cell abundance. The change in relative abundance for all remaining orders in both depth horizons over the station occupation of N2S4 were less than 1%. However, many of the bacterioplankton families within these orders increased in estimated 16S rRNA-estimated

cell abundance despite not changing in relative abundance. For instance, while members of the SAR202 subclade I remained at a constant relative abundance of 5 ± 1% within the upper mesopelagic community, the overall bacterioplankton cell abundance increased by two-fold; thus, throughout the occupation of N2S4 we estimate that members of SAR202 also increased in 16S rRNA-estimated cell abundance by a factor of two. Similarly, members of *Acidimicrobiales* subgroup OM1, SAR116, and *Salinisphaeraceae* all did not change in relative abundance in the upper mesopelagic over the occupation of N2S4, but the change in 16S rRNA-estimated cell abundances is estimated to have increased by 115%, 107%, and 86%, respectively (Figure 4.6, 4.7).

Discussion

Microbial Response in the Mesopelagic

Over the three-day occupation of N2S4, net primary production coincided with inorganic nitrogen utilization and the reduction of AOU in the euphotic zone (0 – 75 m) (Figure 1c – g). Increases in phytoplankton relative abundance were primarily attributed to prasinophytes and diatoms (Bolaños et al., 2021), but growth rates of other picoeukaryotes and cyanobacteria also increased over the occupation (Morison et al., 2019).

Bacterioplankton growth and production in the euphotic zone also responded positively to mixed layer shoaling following deep convection (Figure 4.1f, 4.1h, 4.1i, 4.2d). Though NPP outpaced BCD, changes in the bulk DOC concentration were not resolvable over the timescale of station occupation. Despite our inability to resolve changes in the bulk DOM pool, increases in both the concentration and the relative contribution of TDAA to the bulk DOC pool (Figure 4.1j, 4.1k, 4.2g, 4.2h) suggest that the quality of the accumulated DOM pool changed to less diagenetically altered composition (i.e., fresh and less

recalcitrant) within the euphotic zone throughout station occupation. Amino acids comprise a large proportion of labile DOC and are preferentially and rapidly consumed by heterotrophic bacterioplankton (Keil and Kirchman, 1993; Cowie and Hedges, 1994; Davis and Benner, 2005). The elevated contribution of TDAA to the bulk DOC pool is thus indicative of newly produced DOM and can result from a variety of pathways including direct release from phytoplankton (Granum et al., 2002) or archaea (Bayer et al., 2019), through zooplankton egestion and excretion (Maas et al., 2020), or particle solubilization via processes like grazer sloppy feeding (Lampert, 1978) and viral lysis (Middelboe and Jørgensen, 2006). The change in DOM composition supports the hypothesis that the flux of labile DOM at the nmol L^{-1} level partially supported the enhanced BP and associated BCD.

In the upper mesopelagic zone (100 – 200 m), declines in both chlorophyll *a* and NPP and the increase in AOU reflect net heterotrophy. Furthermore, the decrease in phytoplankton cell abundance is suggestive of active loss through grazing or particle solubilization (Figure 4.1d, 4.1e, 4.2a, 4.2b). These trends in AOU and phytoplankton carbon provide support for the proposed pathway in which the mixed layer pump exports dissolved and suspended particulate organic carbon to depth by convection, which then fuels mesopelagic food webs and metabolic demand (Carlson et al., 1994; Dall'Olmo et al., 2016; Lacour et al., 2019).

During the occupation of hydrostation N2S4, bacterioplankton cell abundance, production, and BCD increased throughout the upper mesopelagic as NPP and phytoplankton carbon declined (Figure 4.2h, 4.2i). The BCD was supported by the flux of labile DOM, but the source of this labile material remains unknown. The increase in BCD and coincident loss of mesopelagic chlorophyll *a* and phytoplankton cell abundance suggests

that POM losses through grazing or solubilization delivered into the upper mesopelagic by recent deep convection mixing may have been a potential source of freshly produced labile DOC, as suggested in previous studies (Cho and Azam, 1988; Smith and Azam, 1992; Smith et al., 1995).

^{3}H-Leucine incorporation in the upper mesopelagic at N2S4 was 6.4 ± 1.6 pmol C L^{-1} d^{-1} upon occupation (Figure 4.1i), well above the background ^{3}H-Leucine incorporation rate observed in the mesopelagic of the stratified station of N3S6 (0.4 ± 0.2 pmol C L^{-1} d^{-1}, Figure 4.3i). The mean and median background ^{3}H-Leucine incorporation rates, considered here to be for depths between 100 and 500 m, for all stations occupied during NAAMES 3 when stratification was strongest throughout the study region were 2.6 pmol C L^{-1} d^{-1} and 1.7 pmol C L^{-1} d^{-1}, respectively (see data in OB.DAAC SeaBASS [https://seabass.gsfc.nasa.gov/naames] or BCO-DMO [DOI: 10.26008/1912/bco-dmo.824623.1]). This finding indicates either that the extant bacterioplankton community was responding to labile DOC delivered from the euphotic as well as production in the mesopelagic or that the elevated activity was mixed in from the surface and then continued to increase over the station occupation. Upper mesopelagic ^{3}H-Leucine incorporation continued to increase over the subsequent two days at N2S4 to reach a maximum of 11.7 ± 1.9 pmol C L^{-1} d^{-1} (Figure 4.1i).

Although the decreasing trend in bulk DOC in the upper mesopelagic over the course of hydrostation N2S4 occupation was not statistically significant, changes in the TDAA concentration and contribution to bulk DOM indicated that DOM quality was being transformed to a more altered state in the upper mesopelagic zone (Figure 4.2g, 4.2h). This observation is consistent with the argument that heterotrophic bacterioplankton can alter

DOM concentration and quality once isolated in the mesopelagic (Goldberg et al., 2009; Kaiser and Benner, 2009).

While the data presented here do not provide unequivocal evidence for the degradation of surface accumulated DOC by mesopelagic heterotrophic microbes, they do demonstrate that microbes respond rapidly to the export of less diagenetically altered organic matter from the euphotic zone as the water column physically stratifies following deep convection. Changes in the upper mesopelagic accounted for 35% and 65% of the total increases in bacterioplankton cell abundance and BCD observed in the surface 200 m, respectively.

Gradual Changes in Bacterioplankton Community Composition

In the persistently stratified water column of NAAMES 3 Hydrostation 6 (N3S6, Figure 4.3), bacterioplankton communities were structured over depth (Figure 4.4b), with euphotic communities differentiating from upper mesopelagic communities (Figure 4.5a, 4.5b). These observations have been previously reported for the NAAMES region and are consistent with those of studies in pelagic systems (Giovannoni et al., 1996; Field et al., 1997; DeLong et al., 2006b; Treusch et al., 2009; Sunagawa et al., 2015; Bolaños et al., 2021). Community composition within the respective euphotic and mesopelagic zones did not change significantly over the N3S6 occupation. Taxonomic richness increased with increasing depth (Figure 4.4), a pattern also observed throughout the global ocean (Treusch et al., 2009; Sunagawa et al., 2015) that reflects the range of niches resulting from heterogeneity in organic and inorganic matter quality and availability.

In contrast to the vertical structure observed at N3S6, the microbial community at N2S4 was homogenized throughout the surface 250 m during and shortly following mixing. The taxonomic richness of N2S4 in the euphotic and mesopelagic zones was 642 ± 123 and

693 ± 152, respectively, compared to 428 ± 92 and 652 ± 108 for the euphotic and mesopelagic zone of N3S6, respectively (Figure 4.4). This pattern suggests that deep convection was a mechanism that enhanced community richness in the euphotic zone, while not simultaneously reducing richness in the upper mesopelagic. Differences in community composition between the two stations may not only be attributed to differences in physical dynamics, but also to location in the Western North Atlantic, with N2S4 located in the subtropics and N3S6 in the subarctic.

Over timescales of weeks to months, shifts in upper mesopelagic bacterioplankton community composition have been observed at sites where deep convection occurs, including BATS (Carlson et al., 2009; Treusch et al., 2009; Giovannoni and Vergin, 2012), with increases in the relative abundance of SAR202, *Acidimicrobiales* clade OM1, *Salinisphaeraceae*, OCS116, and SAR11 subclade II, (Morris et al., 2005; Carlson et al., 2009; Treusch et al., 2009; Vergin et al., 2013). Some of these mesopelagic bacterioplankton are hypothesized to retain the metabolic capability to degrade functionally recalcitrant DOC that accumulates in surface waters on the timescales of weeks (Morris et al., 2005; DeLong et al., 2006b; Landry et al., 2017; Saw et al., 2020).

SAR202, a free-living member of the phylum *Chloroflexi*, have been observed to oxidize lignin, a recalcitrant CRAM-like polymeric compound (Liu et al., 2020b). These bacterioplankton contribute ~ 10% of the total bacterioplankton abundance in the mesopelagic and bathypelagic realms of the Atlantic and Pacific (Morris et al., 2004; Mehrshad et al., 2018; Saw et al., 2020; Bolaños et al., 2021), suggesting that they may play an important role in the remineralization of surface-accumulated DOC (Landry et al., 2017). *Acidimicrobiales* and *Salinisphaeraceae* have also been shown to be capable of using

complex carbon sources derived from phytoplankton (Liu et al., 2020a). SAR11, a group of free-living aerobic heterotrophic alphaproteobacteria that are ubiquitous in the ocean, is made up of a variety of ecotypes adapted to different ocean niches (Brown et al., 2012; Vergin et al., 2013). Over a seven year time-series in the NW Mediterranean Sea, Salter et al (2015) observed that the diversity of SAR11 ecotypes in the upper 5 m increased following physical mixing, with the elevated contributions of subclades Ib and II interrupting the predominance of subclade Ia during periods of stratification, low phytoplankton biomass, and severe phosphate limitation. Similarly at BATS, SAR11 subclade II becomes annually prevalent in the upper mesopelagic as the water column stratifies in the late spring, after semi-labile DOM is delivered to the upper mesopelagic from the surface by winter deep convection (Carlson et al., 2009). In fact, SAR11 subclade II dominated the upper mesopelagic following deep convective overturn in the late winter and early spring throughout the subtropics in the NAAMES study region (Bolaños et al., 2021).

As N2S4 thermally stratified over the hydrostation occupation, microbial populations and organic matter became trapped at depth. Our expectation was that a succession in bacterioplankton community structure would be observed over time that differentiated the upper mesopelagic from the euphotic zone. Specifically, we hypothesized that the upper mesopelagic community would become more represented by lineages typifying mesopelagic zones in the subtropical regions of the Western North Atlantic, including SAR202 and SAR11 subclade II (Bolaños et al., 2021). What we observed was that the temporal turnover of bacterioplankton community structure over the three-day occupation at N2S4 was significant but subtle and that communities did not clearly diverge between the euphotic and upper mesopelagic (Figure 4.5b) over such a short time scale. We interpret these findings at

N2S4 as reflecting a transient phase in microbial community structuring that, if sustained over a longer period, transitions from a mixed system to a persistently stratified water column like that of N3S6 (Figure 4.5c).

Despite observing rapid changes in bacterioplankton cell abundance and BCD, the duration of our occupation of N2S4 was simply not long enough to resolve a clear separation in community composition between the euphotic and mesopelagic zones. Upper mesopelagic increases in the relative abundance and/or cell abundance of bacterioplankton taxa that typically dominate the euphotic zone, like SAR11 subclade Ia and members of order *Flavobacteriales* (Bolaños et al., 2021), indicate that some of the organic matter exported to depth by deep convection was labile in character and could support the growth of these more surface-associated lineages. Given more time, we hypothesize that a clear vertical separation of community structure would become evident as the sources of labile DOM become scarce. These conditions would be unfavorable to taxa typical of euphotic zone communities, like SARII subclade Ia and *Flavobacteriales*, which would be outcompeted in the upper mesopelagic by taxa that are better adapted to utilizing surface-accumulated, more recalcitrant DOM. Furthermore, our observations relied on 16S rRNA gene amplification using V1-V2 primers that only targets bacterioplankton and plastid. As such, our analysis excluded archaeal responses (Wear et al., 2018) that could have been important given that deep-sea archaea have the capacity to degrade complex carbon compounds (Ouverney and Fuhrman, 2000; Li et al., 2015; Bergauer et al., 2018) and have been observed to assimilate phytoplankton-derived exopolymeric substances (Boutrif et al., 2011).

Interestingly, a significant, albeit subtle, shift in bacterioplankton community composition (Figure 5b, $p = 0.04$) was observed in the mesopelagic of N2S4, indicating that separation of communities between the euphotic and mesopelagic zones was beginning to occur. Notable changes in relative abundance in the mesopelagic zone were attributed to an increase in the SAR11 clade, particularly subclade Ia, and decreases in members of *Oceanospirillales* (Figure 4.6, Figure 4.7). While there was little, if any, change in the relative abundance of other bacterioplankton orders and families, inferring microbial responses or the lack thereof solely from relative abundance data can be misleading (Figure 4.7).

In a community that increases in cell density and biomass, an individual taxonomic group that does not change in relative abundance would increase in 16S rRNA-estimated cell abundance and would actually be considered a responder to new environmental conditions. For example, the relative abundance of taxonomic groups like SAR202 subclade I, *Acidimicrobiales* clade OM1, and *Salinisphaeraceae* did not change significantly in the upper mesopelagic throughout the occupation of N2S4, but they did experience a 2-fold-change in 16S rRNA-estimated cell abundance (Figure 4.6, Figure 4.7). Furthermore, while the relative abundance of *Oceanospirillales* decreased in the upper mesopelagic over the occupation of N2S4, the 16S rRNA gene-estimated cell abundance of its constituents increased. Indeed, increases in 16S rRNA-estimated cell abundance throughout the upper mesopelagic zone were observed for most of the community members, indicating that a substantial fraction of the upper mesopelagic community contributed to the increase in BCD (Figure 4.6, 4.7). We caution that our 16S rRNA-estimated cell abundances should not be taken as absolute values as they are biased against archaea, reflecting the relative

abundances of only bacterioplankton applied to total prokaryotic counts. Even so, bacterioplankton families that did not change in relative abundance would still be revealed as responders because of the increase in total prokaryotic abundance over the station occupation would still reveal responses. It is noteworthy that SAR202 subclade I emerges as a responder to the changing conditions of the upper mesopelagic. Though SAR202 cells are often associated with the meso- and bathy-pelagic, it was recently reported that subclade I is predominantly an epipelagic subclade that encodes multiple arylsulfatases and enolases in its genomes (Saw et al., 2020). These enzymes are predicted to play roles in the degradation of complex sulfated polysaccharides, such as fucoidan, which are products of eukaryotic phytoplankton (Mühlenbruch et al., 2018). The increase in SAR202 subclade I in the upper mesopelagic of N2S4 may result from the availability of labile or semi-labile DOM, including complex sulfated polysaccharides, that was delivered to the upper mesopelagic by convective mixing.

Station N2S4 provided an opportunity to observe a rapid response in the mesopelagic zone by some typically upper-euphotic zone-associated bacterioplankton, like SAR11 subclade Ia (Salter et al., 2015; Giovannoni, 2017) (Figure 4.6). Such rapid responses of "surface" lineages in the mesopelagic would be difficult to capture in coarsely resolved time series sampling (e.g., monthly sampling at BATS). It is intriguing that SAR11 subclade Ia increased in relative and 16S rRNA gene-estimated cell abundances in the upper mesopelagic over the short occupation of N2S4, as it is associated with life in the surface ocean under nutrient-limited conditions (Salter et al., 2015; Giovannoni, 2017) and has been shown to decline in the mesopelagic following annual deep convection at BATS (Carlson et al., 2009). Members of SAR11 clade do possess a high abundance of transporters targeting

low-molecular-weight DOM such as amino acids and osmolytes, and have C1 pathways for oxidizing volatile compounds (Giovannoni, 2017). Thus, SARII subclade Ia may have benefited from scavenging hydrolysis products and leaked compounds released by other bacterioplankton, such as attached *Flavobacteria* that can solubilize exported POM (Williams et al., 2013). As those bacterioplankton solubilized particles, they may have released amino acids and other DOM that fueled production of SAR11 subclade Ia (Giovannoni, 2017; Arnosti et al., 2018). Additionally, SARII subclade Ia and other surface-associated lineages like *Flavobacteriales* that rely on the flux of labile organic matter may have been supported by surface-derived DOC that had been delivered by deep convection.

The energy from storm events can erode the thermocline and deliver organic matter from the euphotic zone to the upper mesopelagic. As those storms subside, water column stratification promotes phytoplankton bloom conditions and the production of labile organic matter, some of which can then be delivered with any accumulated organic matter to the upper mesopelagic upon the next storm event. We hypothesize that the dynamics observed at N2S4 reflect a pattern by which labile organic matter, along with recalcitrant accumulated organic matter, is injected into the upper mesopelagic. This export pathway supports the growth of surface-associated bacterioplankton lineages in the upper mesopelagic until the frequency and magnitude of storms and vertical injections of labile organic matter subside in the summer and autumn, when they are outcompeted by bacterioplankton capable of utilizing surface-accumulated and recalcitrant DOM. We hypothesize that the shift between a mixed heterotrophic community (i.e., N2S4) to a well-stratified community (i.e., N3S6) occurs as the mesopelagic community changes on timescales greater than days, where deeper lineages like SAR202 subclade I, *Acidimicrobiales* clade OM1, *Salinisphaeraceae*,

OCS116, and SAR11 subclade II supplant surface-associated lineages that had been mixed to depth.

Conclusions

The bacterioplankton diversity patterns observed at N2S4 likely reflect an initial and fleeting moment in the maturation of community structure following stratification of a deeply mixed layer. The delivery of surface accumulated DOC to the upper mesopelagic zone changes the composition of the extant community. However, the community composition changes on timescales of days are subtle and more gradual than changes in bacterioplankton stocks and secondary rates because the continued availability of labile organic matter temporarily supports the growth of surface-associated bacterioplankton. The shift in mesopelagic bacterioplankton community structure from a mixed community to one that is more typical of the mesopelagic likely becomes more pronounced as the source and stock of labile organic matter becomes depleted and the extant community shifts to lineages capable of consuming more recalcitrant organic matter.

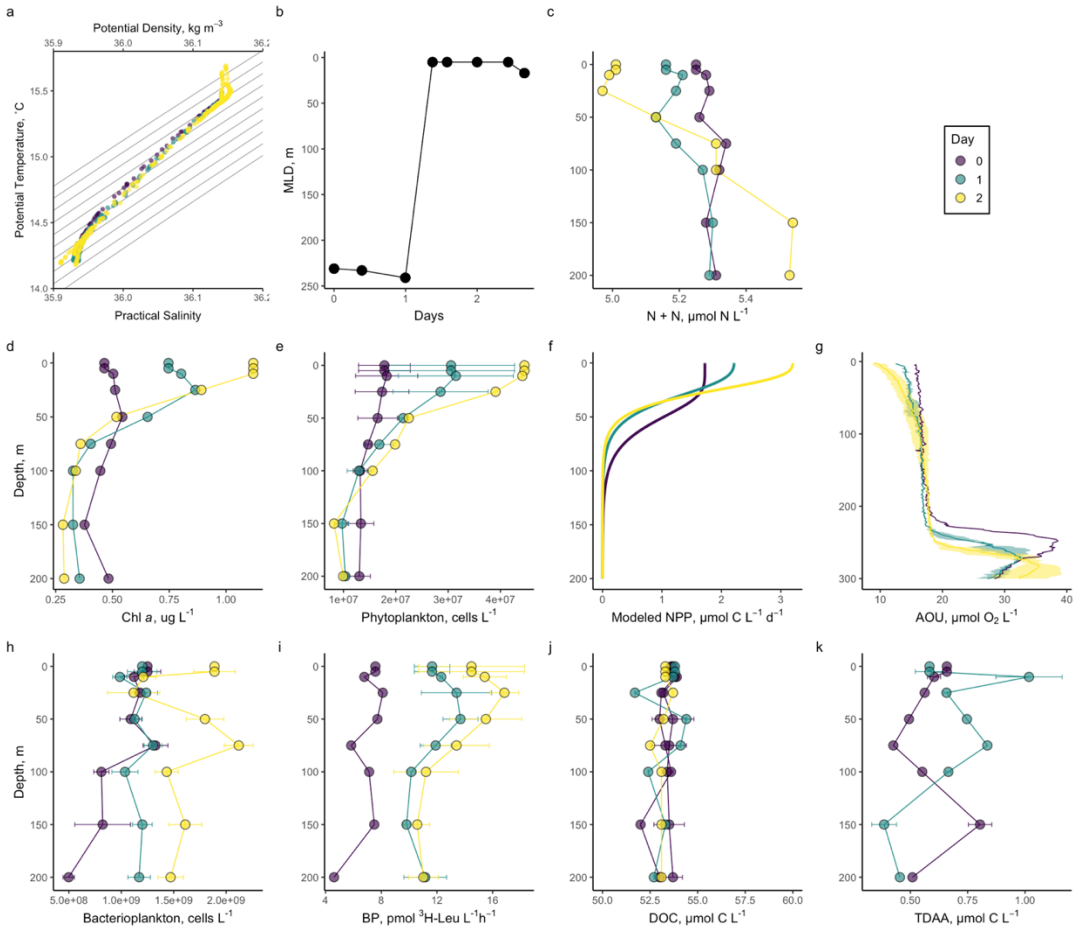

Figure 4.1. Physical, biological, and biogeochemical properties of NAAMES 2 Station 4 (N2S4). (a) Temperature-Salinity diagram over the three-day occupation of the eddy core at N2S4 (47.46˚N, -38.72˚W) in May 2016. Black lines represent isopycnals. (b) Mixed layer depth over the occupation of N2S4. (c – k) Depth profiles taken over the occupation of N2S4. N + N is nitrate + nitrite, NPP is net primary production, AOU is apparent oxygen utilization, BP is bacterioplankton production, DOC is dissolved organic carbon, and TDAA is total dissolved amino acids. In panels c – e and h – k, filled circles represent the mean estimate for each depth between different casts on the same day. In panel g, AOU data was binned to 1 m and lines represent the mean profile for different casts on the same day. Error bars and shaded regions represent the standard deviation from the mean.

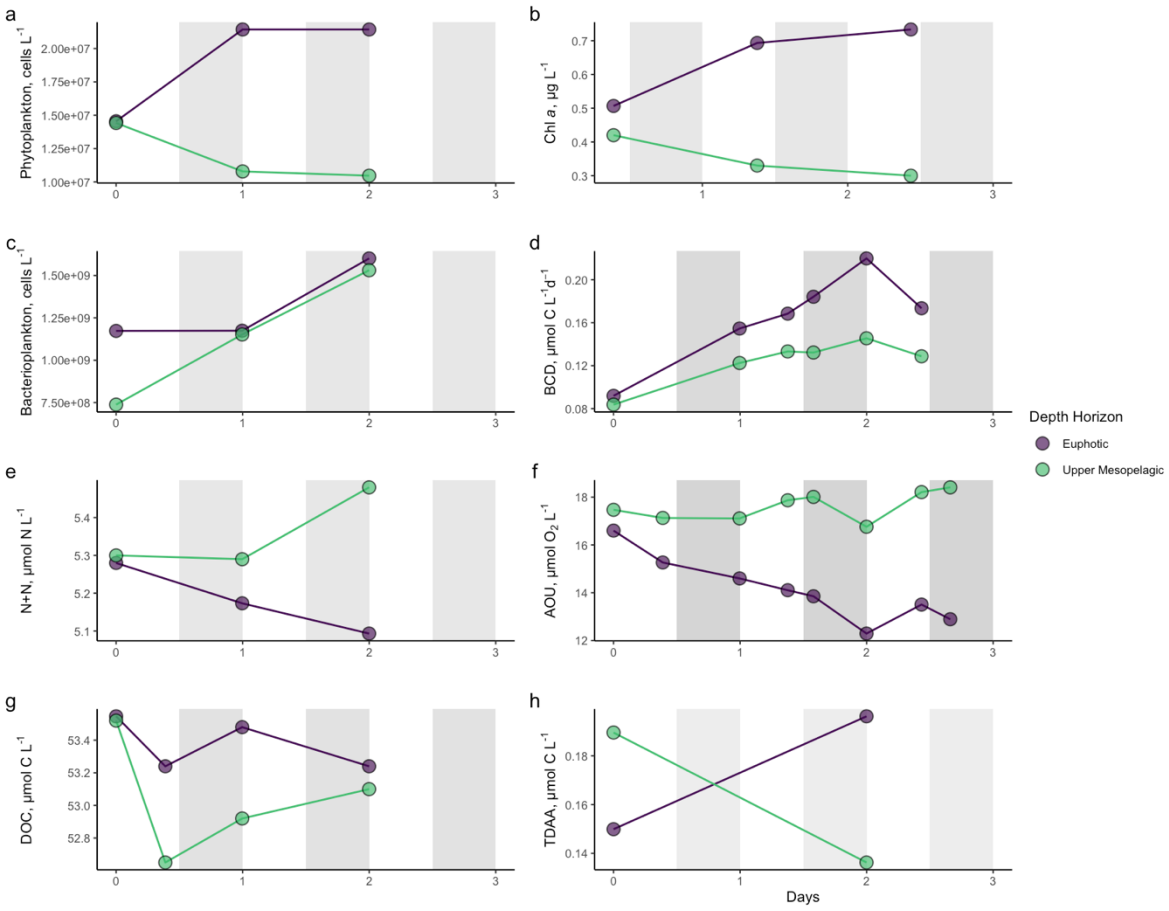

Figure 4.2. Depth-normalized integrations of biological and biogeochemical properties of NAAMES 2 Station 4 (N2S4). Stocks and rates for the euphotic and the upper mesopelagic zones over the three-day occupation of the eddy core at N2S4(47.46˚N, -38.72˚W) in May 2016. Unshaded time periods indicate day, while shaded time periods indicate night. BCD is bacterioplankton carbon demand, N + N is nitrate + nitrite, AOU is apparent oxygen utilization, DOC is dissolved organic carbon, and TDAA is total dissolved amino acids. The volumetric values presented represent mean value for the euphotic an upper mesopelagic zone, respectively. Mean values were determined by integrating values within each depth zone and normalizing by integration depth. The depth of integration for the euphotic zone and mesopelagic zone was 0 – 75 m and 100 – 200 m, respectively. 100 – 200 m, respectively.

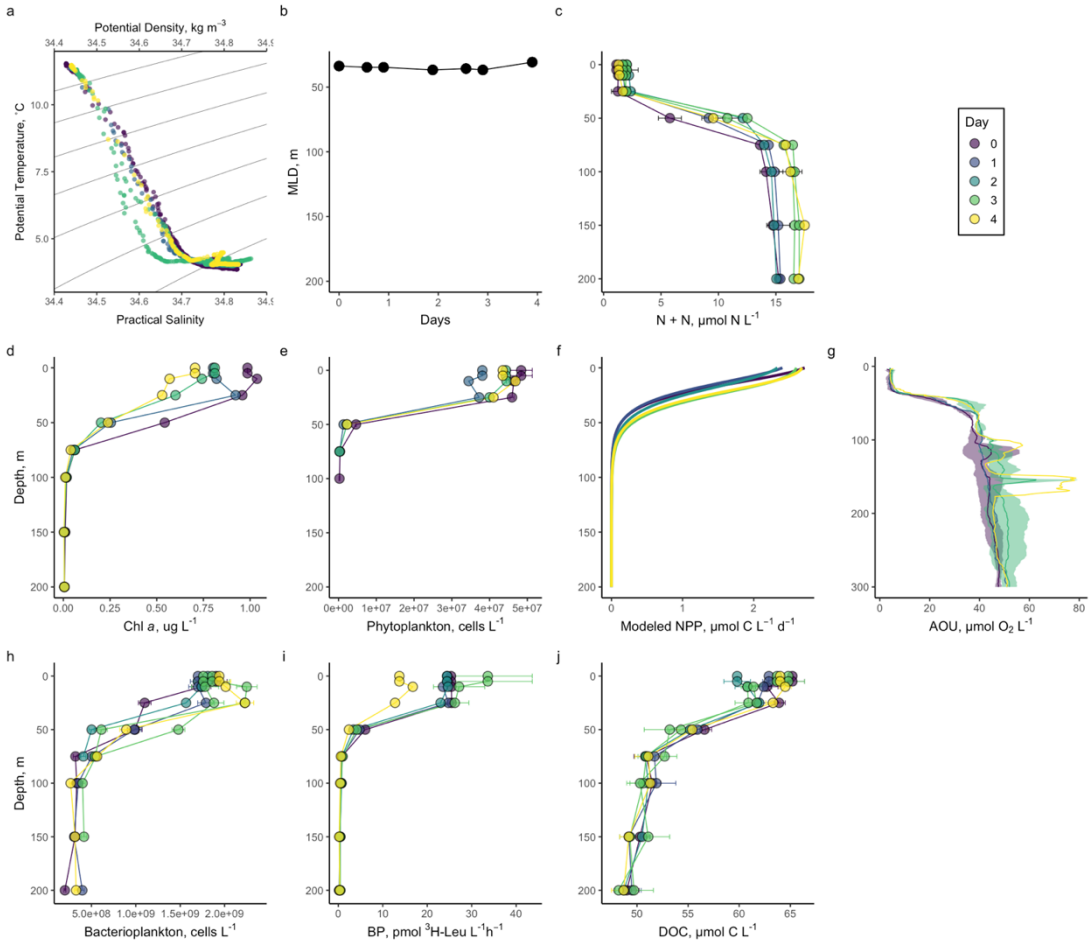

Figure 4.3. Physical, biological, and biogeochemical properties of NAAMES 3 Station 6 (N3S6). (a) Temperature-Salinity diagram over the three-day occupation of N3S6 (53.38˚N, -39.54˚W) in September 2017. Black lines represent isopycnals. (b) Mixed layer depth over the occupation of N3S6. (c – k) Depth profiles taken over the occupation of N2S4. N + N is nitrate + nitrite, NPP is net primary production, AOU is apparent oxygen utilization, BP is bacterioplankton production, and DOC is dissolved organic carbon. In panels c – e and h – k, filled circles represent the mean estimate for each depth between different casts on the same day. In panel g, AOU data was binned to 1 m and lines represent the mean profile for different casts on the same day. Error bars and shaded regions represent the standard deviation from the mean.

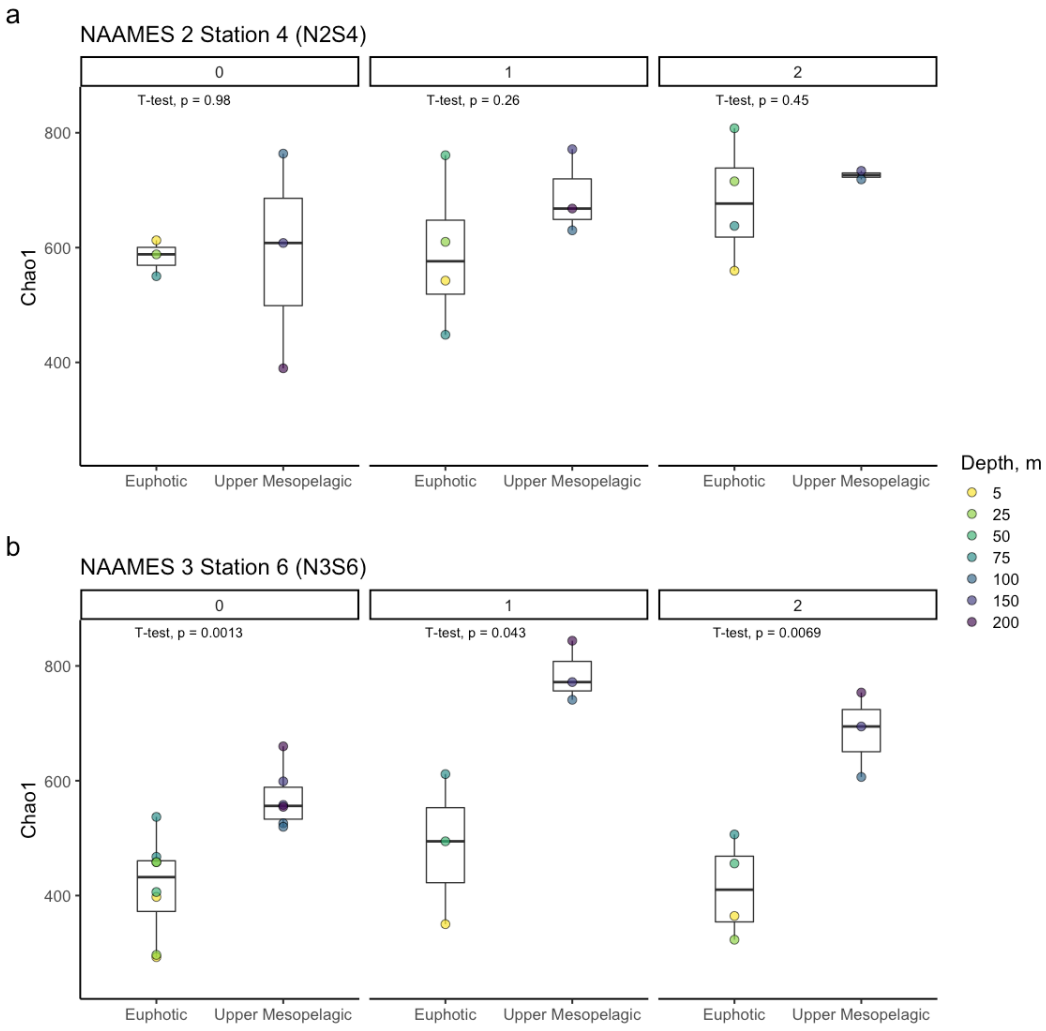

Figure 4.4. Alpha diversity of NAAMES 2 Station 4 (N2S4) and NAAMES 3 Station 6 (N3S6). Chao1 alpha diversity index of bacterioplankton communities for NAAMES 2 hydrostation 4 (a) and NAAMES 3 hydrostation 6 (b). Filled circles represent estimates of each sample, with color representing the depth at which each sample was collected. Boxes represent the 1.5 interquartile range, with the internal solid line representing the median. *p*-values are reported for t-tests between the mean of the Chao1 indices of groups based on depth horizon and time.

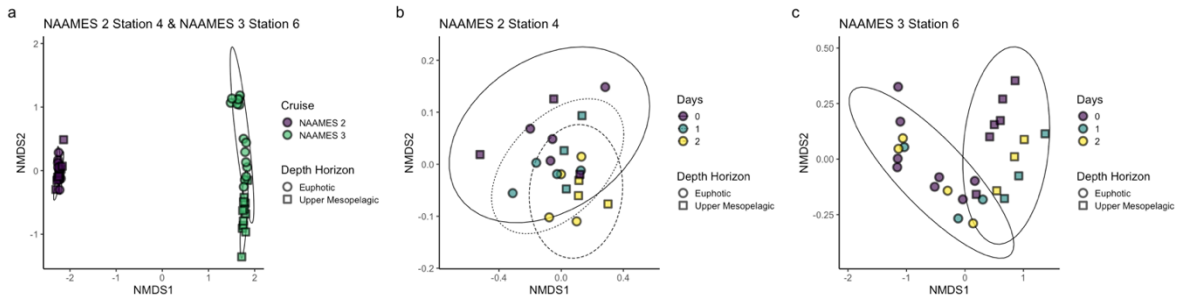

Figure 4.5. Beta diversity of NAAMES 2 Station 4 (N2S4) and NAAMES 3 Station 6 (N3S6). NMDS ordinations with Bray-Curtis dissimilarities for (a) all samples taken at NAAMES 2 hydrostation 4 (N2S4) and NAAMES 3 hydrostation 6 (N3S6) (stress = 0.02), (b) samples only taken at N2S4 (stress = 0.10), and (c) samples only taken at N3S6 (stress = 0.02). 95% confidence interval ellipses are drawn around group centroids based on depth horizon in panels a and c, while they are drawn based on time in panel b.

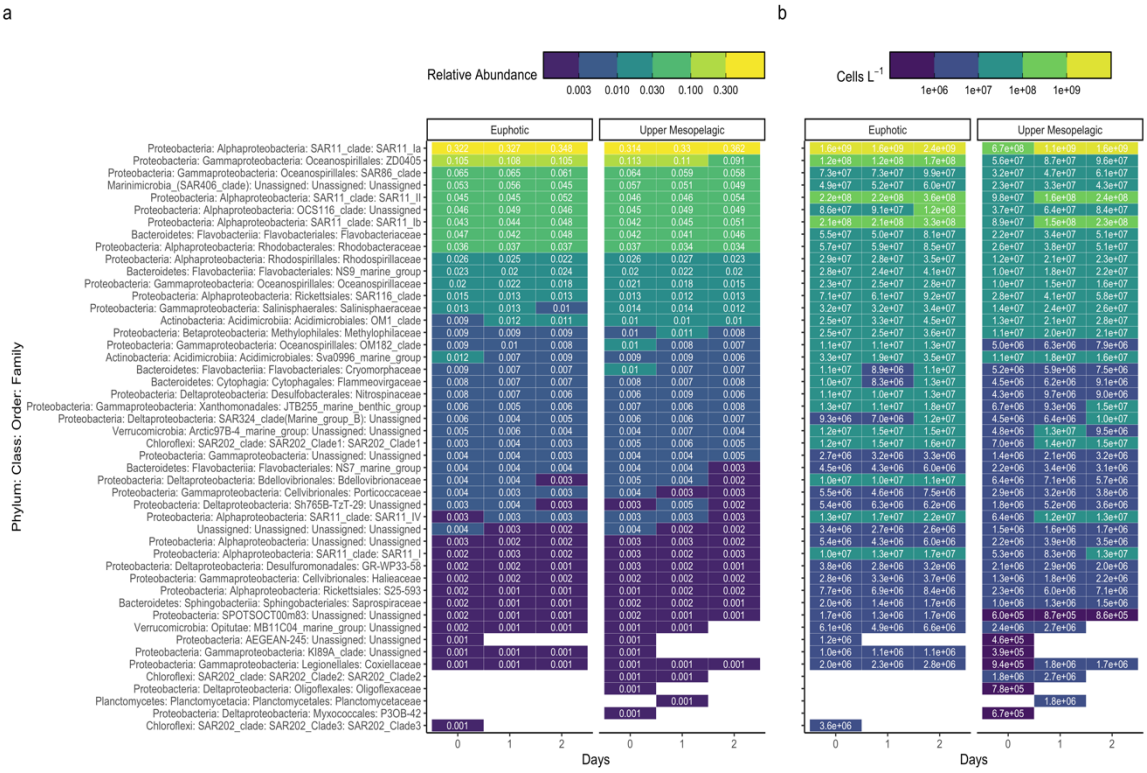

Figure 4.6. Taxonomic abundances at NAAMES 2 Station 4 (N2S4). Relative abundances (a) and estimated cell abundances (b) of taxonomic groups to the family level for the euphotic and upper mesopelagic zones at NAAMES 2 hydrostation 4. For each the euphotic and upper mesopelagic zones, the relative abundance of a taxonomic group was calculated by summing its ASV counts across all depths in the depth horizon and then dividing the summed counts by the total counts in the depth horizon. Taxonomic group cell abundance for each family was estimated for the euphotic and mesopelagic zones as the product between its relative abundance and the total cell abundance in the respective depth horizon, normalized to its gene copy number. Only shown are taxonomic groups that were present > 0.1% in either depth horizon.

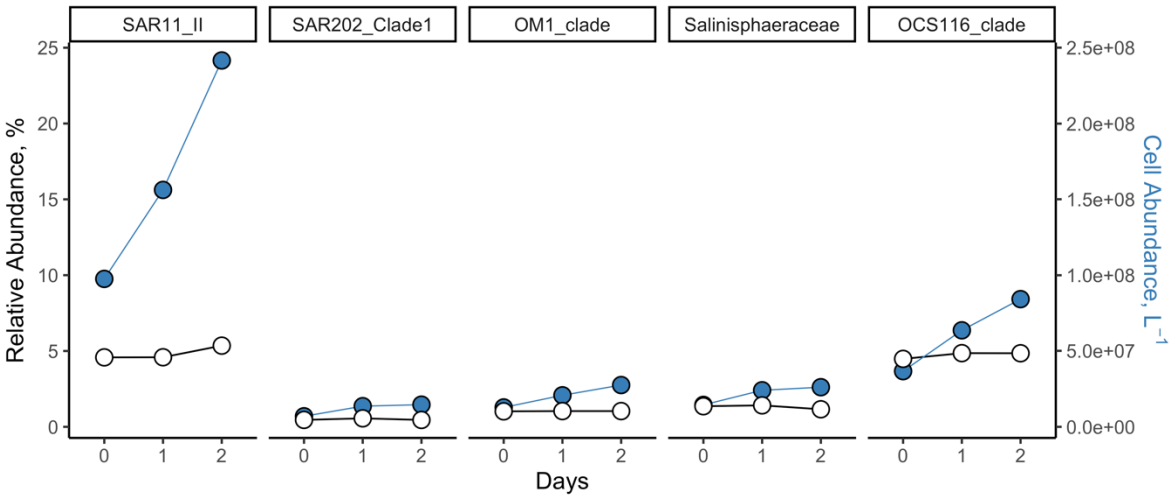

Figure 4.7. Taxonomic abundances of select bacterioplankton in the upper mesopelagic at NAAMES 2 Station 4 (N2S4). Relative and cell abundance in the upper mesopelagic of select bacterioplankton taxa that have been observed from previous studies to utilize or able to utilize surface-accumulated, more recalcitrant DOM.

References

Alkire, M. B., D'Asaro, E., Lee, C., Jane Perry, M., Gray, A., Cetinić, I., et al. (2012). Estimates of net community production and export using high-resolution, Lagrangian measurements of O 2, NO 3-, and POC through the evolution of a spring diatom bloom in the North Atlantic. *Deep. Res. Part I Oceanogr. Res. Pap.* 64, 157–174. doi:10.1016/j.dsr.2012.01.012.

Alonso-Sáez, L., Gasol, J. M., Arístegui, J., Vilas, J. C., Vaqué, D., Duarte, C. M., et al. (2007). Large-scale variability in surface bacterial carbon demand and growth efficiency in the subtropical northeast Atlantic Ocean. *Limnol. Oceanogr.* 52, 533–546. doi:10.4319/lo.2007.52.2.0533.

Alonso-Sáez, L., Vázquez-Domínguez, E., Cardelús, C., Pinhassi, J., Sala, M. M., Lekunberri, I., et al. (2008). Factors controlling the year-round variability in carbon flux through bacteria in a coastal marine system. *Ecosystems* 11, 397–409. doi:10.1007/s10021-008-9129-0.

Aluwihare, L. I., and Repeta, D. J. (1999). A comparison of the chemical characteristics of oceanic DOM and extracellular DOM produced by marine algae. *Mar. Ecol. Prog. Ser.* 186, 105–117. doi:10.3354/meps186105.

Aluwihare, L. I., Repeta, D. J., and Chen, R. F. (1997). A major biopolymeric component to dissolved organic carbon in surface sea water. *Nature* 387, 166–169. doi:10.1038/387166a0.

Amon, R. M. W., and Benner, R. (1994). Rapid cycling of high-molecular-weight dissolved organic matter in the ocean. *Nature*. doi:10.1038/369549a0.

Anderson, M. J. (2001). A new method for non-parametric multivariate analysis of variance. *Austral Ecol.* 26, 32–46. doi:10.1046/j.1442-9993.2001.01070.x.

Anderson, M. J. (2006). Distance-based tests for homogeneity of multivariate dispersions. *Biometrics* 62, 245–253. doi:10.1111/j.1541-0420.2005.00440.x.

Arakawa, N., Aluwihare, L. I., Simpson, A. J., Soong, R., Stephens, B. M., and Lane-Coplen, D. (2017). Carotenoids are the likely precursor of a significant fraction of marine dissolved organic matter. *Sci. Adv.* 3, 1–12. doi:10.1126/sciadv.1602976.

Arnosti, C., Reintjes, G., and Amann, R. (2018). A mechanistic microbial underpinning for the size-reactivity continuum of dissolved organic carbon degradation. *Mar. Chem.* doi:10.1016/j.marchem.2018.09.008.

Arnosti, C., Wietz, M., Brinkhoff, T., Hehemann, J. H., Probandt, D., Zeugner, L., et al. (2021). The Biogeochemistry of Marine Polysaccharides: Sources, Inventories, and Bacterial Drivers of the Carbohydrate Cycle. *Ann. Rev. Mar. Sci.* doi:10.1146/annurev-marine-032020-012810.

Arrieta, J. M., Mayol, E., Hansman, R. L., Herndl, G. J., Dittmar, T., and Duarte, C. M. (2015). Ocean chemistry: Dilution limits dissolved organic carbon utilization in the deep ocean. *Science (80-.).* 348, 331–333. doi:10.1126/science.1258955.

Azam, F. (1998). Microbial control of oceanic carbon flux: the plot thickens. *Science (80-.).* 280, 694–696.

Azam, F., Fenchel, T., Field, J. G., Gray, J. S., Meyer-Reil, L. A., and Thingstad, F. (1983). The ecological role of water-column microbes in the sea. *Mar. Ecol. Prog. Ser.*, 257–263.

Azam, F., Smith, D. C., Steward, G. F., and Hagström, Å. (1993). Bacteria-Organic Matter

Coupling and Its Significance for Oceanic Carbon Cycling. *Microb. Ecol.* 28, 167–179. doi:10.1002/9781118015841.

Baetge, N., Graff, J. R., Behrenfeld, M. J., and Carlson, C. A. (2020). Net Community Production, Dissolved Organic Carbon Accumulation, and Vertical Export in the Western North Atlantic. *Front. Mar. Sci.* 7. doi:10.3389/fmars.2020.00227.

Bates, N. R., Hansell, D. A., Carlson, C. A., and Gordon, L. I. (1998). Distribution of CO 2 species, estimates of net community production, and air-sea CO 2 exchange in the Ross Sea polynya. *J. Geophys. Res. Ocean.* 103, 2883–2896. doi:10.1029/97jc02473.

Bayer, B., Hansman, R. L., Bittner, M. J., Noriega-Ortega, B. E., Niggemann, J., Dittmar, T., et al. (2019). Ammonia-oxidizing archaea release a suite of organic compounds potentially fueling prokaryotic heterotrophy in the ocean. *Environ. Microbiol.* 21, 4062–4075. doi:10.1111/1462-2920.14755.

Behrenfeld, M. J. (2010). Abandoning sverdrup's critical depth hypothesis on phytoplankton blooms. *Ecology* 91, 977–989. doi:10.1890/09-1207.1.

Behrenfeld, M. J., and Boss, E. S. (2018). Student's tutorial on bloom hypotheses in the context of phytoplankton annual cycles. *Glob. Chang. Biol.* 24, 55–77. doi:10.1111/gcb.13858.

Behrenfeld, M. J., Moore, R. H., Hostetler, C. A., Graff, J., Gaube, P., Russell, L. M., et al. (2019). The North Atlantic Aerosol and Marine Ecosystem Study (NAAMES): Science motive and mission overview. *Front. Mar. Sci.* 6, 1–25. doi:10.3389/fmars.2019.00122.

Behrenfeld, M. J., O'Malley, R. T., Boss, E. S., Westberry, T. K., Graff, J. R., Halsey, K. H., et al. (2016). Revaluating ocean warming impacts on global phytoplankton. *Nat. Clim. Chang.* 6, 323–330. doi:10.1038/nclimate2838.

Benner, R., and Amon, R. M. W. (2015). The Size-Reactivity Continuum of Major Bioelements in the Ocean. *Ann. Rev. Mar. Sci.* 7, 185–205. doi:10.1146/annurev-marine-010213-135126.

Benner, R., and Biddanda, B. (1998). Photochemical transformations of surface and deep marine dissolved organic matter: Effects on bacterial growth. *Limnol. Oceanogr.* 43, 1373–1378. doi:10.4319/lo.1998.43.6.1373.

Benner, R., and Herndl, G. J. (2011). Bacterially Derived Dissolved Organic Matter in the Microbial Carbon Pump. *Science (80-.).*, 46–48.

Benner, R., Pakulski, J. D., McCarthy, M., Hedges, J. I., and Hatcher, P. G. (1992). Bulk Chemical Characteristics of Dissolved Organic Matter in the Ocean. *Science (80-.).* 255, 1561 LP – 1564. doi:10.1126/science.255.5051.1561.

Bergauer, K., Fernandez-Guerra, A., Garcia, J. A. L., Sprenger, R. R., Stepanauskas, R., Pachiadaki, M. G., et al. (2018). Organic matter processing by microbial communities throughout the Atlantic water column as revealed by metaproteomics. *Proc. Natl. Acad. Sci. U. S. A.* 115, E400–E408. doi:10.1073/pnas.1708779115.

Bif, M. B., and Hansell, D. A. (2019). Seasonality of Dissolved Organic Carbon in the Upper Northeast Pacific Ocean. *Global Biogeochem. Cycles* 33, 526–539. doi:10.1029/2018GB006152.

Billen, G. (1990). Delayed development of bacterioplankton with respect to phytoplankton: a cue for understanding their trophic relationships. *Arch. f{ü}r Hydrobiol. Beih.* 34, 191–201.

Billen, G., and Fontigny, A. (1987). Dynamics of a Phaeocystis-dominated spring bloom in Belgian coastal waters. II. Bacterioplankton dynamics. *Mar. Ecol. Prog. Ser.* 37, 249–

257. doi:10.3354/meps037249.
Bolaños, L. M., Choi, C. J., Worden, A. Z., Baetge, N., Carlson, C. A., and Giovannoni, S. (2021). Seasonality of the Microbial Community Composition in the North Atlantic. *Front. Mar. Sci.* 8, 1–16. doi:10.3389/fmars.2021.624164.
Borch, N. H., and Kirchman, D. L. (1997). Concentration and composition of dissolved combined neutral sugars (polysaccharides) in seawater determined by HPLC-PAD. *Mar. Chem.* 57, 85–95. doi:10.1016/S0304-4203(97)00002-9.
Børsheim, K. Y., and Myklestad, S. M. (1997). Dynamics of DOC in the Norwegian sea inferred from monthly profiles collected during 3 years at 66°N, 2°E. *Deep. Res. Part I Oceanogr. Res. Pap.* 44, 593–601. doi:10.1016/S0967-0637(96)00106-9.
Boutrif, M., Garel, M., Cottrell, M. T., and Tamburini, C. (2011). Assimilation of marine extracellular polymeric substances by deep-sea prokaryotes in the NW Mediterranean Sea. *Environ. Microbiol. Rep.* 3, 705–709. doi:10.1111/j.1758-2229.2011.00285.x.
Boyd, P. W., Claustre, H., Levy, M., Siegel, D. A., and Weber, T. (2019). Multi-faceted particle pumps drive carbon sequestration in the ocean. *Nature* 568, 327–335. doi:10.1038/s41586-019-1098-2.
Braakman, R., Follows, M. J., and Chisholm, S. W. (2017). Metabolic evolution and the self-organization of ecosystems. *Proc. Natl. Acad. Sci. U. S. A.* 114, E3091–E3100. doi:10.1073/pnas.1619573114.
Brown, M. V., Lauro, F. M., Demaere, M. Z., Muir, L., Wilkins, D., Thomas, T., et al. (2012). Global biogeography of SAR11 marine bacteria. *Mol. Syst. Biol.* 8, 1–13. doi:10.1038/msb.2012.28.
Buchan, A., LeCleir, G. R., Gulvik, C. A., and González, J. M. (2014). Master recyclers: features and functions of bacteria associated with phytoplankton blooms. *Nat. Rev. Microbiol.* doi:10.1038/nrmicro3326.
Burd, A. B., Hansell, D. A., Steinberg, D. K., Anderson, T. R., Arístegui, J., Baltar, F., et al. (2010). Assessing the apparent imbalance between geochemical and biochemical indicators of meso- and bathypelagic biological activity: What the @$#! is wrong with present calculations of carbon budgets? *Deep. Res. Part II Top. Stud. Oceanogr.* 57, 1557–1571. doi:10.1016/j.dsr2.2010.02.022.
Bury, S. J., Boyd, P. W., Preston, T., Savidge, G., and Owens, N. J. P. (2001). Size-fractionated primary production and nitrogen uptake during a North Atlantic phytoplankton bloom: Implications for carbon export estimates. *Deep. Res. Part I Oceanogr. Res. Pap.* 48, 689–720. doi:10.1016/S0967-0637(00)00066-2.
Callahan, B. J., McMurdie, P. J., Rosen, M. J., Han, A. W., Johnson, A. J. A., and Holmes, S. P. (2016). DADA2: High-resolution sample inference from Illumina amplicon data. *Nat. Methods* 13, 581–583. doi:10.1038/nmeth.3869.
Carlson, C. A., Bates, N. R., Ducklow, H. W., and Hansell, D. A. (1999). Estimation of bacterial respiration and growth efficiency in the Ross Sea, Antarctica. *Aquat. Microb. Ecol.* doi:10.3354/ame019229.
Carlson, C. A., and Ducklow, H. W. (1996). Growth of bacterioplankton and consumption of dissolved organic carbon in the Sargasso Sea. *Aquat. Microb. Ecol.* 10, 69–85. doi:10.3354/ame010069.
Carlson, C. A., Ducklow, H. W., Hansell, D. A., and Smith, W. O. (1998). Organic carbon partitioning during spring phytoplankton blooms in the Ross Sea polynya and the Sargasso Sea. *Limnol. Oceanogr.* 43, 375–386. doi:10.4319/lo.1998.43.3.0375.

Carlson, C. A., Ducklow, H. W., and Michaels, A. F. (1994). Annual Flux of dissolved organic carbon from the euphotic zone in the northwestern Sargasso Sea. *Nature* 371, 405–408.

Carlson, C. A., Giovannoni, S. J., Hansell, D. A., Goldberg, S. J., Parsons, R., Otero, M. P., et al. (2002). Effect of nutrient amendments on bacterioplankton production, community structure, and DOC utilization in the northwestern Sargasso Sea. *Aquat. Microb. Ecol.* 30, 19–36. doi:10.3354/ame030019.

Carlson, C. A., Giovannoni, S. J., Hansell, D. A., Goldberg, S. J., Parsons, R., and Vergin, K. (2004). Interactions among dissolved organic carbon, microbial processes, and community structure in the mesopelagic zone of the northwestern Sargasso Sea. *Limnol. Oceanogr.* 49, 1073–1083. doi:10.4319/lo.2004.49.4.1073.

Carlson, C. A., and Hansell, D. A. (2003). The contribution of dissolved organic carbon and nitrogen to the biogeochemistry of the Ross Sea. *Biogeochem. Ross Sea* 78, 123–142. doi:10.1029/078ars08.

Carlson, C. A., and Hansell, D. A. (2015). *DOM Sources, Sinks, Reactivity, and Budgets*. doi:10.1016/B978-0-12-405940-5.00003-0.

Carlson, C. A., Hansell, D. A., Nelson, N. B., Siegel, D. A., Smethie, W. M., Khatiwala, S., et al. (2010). Dissolved organic carbon export and subsequent remineralization in the mesopelagic and bathypelagic realms of the North Atlantic basin. *Deep. Res. Part II Top. Stud. Oceanogr.* 57, 1433–1445. doi:10.1016/j.dsr2.2010.02.013.

Carlson, C. A., Hansell, D. A., Peltzer, E. T., and Smith, J. (2000). Stocks and dynamics of dissolved and particulate organic matter in the Southern Ross Sea, Antarctica. *Deep. Res. Part II Top. Stud. Oceanogr.* 47, 3201–3225. doi:10.1016/S0967-0645(00)00065-5.

Carlson, C. A., Hansell, D. A., and Tamburini, C. (2011). DOC Persistence and Its Fate After Export Within the Ocean Interior. *Science (80-.).*, 57–59.

Carlson, C. A., Morris, R., Parsons, R., Treusch, A. H., Giovannoni, S. J., and Vergin, K. (2009). Seasonal dynamics of SAR11 populations in the euphotic and mesopelagic zones of the northwestern Sargasso Sea. *ISME J.* doi:10.1038/ismej.2008.117.

Cho, B. C., and Azam, F. (1988). Major role of bacteria in biogeochemical fluxes in the ocean's interior. *Nature* 332, 441–443. doi:10.1038/332441a0.

Church, M. J. (2008). Resource control of bacterial dynamics in the sea. *Microb. Ecol. Ocean.* 1, 335–382. doi:10.1002/9780470281840.ch10.

Claustre, H., Johnson, K. S., and Takeshita, Y. (2020). Observing the Global Ocean with Biogeochemical-Argo. *Ann. Rev. Mar. Sci.* 12, 23–48. doi:10.1146/annurev-marine-010419-010956.

Codispoti, L. A., Friederich, G. E., and Hood, D. W. (1986). Variability in the inorganic carbon system over the southeastern Bering Sea shelf during spring 1980 and spring-summer 1981. *Cont. Shelf Res.* 5, 133–160. doi:10.1016/0278-4343(86)90013-0.

Cole, J., Findlay, S., and Pace, M. (1988). Bacterial production in fresh and saltwater ecosystems: a cross-system overview. *Mar. Ecol. Prog. Ser.* 43, 1–10. doi:10.3354/meps043001.

Conan, P., Søndergaard, M., Kragh, T., Thingstad, F., Pujo-Pay, M., Williams, P. J. L. B., et al. (2007). Partitioning of organic production in marine plankton communities: The effects of inorganic nutrient ratios and community composition on new dissolved organic matter. *Limnol. Oceanogr.* 52, 753–765. doi:10.4319/lo.2007.52.2.0753.

Copin-Montégut, G., and Avril, B. (1993). Vertical distribution and temporal variation of dissolved organic carbon in the North-Western Mediterranean Sea. *Deep. Res. Part I* 40, 1963–1972. doi:10.1016/0967-0637(93)90041-Z.

Cotner, J. B., Ammerman, J. W., Peele, E. R., and Bentzen, E. (1997). Phosphorus-limited bacterioplankton growth in the Sargasso Sea. *Aquat. Microb. Ecol.* 13, 141–149. doi:10.3354/ame013141.

Cowie, G. L., and Hedges, J. I. (1994). Biochemical indicators of diagenetic alteration in natural organic matter mixtures. *Nature* 369, 489–492. doi:10.1038/369304a0.

Dall'Olmo, G., Dingle, J., Polimene, L., Brewin, R. J. W., and Claustre, H. (2016). Substantial energy input to the mesopelagic ecosystem from the seasonal mixed-layer pump. *Nat. Geosci.* 9, 820–823. doi:10.1038/ngeo2818.

Davie-Martin, C. L., Giovannoni, S. J., Behrenfeld, M. J., Penta, W. B., and Halsey, K. H. (2020). Seasonal and Spatial Variability in the Biogenic Production and Consumption of Volatile Organic Compounds (VOCs) by Marine Plankton in the North Atlantic Ocean. *Front. Mar. Sci.* 7, 611870. doi:10.3389/fmars.2020.611870.

Davis, J., and Benner, R. (2005). Seasonal trends in the abundance, composition and bioavailability of particulate and dissolved organic matter in the Chukchi/Beaufort Seas and western Canada Basin. *Deep. Res. Part II Top. Stud. Oceanogr.* 52, 3396–3410. doi:10.1016/j.dsr2.2005.09.006.

de Boyer Montégut, C., Madec, G., Fischer, A. S., Lazar, A., and Iudicone, D. (2004). Mixed layer depth over the global ocean: An examination of profile data and a profile-based climatology. *J. Geophys. Res. C Ocean.* 109, 1–20. doi:10.1029/2004JC002378.

Del Giorgio, P. A., and Cole, J. J. (1998). Bacterial growth efficiency in natural aquatic systems. *Annu. Rev. Ecol. Syst.* 29, 503–541. doi:10.1146/annurev.ecolsys.29.1.503.

del Giorgio, P. A., Cole, J. J., and Cimbleris, A. (1997). Respiration rates in bacteria exceed phytoplankton production in unproductive aquatic systems. *Nature* 385, 148–151. doi:10.1038/385148a0.

Del Giorgio, P. A., Condon, R., Bouvier, T., Longnecker, K., Bouvier, C., Sherr, E., et al. (2011). Coherent patterns in bacterial growth, growth efficiency, and leucine metabolism along a northeastern Pacific inshore-offshore transect. *Limnol. Oceanogr.* 56, 1–16. doi:10.4319/lo.2011.56.1.0001.

Della Penna, A., and Gaube, P. (2019). Overview of (sub)mesoscale ocean dynamics for the NAAMES field program. *Front. Mar. Sci.* 6, 384. doi:10.3389/fmars.2019.00384.

Della Penna, A., and Gaube, P. (2020). Mesoscale Eddies Structure Mesopelagic Communities. *Front. Mar. Sci.* 7, 1–9. doi:10.3389/fmars.2020.00454.

DeLong, E. F., Preston, C. M., Mincer, T., Rich, V., Hallam, S. J., Frigaard, N., et al. (2006a). Community Genomics Among Stratified Microbial Assemblages in the Ocean's Interior. *Science (80-.).* 311, 496–503.

DeLong, E. F., Preston, C. M., Mincer, T., Rich, V., Hallam, S. J., Frigaard, N. U., et al. (2006b). Community genomics among stratified microbial assemblages in the ocean's interior. *Science (80-.).* 311, 496–503. doi:10.1126/science.1120250.

DeVries, T., and Weber, T. (2017). The export and fate of organic matter in the ocean: New constraints from combining satellite and oceanographic tracer observations. *Global Biogeochem. Cycles* 31, 535–555. doi:10.1002/2016GB005551.

Dickson, R., and Brown, J. (1994). The production of North Atlantic Deep Water : Sources , rates , and pathways la . Worthington ' s scheme conversion paths North Circled

numbers are transport estimates in Sverdrups , where lb . The recasting of Worthington ' s scheme by McCartney and. *J. Geophys. Res.* 99, 12319–12341. Available at: https://agupubs.onlinelibrary.wiley.com/doi/abs/10.1029/94JC00530.

Dittmar, T. (2015). "Reasons Behind the Long-Term Stability of Dissolved Organic Matter," in *Biogeochemistry of Marine Dissolved Organic Matter: Second Edition* (Elsevier), 369–388. doi:10.1016/B978-0-12-405940-5.00007-8.

Duarte, C. M., and Agustí, S. (1998). The CO2 balance of unproductive aquatic ecosystems. *Science (80-.).* doi:10.1126/science.281.5374.234.

Ducklow, H. (2000). "Bacterial Production and Biomass in the Oceans," in *Microbial ecology of the oceans*, ed. D. Kirchman (New York: Wiley), 1–47.

Ducklow, H., Carlson, C., and Smith, W. (1999). Bacterial growth in experimental plankton assemblages and seawater cultures from the Phaeocystis antarctica bloom in the Ross Sea, Antarctica. *Aquat. Microb. Ecol.* 19, 215–227. doi:10.3354/ame019215.

Ducklow, H. W., Dickson, M. L., Kirchman, D. L., Steward, G., Orchardo, J., Marra, J., et al. (2000). Constraining bacterial production, conversion efficiency and respiration in the Ross Sea, Antarctica, January - February, 1997. *Deep. Res. Part II Top. Stud. Oceanogr.* 47, 3227–3247. doi:10.1016/S0967-0645(00)00066-7.

Ducklow, H. W., Kirchman, D. L., and Anderson, T. R. (2002). The magnitude of spring bacterial production in the North Atlantic Ocean. *Limnol. Oceanogr.* 47, 1684–1693. doi:10.4319/lo.2002.47.6.1684.

Ducklow, H. W., Kirchman, D. L., Quinby, H. L., Carlson, C. A., and Dam, H. G. (1993). Stocks and dynamics of bacterioplankton carbon during the spring bloom in the eastern North Atlantic Ocean. *Deep. Res. Part II* 40, 245–263. doi:10.1016/0967-0645(93)90016-G.

Ducklow, H. W., Purdie, D. A., Williams, P. J. L. B., and Davies, J. M. (1986). Bacterioplankton: A sink for carbon in a coastal marine plankton community. *Science (80-.).* doi:10.1126/science.232.4752.865.

Ducklow, H. W., Smith, D. C., Campbell, L., Landry, M. R., Quinby, H. L., Steward, G. F., et al. (2001a). Heterotrophic bacterioplankton in the Arabian Sea: Basinwide response to year-round high primary productivity. *Deep. Res. Part II Top. Stud. Oceanogr.* 48, 1303–1323. doi:10.1016/S0967-0645(00)00140-5.

Ducklow, H. W., Steinberg, D. K., and Buesseler, K. O. (2001b). Upper Ocean Carbon Export and the Biological Pump. *Oceanography* 14.

Dugdale, R. C., and Goering, J. J. (1967). Uptake of New and Regenerated Forms of Nitrogen in Primary Productivity. *Limnol. Oceanogr.* 12, 196–206. doi:10.4319/lo.1967.12.2.0196.

Dunne, J. P., Sarmiento, J. L., and Gnanadesikan, A. (2007). A synthesis of global particle export from the surface ocean and cycling through the ocean interior and on the seafloor. *Global Biogeochem. Cycles* 21, 1–16. doi:10.1029/2006GB002907.

Duursma, E. K. (1963). The production of dissolved organic matter in the sea, as related to the primary gross production of organic matter. *Netherlands J. Sea Res.* 2, 85–94. doi:10.1016/0077-7579(63)90007-3.

Eberlein, K., Leal, M. T., Hammer, K. D., and Hickel, W. (1985). Dissolved organic substances during a Phaeocystis pouchetii bloom in the German Bight (North Sea). *Mar. Biol.* 89, 311–316. doi:10.1007/BF00393665.

Falkowski, P. G., Barber, R. T., and Smetacek, V. (1998). Biogeochemical controls and

feedbacks on ocean primary production. *Science (80-.).* 281, 200–206. doi:10.1126/science.281.5374.200.
Fawcett, S. E., Ward, B. B., Lomas, M. W., and Sigman, D. M. (2015). Vertical decoupling of nitrate assimilation and nitrification in the Sargasso Sea. *Deep. Res. Part I Oceanogr. Res. Pap.* 103, 64–72. doi:10.1016/j.dsr.2015.05.004.
Field, C. B., Behrenfeld, M. J., Randerson, J. T., and Falkowski, P. (1998). Primary production of the biosphere: Integrating terrestrial and oceanic components. *Science (80-.).* 281, 237–240. doi:10.1126/science.281.5374.237.
Field, K. G., Gordon, D., Wright, T., Rappé, M., Urbach, E., Vergin, K., et al. (1997). Diversity and depth-specific distribution of SAR11 cluster rRNA genes from marine planktonic bacteria. *Appl. Environ. Microbiol.* 63, 63–70. doi:10.1128/aem.63.1.63-70.1997.
Fox, J., Behrenfeld, M. J., Haëntjens, N., Chase, A., Kramer, S. J., Boss, E., et al. (2020). Phytoplankton Growth and Productivity in the Western North Atlantic: Observations of Regional Variability From the NAAMES Field Campaigns. *Front. Mar. Sci.* 7, 24. doi:10.3389/fmars.2020.00024.
Fukuda, R., Ogawa, H., Nagata, T., and Koike, I. (1998). Direct determination of carbon and nitrogen contents of natural bacterial assemblages in marine environments. *Appl. Environ. Microbiol.* 64, 3352–3358. doi:10.1128/aem.64.9.3352-3358.1998.
García-Martín, E. E., Daniels, C. J., Davidson, K., Lozano, J., Mayers, K. M. J., McNeill, S., et al. (2019). Plankton community respiration and bacterial metabolism in a North Atlantic Shelf Sea during spring bloom development (April 2015). *Prog. Oceanogr.* 177, 101873. doi:10.1016/j.pocean.2017.11.002.
Giovannoni, S. J. (2017). SAR11 Bacteria: The Most Abundant Plankton in the Oceans. *Ann. Rev. Mar. Sci.* 9, 231–255. doi:10.1146/annurev-marine-010814-015934.
Giovannoni, S. J., Rappé, M. S., Vergin, K. L., and Adair, N. L. (1996). 16S rRNA genes reveal stratified open ocean bacterioplankton populations related to the green non-sulfur bacteria. *Proc. Natl. Acad. Sci. U. S. A.* 93, 7979–7984. doi:10.1073/pnas.93.15.7979.
Giovannoni, S. J., and Vergin, K. L. (2012). Seasonality in ocean microbial communities. *Science (80-.).* doi:10.1126/science.1198078.
Goldberg, S. J., Carlson, C. A., Hansell, D. A., Nelson, N. B., and Siegel, D. A. (2009). Temporal dynamics of dissolved combined neutral sugars and the quality of dissolved organic matter in the Northwestern Sargasso Sea. *Deep. Res. Part I Oceanogr. Res. Pap.* 56, 672–685. doi:10.1016/j.dsr.2008.12.013.
Graff, J. R., and Behrenfeld, M. J. (2018). Photoacclimation responses in subarctic Atlantic phytoplankton following a natural mixing-restratification event. *Front. Mar. Sci.* 5, 209. doi:10.3389/fmars.2018.00209.
Granum, E., Kirkvold, S., and Myklestad, S. M. (2002). Cellular and extracellular production of carbohydrates and amino acids by the marine diatom Skeletonema costatum: Diel variations and effects of N depletion. *Mar. Ecol. Prog. Ser.* doi:10.3354/meps242083.
Gruber, D. F., Simjouw, J. P., Seitzinger, S. P., and Taghon, G. L. (2006). Dynamics and characterization of refractory dissolved organic matter produced by a pure bacterial culture in an experimental predator-prey system. *Appl. Environ. Microbiol.* 72, 4184–4191. doi:10.1128/AEM.02882-05.

Gundersen, K., Heldal, M., Norland, S., Purdie, D. A., and Knap, A. H. (2002). Elemental C, N, and P cell content of individual bacteria collected at the Bermuda Atlantic Time-series Study (BATS) site. *Limnol. Oceanogr.* 47, 1525–1530. doi:10.4319/lo.2002.47.5.1525.

Halewood, E. R., Carlson, C. A., Brzezinski, M. A., Reed, D. C., and Goodman, J. (2012). Annual cycle of organic matter partitioning and its availability to bacteria across the Santa Barbara Channel continental shelf. *Aquat. Microb. Ecol.* 67, 189–209. doi:10.3354/ame01586.

Hansell, D. A. (2005). Dissolved Organic Carbon Reference Material Program. *EOS Trans. Am. Geophys. Union* 86, 318. doi:10.1029/2004GL020684.w.

Hansell, D. A. (2013). Recalcitrant dissolved organic carbon fractions. *Ann. Rev. Mar. Sci.* doi:10.1146/annurev-marine-120710-100757.

Hansell, D. A., Bates, N. R., and Carlson, C. A. (1997a). Predominance of vertical loss of carbon from surface waters of the equatorial Pacific Ocean. *Nature* 386, 59–61. doi:10.1038/386059a0.

Hansell, D. A., and Carlson, C. A. (1998a). Deep-ocean gradients in the concentration of dissolved organic carbon. *Nature* 395, 263–266. doi:10.1038/26200.

Hansell, D. A., and Carlson, C. A. (1998b). Net community production in dissolved organic carbon. *Global Biogeochem. Cycles* 12, 443–453. doi:10.1029/98GB01928.

Hansell, D. A., and Carlson, C. A. (2001a). Biogeochemistry of total organic carbon and nitrogen in the Sargasso Sea: Control by convective overturn. *Deep. Res. Part II Top. Stud. Oceanogr.* 48, 1649–1667. doi:10.1016/S0967-0645(00)00153-3.

Hansell, D. A., and Carlson, C. A. (2001b). Marine dissolved organic matter and the carbon cycle. *Oceanography*. doi:10.5670/oceanog.2001.05.

Hansell, D. A., Carlson, C. A., Bates, N. R., and Poisson, A. (1997b). Horizontal and vertical removal of organic carbon in the equatorial pacific ocean: A mass balance assessment. *Deep. Res. Part II Top. Stud. Oceanogr.* 44, 2115–2130. doi:10.1016/S0967-0645(97)00021-0.

Hansell, D. A., Carlson, C. A., Repeta, D. J., and Schlitzer, R. (2009). Dissolved organic matter in the ocean a controversy stim ulates new insights. *Oceanography*. doi:10.5670/oceanog.2009.109.

Hansell, D. A., Carlson, C. A., and Schlitzer, R. (2012). Net removal of major marine dissolved organic carbon fractions in the subsurface ocean. *Global Biogeochem. Cycles* 26, 1–9. doi:10.1029/2011GB004069.

Hansell, D. A., Whitledge, T. E., and Goering, J. J. (1993). Patterns of nitrate utilization and new production over the Bering-Chukchi shelf. *Cont. Shelf Res.* 13, 601–627. doi:10.1016/0278-4343(93)90096-G.

Hertkorn, N., Benner, R., Frommberger, M., Schmitt-Kopplin, P., Witt, M., Kaiser, K., et al. (2006). Characterization of a major refractory component of marine dissolved organic matter. *Geochim. Cosmochim. Acta* 70, 2990–3010. doi:10.1016/j.gca.2006.03.021.

Hobbie, J. E., Daley, R. J., and Jasper, S. (1977). Use of Nuclepore Filters for Counting Bacteria by Fluorescence Microscopy. *Appl. Environ. Microbiol.* 33, 1225–1228.

Holte, J., Talley, L. D., Gilson, J., and Roemmich, D. (2017). An Argo mixed layer climatology and database. *Geophys. Res. Lett.* 44, 5618–5626. doi:10.1002/2017GL073426.

Hopkinson, C. S., and Vallino, J. J. (2005). Efficient export of carbon to the deep ocean

through dissolved organic matter. *Nature* 433, 142–145. doi:10.1038/nature03191.
Hoppe, H. G., Gocke, K., Koppe, R., and Begler, C. (2002). Bacterial growth and primary production along a north-south transect of the Atlantic Ocean. *Nature* 416, 168–171. doi:10.1038/416168a.
Ittekkot, V., Brockmann, U., Michaelis, W., and Degens, E. (1981). Dissolved Free and Combined Carbohydrates During a Phytoplankton Bloom in the Northern. *Mar. Ecol. Prog. Ser.* 4, 299–305.
Jiao, N., Herndl, G. J., Hansell, D. A., Benner, R., Kattner, G., Wilhelm, S. W., et al. (2010). Microbial production of recalcitrant dissolved organic matter: Long-term carbon storage in the global ocean. *Nat. Rev. Microbiol.* 8, 593–599. doi:10.1038/nrmicro2386.
Kaiser, K., and Benner, R. (2009). Biochemical composition and size distribution of organic matter at the Pacific and Atlantic time-series stations. *Mar. Chem.* 113, 63–77. doi:10.1016/j.marchem.2008.12.004.
Karl, D. M., Christian, J. R., Dore, J. E., and Letelier, R. M. (1996). Microbiological oceanography in the region west of the Antarctic Peninsula: microbial dynamics, nitrogen cycle and carbon flux. *Antarct Res Ser* 70, 303–332.
Kattner, G., Meinhard, S., and Koch, B. P. (2011). Molecular Characterization of Dissolved Organic Matter and Constraints for Prokaryotic Utilization. *Science (80-.).*, 60–61.
Kawasaki, N., and Benner, R. (2006). Bacterial release of dissolved organic matter during cell growth and decline: Molecular origin and composition. *Limnol. Oceanogr.* doi:10.4319/lo.2006.51.5.2170.
Keil, R. G., and Kirchman, D. L. (1993). Dissolved combined amino acids: Chemical form and utilization by marine bacteria. *Limnol. Oceanogr.* 38, 1256–1270. doi:10.4319/lo.1993.38.6.1256.
Kieber, R. J., Hydro, L. H., and Seaton, P. J. (1997). Photooxidation of triglycerides and fatty acids in seawater: Implication toward the formation of marine humic substances. *Limnol. Oceanogr.* 42, 1454–1462. doi:10.4319/lo.1997.42.6.1454.
Kirchman, D. L., Ducklow, H. W., McCarthy, J. J., and Garside, C. (1994). Biomass and nitrogen uptake by heterotrophic bacteria during the spring phytoplankton bloom in the North Atlantic Ocean. *Deep. Res. Part I* 41, 879–895. doi:10.1016/0967-0637(94)90081-7.
Körtzinger, A., Koeve, W., Kähler, P., and Mintrop, L. (2001). C : N ratios in the mixed layer during the productive season in the northeast Atlantic Ocean. *Deep. Res. Part I Oceanogr. Res. Pap.* 48, 661–688. doi:10.1016/S0967-0637(00)00051-0.
Lacour, L., Briggs, N., Claustre, H., Ardyna, M., and Dall'Olmo, G. (2019). The Intraseasonal Dynamics of the Mixed Layer Pump in the Subpolar North Atlantic Ocean: A Biogeochemical-Argo Float Approach. *Global Biogeochem. Cycles* 33, 266–281. doi:10.1029/2018GB005997.
Lampert, W. (1978). Release of dissolved organic carbon by grazing zooplankton. *Limnol. Oceanogr.* 23, 831–834. doi:10.4319/lo.1978.23.4.0831.
Landry, Z., Swa, B. K., Herndl, G. J., Stepanauskas, R., and Giovannoni, S. J. (2017). SAR202 genomes from the dark ocean predict pathways for the oxidation of recalcitrant dissolved organic matter. *MBio*. doi:10.1128/mBio.00413-17.
LaRowe, D. E., Dale, A. W., Amend, J. P., and Van Cappellen, P. (2012). Thermodynamic limitations on microbially catalyzed reaction rates. *Geochim. Cosmochim. Acta*. doi:10.1016/j.gca.2012.05.011.

Laws, E. (1991). Photosynthetic quotients, new production and net community production in the open ocean. *Deep. Res. Part I* 38, 143–167.
Lee, S., Fuhrman, J. (1987). Relationships between Biovolume and Biomass of Naturally Derived Marine Bacterioplankton. *Appl. Environ. Microbiol.* 53, 1298–1303.
Li, M., Baker, B. J., Anantharaman, K., Jain, S., Breier, J. A., and Dick, G. J. (2015). Genomic and transcriptomic evidence for scavenging of diverse organic compounds by widespread deep-sea archaea. *Nat. Commun.* 6. doi:10.1038/ncomms9933.
Liu, S., Baetge, N., Comstock, J., Opalk, K., Parsons, R., Halewood, E., et al. (2020a). Stable Isotope Probing Identifies Bacterioplankton Lineages Capable of Utilizing Dissolved Organic Matter Across a Range of Bioavailability. *Front. Microbiol.* 11. doi:10.3389/fmicb.2020.580397.
Liu, S., Parsons, R., Opalk, K., Baetge, N., Giovannoni, S., Bolaños, L. M., et al. (2020b). Different carboxyl-rich alicyclic molecules proxy compounds select distinct bacterioplankton for oxidation of dissolved organic matter in the mesopelagic Sargasso Sea. *Limnol. Oceanogr.* doi:10.1002/lno.11405.
Lochte, K., Ducklow, H. W., Fasham, M. J. R., and Stienen, C. (1993). Plankton succession and carbon cycling at 47°N 20°W during the JGOFS North Atlantic Bloom Experiment. *Deep. Res. Part II* 40, 91–114. doi:10.1016/0967-0645(93)90008-B.
Lønborg, C., Martínez-García, S., Teira, E., and Álvarez-Salgado, X. A. (2011). Bacterial carbon demand and growth efficiency in a coastal upwelling system. *Aquat. Microb. Ecol.* 63, 183–191. doi:10.3354/ame01495.
Maas, A. E., Liu, S., Bolaños, L. M., Widner, B., Parsons, R., Kujawinski, E. B., et al. (2020). Migratory Zooplankton Excreta and Its Influence on Prokaryotic Communities. *Front. Mar. Sci.* 7. doi:10.3389/fmars.2020.573268.
Marañón, E., Pérez, V., Fernández, E., Anadón, R., Bode, A., González, N., et al. (2007). Planktonic carbon budget in the eastern subtropical North Atlantic. *Aquat. Microb. Ecol.* 48, 261–275. doi:10.3354/ame048261.
Martin, M. (2011). Cutadapt removes adapter sequences from high-throughput sequencing reads. *EMBnet. J.* 17, 10–12.
McCarthy, M. D., Hedges, J. I., and Benner, R. (1998). Major bacterial contribution to marine dissolved organic nitrogen. *Science (80-.).* doi:10.1126/science.281.5374.231.
McCarthy, M., Hedges, J., and Benner, R. (1996). Major biochemical composition of dissolved high molecular weight organic matter in seawater. *Mar. Chem.* 55, 281–297. doi:10.1016/S0304-4203(96)00041-2.
McCave, I. N. (1975). Vertical flux of particles in the ocean. *Deep. Res. Oceanogr. Abstr.* 22, 491–502. doi:10.1016/0011-7471(75)90022-4.
McMurdie, P. J., and Holmes, S. (2013). phyloseq: an R package for reproducible interactive analysis and graphics of microbiome census data. *PLoS One* 8, e61217.
Mehrshad, M., Rodriguez-Valera, F., Amoozegar, M. A., López-García, P., and Ghai, R. (2018). The enigmatic SAR202 cluster up close: Shedding light on a globally distributed dark ocean lineage involved in sulfur cycling. *ISME J.* 12, 655–668. doi:10.1038/s41396-017-0009-5.
Middelboe, M., and Jørgensen, N. O. G. (2006). Viral lysis of bacteria: An important source of dissolved amino acids and cell wall compounds. *J. Mar. Biol. Assoc. United Kingdom* 86, 605–612. doi:10.1017/S0025315406013518.
Mitra, A., Flynn, K. J., Burkholder, J. M., Berge, T., Calbet, A., Raven, J. A., et al. (2014).

The role of mixotrophic protists in the biological carbon pump. *Biogeosciences*. doi:10.5194/bg-11-995-2014.

Mojica, K., and Gaube, P. Estimates of mixing depth and stratification for the North Atlantic Aerosol and Marine Ecosystem Study.

Moore, E. R., Davie-Martin, C. L., Giovannoni, S. J., and Halsey, K. H. (2020). Pelagibacter metabolism of diatom-derived volatile organic compounds imposes an energetic tax on photosynthetic carbon fixation. *Environ. Microbiol.* 22, 1720–1733. doi:10.1111/1462-2920.14861.

Moran, M. A., and Hodson, R. E. (1990). Bacterial production on humic and nonhumic components of dissolved organic carbon. *Limnol. Oceanogr.* 35, 1744–1756. doi:10.4319/lo.1990.35.8.1744.

Moran, M. A., and Hodson, R. E. (1994). Support of bacterioplankton production by dissolved humic substances from 3 marine environments. *Mar. Ecol. Prog. Ser.* 110, 241–248. doi:10.3354/meps110241.

Morison, F., Harvey, E., Franzè, G., and Menden-Deuer, S. (2019). Storm-induced predator-prey decoupling promotes springtime accumulation of north atlantic phytoplankton. *Front. Mar. Sci.* 6, 608. doi:10.3389/fmars.2019.00608.

Morris, R. M., Rappé, M. S., Urbach, E., Connon, S. A., and Giovannoni, S. J. (2004). Prevalence of the Chloroflexi-related SAR202 bacterioplankton cluster throughout the mesopelagic zone and deep ocean. *Appl. Environ. Microbiol.* 70, 2836–2842. doi:10.1128/AEM.70.5.2836-2842.2004.

Morris, R. M., Vergin, K. L., Cho, J. C., Rappé, M. S., Carlson, C. A., and Giovannoni, S. J. (2005). Temporal and spatial response of bacterioplankton lineages to annual convective overturn at the Bermuda Atlantic Time-series Study site. *Limnol. Oceanogr.* 50, 1687–1696. doi:10.4319/lo.2005.50.5.1687.

Mueller, J. L., Clark, D. K., Kuwahara, V. S., Lazin, G., Brown, S. W., Fargion, G. S., et al. (2003). Ocean optics protocols for satellite ocean color semsor validation, revision 4, Volume VI: Special topics in ocean protocols and appendices. *NASA Tech. Memo.* VOL VI, 1–124.

Mühlenbruch, M., Grossart, H. P., Eigemann, F., and Voss, M. (2018). Mini-review: Phytoplankton-derived polysaccharides in the marine environment and their interactions with heterotrophic bacteria. *Environ. Microbiol.* 20, 2671–2685. doi:10.1111/1462-2920.14302.

Nagata, T. (2008). Organic Matter–Bacteria Interactions in Seawater. *Microb. Ecol. Ocean.*, 207–241. doi:doi:10.1002/9780470281840.ch7.

Ogawa, H., Amagai, Y., Koike, I., Kaiser, K., and Benner, R. (2001). Production of refractory dissolved organic matter by bacteria. *Science (80-.).* 292, 917–920. doi:10.1126/science.1057627.

Oksanen, J., Blanchet, F. G., Kindt, R., Legendre, P., Minchin, P. R., O'hara, R. B., et al. (2013). Package 'vegan.' *Community Ecol. Packag. version* 2, 1–295.

Olsen, A., Key, R. M., Van Heuven, S., Lauvset, S. K., Velo, A., Lin, X., et al. (2016). The global ocean data analysis project version 2 (GLODAPv2) - An internally consistent data product for the world ocean. *Earth Syst. Sci. Data* 8, 297–323. doi:10.5194/essd-8-297-2016.

Omand, M. M., D'Asaro, E. A., Lee, C. M., Perry, M. J., Briggs, N., Cetinić, I., et al. (2015). Eddy-driven subduction exports particulate organic carbon from the spring

bloom. *Science (80-.).* 348, 222–225. doi:10.1126/science.1260062.
Ouverney, C. C., and Fuhrman, J. A. (2000). Marine planktonic archaea take up amino acids. *Appl. Environ. Microbiol.* 66, 4829–4833. doi:10.1128/AEM.66.11.4829-4833.2000.
Parsons, R. J., Breitbart, M., Lomas, M. W., and Carlson, C. A. (2012). Ocean time-series reveals recurring seasonal patterns of virioplankton dynamics in the northwestern Sargasso Sea. *ISME J.* 6, 273–284. doi:10.1038/ismej.2011.101.
Passow, U., and Carlson, C. A. (2012). The biological pump in a high CO2 world. *Mar. Ecol. Prog. Ser.* 470, 249–271. doi:10.3354/meps09985.
Peng, X., Fawcett, S. E., van Oostende, N., Wolf, M. J., Marconi, D., Sigman, D. M., et al. (2018). Nitrogen uptake and nitrification in the subarctic North Atlantic Ocean. *Limnol. Oceanogr.* 63, 1462–1487. doi:10.1002/lno.10784.
Plant, J. N., Johnson, K. S., Sakamoto, C. M., Jannasch, H. W., Coletti, L. J., Riser, S. C., et al. (2016). Net community production at Ocean Station Papa observed with nitrate and oxygen sensors on profiling floats: NCP AT OCEAN STATION PAPA. *Global Biogeochem. Cycles* 30, 859–879. doi:10.1002/2015GB005349.
Pomeroy, L. R., and Deibel, D. O. N. (1986). Temperature regulation of bacterial activity during the spring bloom in Newfoundland coastal waters. *Science (80-.).* 233, 359–361.
Pomeroy, L. R., le Williams, P. J. B., Azam, F., and Hobbie, J. E. (2007). The microbial loop. *Oceanography* 20, 28–33. doi:10.5670/oceanog.2007.45.
Pomeroy, L. R., and Wiebe, W. J. (2001). Temperature and substrates as interactive limiting factors for marine heterotrophic bacteria. *Aquat. Microb. Ecol.* 23, 187–204. doi:10.3354/ame023187.
Porter, K. G., and Feig, Y. S. (1980). The use of DAPI for identifying aquatic microfloral. *Limnol. Oceanogr.* 25(5), 943–948.
Quast, C., Pruesse, E., Yilmaz, P., Gerken, J., Schweer, T., Yarza, P., et al. (2013). The SILVA ribosomal RNA gene database project: Improved data processing and web-based tools. *Nucleic Acids Res.* doi:10.1093/nar/gks1219.
Redfield, A. C. (1963). The influence of organisms on the composition of seawater. *sea* 2, 26–77.
Reinthaler, T., and Herndl, G. J. (2005). Seasonal dynamics of bacterial growth efficiencies in relation to phytoplankton in the southern North Sea. *Aquat. Microb. Ecol.* 39, 7–16. doi:10.3354/ame039007.
Reintjes, G., Fuchs, B. M., Scharfe, M., Wiltshire, K. H., Amann, R., and Arnosti, C. (2020). Short-term changes in polysaccharide utilization mechanisms of marine bacterioplankton during a spring phytoplankton bloom. *Environ. Microbiol.* doi:10.1111/1462-2920.14971.
Repeta, D. J. (2015). "Chemical Characterization and Cycling of Dissolved Organic Matter," in *Biogeochemistry of Marine Dissolved Organic Matter: Second Edition* doi:10.1016/B978-0-12-405940-5.00002-9.
Riser, S. C., Freeland, H. J., Roemmich, D., Wijffels, S., Troisi, A., Belbéoch, M., et al. (2016). Fifteen years of ocean observations with the global Argo array. *Nat. Clim. Chang.* 6, 145–153. doi:10.1038/nclimate2872.
Rivkin, R. B., and Legendre, L. (2001). Biogenic carbon cycling in the upper ocean: Effects of microbial respiration. *Science (80-.).* 291, 2398–2400.

doi:10.1126/science.291.5512.2398.
Romera-Castillo, C., Letscher, R. T., and Hansell, D. A. (2016). New nutrients exert fundamental control on dissolved organic carbon accumulation in the surface Atlantic Ocean. *Proc. Natl. Acad. Sci. U. S. A.* 113, 10497–10502. doi:10.1073/pnas.1605344113.
Salter, I., Galand, P. E., Fagervold, S. K., Lebaron, P., Obernosterer, I., Oliver, M. J., et al. (2015). Seasonal dynamics of active SAR11 ecotypes in the oligotrophic Northwest Mediterranean Sea. *ISME J.* 9, 347–360. doi:10.1038/ismej.2014.129.
Sambrotto, R. N., Savidge, G., Robinson, C., Boyd, P., Takahashi, T., Karl, D. M., et al. (1993). Elevated consumption of carbon relative to nitrogen in the surface ocean. *Nature* 363, 248–250. doi:10.1038/363248a0.
Sanders, R., Henson, S. A., Koski, M., De La Rocha, C. L., Painter, S. C., Poulton, A. J., et al. (2014). The Biological Carbon Pump in the North Atlantic. *Prog. Oceanogr.* 129, 200–218. doi:10.1016/j.pocean.2014.05.005.
Santoro, A. E., Casciotti, K. L., and Francis, C. A. (2010). Activity, abundance and diversity of nitrifying archaea and bacteria in the central California Current. *Environ. Microbiol.* 12, 1989–2006. doi:10.1111/j.1462-2920.2010.02205.x.
Saw, J. H. W., Nunoura, T., Hirai, M., Takaki, Y., Parsons, R., Michelsen, M., et al. (2020). Pangenomics analysis reveals diversification of enzyme families and niche specialization in globally abundant SAR202 bacteria. *MBio* 11. doi:10.1128/mBio.02975-19.
Sharp, J. H., Benner, R., Bennett, L., Carlson, C. A., Dow, R., and Fitzwater, S. E. (1993). Re-evaluation of high temperature combustion and chemical oxidation measurements of dissolved organic carbon in seawater. *Limnol. Oceanogr.* 38, 1774–1782. doi:10.4319/lo.1993.38.8.1774.
Shen, Y., and Benner, R. (2020). Molecular properties are a primary control on the microbial utilization of dissolved organic matter in the ocean. *Limnol. Oceanogr.* 65, 1061–1071. doi:10.1002/lno.11369.
Siegel, D. A., Buesseler, K. O., Behrenfeld, M. J., Benitez-Nelson, C. R., Boss, E., Brzezinski, M. A., et al. (2016). Prediction of the export and fate of global ocean net primary production: The exports science plan. *Front. Mar. Sci.* 3, 1–10. doi:10.3389/fmars.2016.00022.
Siegel, D. A., McGillicuddy, D. J., and Fields, E. A. (1999). Mesoscale eddies, satellite altimetry, and new production in the Sargasso Sea. *J. Geophys. Res. Ocean.* 104, 13359–13379. doi:10.1029/1999jc900051.
Sieracki, M. E., Verity, P. G., and Stoecker, D. K. (1993). Plankton community response to sequential silicate and nitrate depletion during the 1989 North Atlantic spring bloom. *Deep. Res. Part II* 40, 213–225. doi:10.1016/0967-0645(93)90014-E.
Simon, M., and Azam, F. (1989). Protein content and protein synthesis rates of planktonic marine bacteria. *Mar. Ecol. Prog. Ser.* 51, 201–213. doi:10.3354/meps051201.
Smith, D. C., and Azam, F. (1992). A simple, economical method for measuring bacterial protein synthesis rates in seawater using. *Mar. Microb. food webs* 6, 107–114.
Smith, D. C., Steward, G. F., Long, R. A., and Azam, F. (1995). Bacterial mediation of carbon fluxes during a diatom bloom in a mesocosm. *Deep. Res. Part II*. doi:10.1016/0967-0645(95)00005-B.
Steinberg, D. K., Carlson, C. A., Bates, N. R., Goldthwait, S. A., Madin, L. P., and

Michaels, A. F. (2000). Zooplankton vertical migration and the active transport of dissolved organic and inorganic carbon in the Sargasso Sea. *Deep. Res. Part I Oceanogr. Res. Pap.* 47, 137–158. doi:10.1016/S0967-0637(99)00052-7.

Stephens, B. M., Opalk, K. L., Petras, D., Liu, S., Comstock, J., Aluwihare, L. I., et al. (2020). Organic matter composition at Ocean Station Papa affects its bioavailability, bacterioplankton growth efficiency and the responding taxa. *Front. Mar. Sci.* 7, 1077.

Stocker, R. (2012). Marine microbes see a sea of gradients. *Science (80-.).* doi:10.1126/science.1208929.

Stoddard, S. F., Smith, B. J., Hein, R., Roller, B. R. K., and Schmidt, T. M. (2015). rrnDB: Improved tools for interpreting rRNA gene abundance in bacteria and archaea and a new foundation for future development. *Nucleic Acids Res.* 43, D593–D598. doi:10.1093/nar/gku1201.

Sunagawa, S., Coelho, L. P., Chaffron, S., Kultima, J. R., Labadie, K., Salazar, G., et al. (2015). Structure and function of the global ocean microbiome. *Science (80-.).* 348, 1–10. doi:10.1126/science.1261359.

Sweeney, C., Hansell, D. A., Carlson, C. A., Codispoti, L. A., Gordon, L. I., Marra, J., et al. (2000). Biogeochemical regimes, net community production and carbon export in the Ross Sea, Antarctica. *Deep. Res. Part II Top. Stud. Oceanogr.* 47, 3369–3394. doi:10.1016/S0967-0645(00)00072-2.

Takahashi, T., Olafsson, J., and Goddard, J. G. (1993). Seasonal Variation of CO2 and Nutrients in the High-Latitude Surface Oceans: A Comparative Study. *Global Biogeochem. Cycles* 7, 843–878.

Teeling, H., Fuchs, B. M., Becher, D., Klockow, C., Gardebrecht, A., Bennke, C. M., et al. (2012). Substrate-controlled succession of marine bacterioplankton populations induced by a phytoplankton bloom. *Science (80-.).* 336, 608–611. doi:10.1126/science.1218344.

Teira, E., Pazó, M. J., Quevedo, M., Fuentes, M. V., Niell, F. X., and Fernández, E. (2003). Rates of dissolved organic carbon production and bacterial activity in the eastern North Atlantic Subtropical Gyre during summer. *Mar. Ecol. Prog. Ser.* 249, 53–67. doi:10.3354/meps249053.

Thingstad, T. F., Hagström, Å., and Rassoulzadegan, F. (1997). Accumulation of degradable DOC in surface waters: Is it caused by a malfunctioning microbial loop? *Limnol. Oceanogr.* 42, 398–404. doi:10.4319/lo.1997.42.2.0398.

Treusch, A. H., Vergin, K. L., Finlay, L. A., Donatz, M. G., Burton, R. M., Carlson, C. A., et al. (2009). Seasonality and vertical structure of microbial communities in an ocean gyre. *ISME J.* doi:10.1038/ismej.2009.60.

Vergin, K. L., Beszteri, B., Monier, A., Cameron Thrash, J., Temperton, B., Treusch, A. H., et al. (2013). High-resolution SAR11 ecotype dynamics at the Bermuda Atlantic Time-series Study site by phylogenetic placement of pyrosequences. *ISME J.* 7, 1322–1332. doi:10.1038/ismej.2013.32.

Wang, W. L., Moore, J. K., Martiny, A. C., and Primeau, F. W. (2019). Convergent estimates of marine nitrogen fixation. *Nature* 566, 205–211. doi:10.1038/s41586-019-0911-2.

Wear, E. K., Carlson, C. A., and Church, M. J. (2020). Bacterioplankton metabolism of phytoplankton lysates across a cyclone-anticyclone eddy dipole impacts the cycling of semi-labile organic matter in the photic zone. *Limnol. Oceanogr.*, lno.11409.

doi:10.1002/lno.11409.
Wear, E. K., Carlson, C. A., James, A. K., Brzezinski, M. A., Windecker, L. A., and Nelson, C. E. (2015a). Synchronous shifts in dissolved organic carbon bioavailability and bacterial community responses over the course of an upwelling-driven phytoplankton bloom. *Limnol. Oceanogr.* 60, 657–677. doi:10.1002/lno.10042.
Wear, E. K., Carlson, C. A., Windecker, L. A., and Brzezinski, M. A. (2015b). Roles of diatom nutrient stress and species identity in determining the short- and long-term bioavailability of diatom exudates to bacterioplankton. *Mar. Chem.* 177, 335–348. doi:10.1016/j.marchem.2015.09.001.
Wear, E. K., Wilbanks, E. G., Nelson, C. E., and Carlson, C. A. (2018). Primer selection impacts specific population abundances but not community dynamics in a monthly time-series 16S rRNA gene amplicon analysis of coastal marine bacterioplankton. *Environ. Microbiol.* 20, 2709–2726. doi:10.1111/1462-2920.14091.
Weiss, R. F. (1970). The solubility of nitrogen, oxygen and argon in water and seawater. *Deep. Res. Oceanogr. Abstr.* 17, 721–735. doi:10.1016/0011-7471(70)90037-9.
Williams, P. J. L. B. (1995). Evidence for the seasonal accumulation of carbon-rich dissolved organic material, its scale in comparison with changes in particulate material and the consequential effect on net CN assimilation ratios. *Mar. Chem.* 51, 17–29. doi:10.1016/0304-4203(95)00046-T.
Williams, P. M., and Druffel, E. (1988). Dissolved Organic Matter in the Ocean: Comments on a Controversy. *Oceanography* 1, 14–17. doi:10.5670/oceanog.1988.33.
Williams, T. J., Wilkins, D., Long, E., Evans, F., Demaere, M. Z., Raftery, M. J., et al. (2013). The role of planktonic Flavobacteria in processing algal organic matter in coastal East Antarctica revealed using metagenomics and metaproteomics. *Environ. Microbiol.* 15, 1302–1317. doi:10.1111/1462-2920.12017.
Yager, P. L., Wallace, D. W. R., Johnson, K. M., Smith, W. O., Minnett, P. J., and Deming, J. W. (1995). The Northeast Water Polynya as an atmospheric CO2 sink: a seasonal rectification hypothesis. *J. Geophys. Res.* 100, 4389–4398. doi:10.1029/94JC01962.
Zakem, E. J., Cael, B. B., and Levine, N. M. (2020). A unified theory for organic matter accumulation. *bioRxiv*. doi:10.1101/2020.09.25.314021.
Zweifel, U. L., Wikner, J., Hagström, Å., Lundberg, E., and Norrman, B. (1995). Dynamics of dissolved organic carbon in a coastal ecosystem. *Limnol. Oceanogr.* 40, 299–305. doi:10.4319/lo.1995.40.2.0299.